INFORMATION TO USERS

This manuscript has been reproduced from the microfilm master. UMI films the text directly from the original or copy submitted. Thus, some thesis and dissertation copies are in typewriter face, while others may be from any type of computer printer.

The quality of this reproduction is dependent upon the quality of the copy submitted. Broken or indistinct print, colored or poor quality illustrations and photographs, print bleedthrough, substandard margins, and improper alignment can adversely affect reproduction.

In the unlikely event that the author did not send UMI a complete manuscript and there are missing pages, these will be noted. Also, if unauthorized copyright material had to be removed, a note will indicate the deletion.

Oversize materials (e.g., maps, drawings, charts) are reproduced by sectioning the original, beginning at the upper left-hand corner and continuing from left to right in equal sections with small overlaps.

Photographs included in the original manuscript have been reproduced xerographically in this copy. Higher quality 6" x 9" black and white photographic prints are available for any photographs or illustrations appearing in this copy for an additional charge. Contact UMI directly to order.

ProQuest Information and Learning
300 North Zeeb Road, Ann Arbor, MI 48106-1346 USA
800-521-0600

UMI®

Induced Optical Fluorescence Spectroscopy of Laser Excited Microorganisms in Water

By

SARHAN MAHMOUD MUSA

A dissertation submitted to Graduate Faculty in partial fulfillment of the requirements for the degree of Doctoral of Philosophy in Engineering,
The City University of New York

Year 2001

This manuscript has been read and accepted for the Graduate Faculty in Engineering in satisfaction of the dissertation requirements for the degree of Doctor in Philosophy.

7/26/01
Date

Chair of the Examining Committee

Professor Samir A. Ahmed

7/26/01
Date

Executive Officer

Dean Mumtaz K. Kassir

Professor S. Ahmed

Professor M. Ali

Professor B. Gross

Professor R. Khanbilvardi

Professor F. Moshary

Professor L. Roytman

DR. k. Szekielda

DR. F. Adib

Supervisory Committee

THE CITY UNIVERSITY OF NEW YORK

Abstract

Induced Optical Fluorescence Spectroscopy of Laser Excited Microorganisms in Water

By

SARHAN MAHMOUD MUSA

Advisor: Professor Samir A. Ahmed

This thesis presents a study of the laser induced optical natural fluorescence of *Giardia lamblia* cysts. It shows that the auto-fluorescence spectra of untagged *Giardia lamblia* cysts excited by visible lasers can be detected using fiber-optical fluorescence microscopy. The peak of the fluorescence spectrum agrees with the amino acid tryptophan in aqueous solution at all the excitation wavelengths used. While *G.lamblia*'s fluorescence is very similar to other translucent microorganisms such as paramecium and rotifer under 458 nm excitation, a clear difference is revealed under blue laser excitation at 401 nm, where only *G.lamblia* matches tryptophan in fluorescence. A reproducible decay of the fluorescence intensity is also observed in *Giardia lamblia* under continuous excitation.

I dedicate this thesis to my lovely mother Fatmeh and my sister Majida.

Acknowledgments

I would like to specially thank my Mentor Professor Samir Ahmed whom I look up to with the utmost respect and admiration and who through his guidance, training, ideas, and motivation encouraged me to continue and successfully finish the doctoral degree.

I want to specially thank Dr. Yiping Zhang for his great help, ideas, and training provided me during the investigations performed for this thesis. In addition, I thank Eugene Leykin, Bahar Zoghimoghadam, Professor John Lee, Professor Ralph Zuzolo, and Dr. Ian Mitchell for their helps and all members of the Remote Sensing lab of City College. I thank Professors M. Ali, B. Gross, R. Khanbilvardi, F. Moshary, L. Roytman Professor, k. Szekielda and Dr. F. Adib for being part of my doctoral dissertation committee.

Table of contents

List of figures

Chapter 1

Introduction

1.1 Background

The spontaneous fluorescence of waterborne microorganisms (such as *Giardia lamblia*, Paramecium, and Rotifer) without adding dyes is referred to in the thesis as optical natural fluorescence (ONF). The autofluorescence spectroscopy is useful because it does not require any chemical manipulation for the sample, gives real time results immediately from the sample reaction, and supplies information about the biological structure of the cell through its fluorophores. This technique is compatible with microscope optics and sensitive to weakly fluorescing microscopic samples. It can be used to distinguish the microorganisms from each other.

Giardia lamblia is a common intestinal protozoan (which consists of a single cell for its body) that causes giardiasis (gastrointestinal disease, symptoms including diarrhea, nausea, and/or stomach cramps, can be fatal to immune suppressed individuals), which has been distributed worldwide and implicated in recent outbreaks of illness in the US [1,2,22-23]. G. lamblia is commonly found in surface waters (rivers, lakes, streams, etc.) especially where there is contamination from sewage or animal wastes [6]. It lives mainly in cysts forms that are resistant to disinfections. The cysts of G. lamblia are oval in shape and are approximately 8 to 14 μm in size (width by length) [3-5,7]. Because of its translucent appearance and low concentration in natural waters [8], G. lamblia is not easy to detect, but even a few cysts are enough to make a person severely sick.

There were a number of methods proposed for the detection of G. lamblia cysts, such as conventional microscopy, flow cytometry (FC) [9-10,24], "UV-VIS Spectroscopy"

method [11-12], enzyme-linked immunosorbent assay (ELISA) [13], and polymerase chain reaction (PCR) [14]. These methods are at various stages of development, some of them being incomplete. Many of them have problems for ascertaining G. lamblia cysts in water [2,6,28]. For example, conventional microscopy needs an experienced person dedicated to the observation and is inefficient in time and prone to error. The FC method relies on the ability of the instrument to analyze particles individually in a suspension, which means the method needs to have a highly trained full-time operator. This method is limited in efficiency due to losses occurring during sample concentration, and the purified and concentrated samples are stained with antibodies specific to G. lamblia cysts. For "UV-VIS Spectroscopy" method, the background particles such as algae and nonbiotic particulate cause spectral patterns that mask the deconvolution of the target organism fingerprint, and the antibody labeling is used to enhance the signal and allow differentiation. In ELISA method algae present in the sample can pick up the antibody reagents and give false-positive readings, which reduce the analytical sensitivity. In addition, the PCR method has limitation during the sample collection and elution. Organic matter and dissolved solids can be concentrated in the sample and these compounds (such as humic substances) can interfere with the activity of the enzymes used in PCR.

The current state-of-the-art technique for detecting G. lamblia relied upon microscopic immunofluorescence assay (IFA) method that uses antibodies directed against the cyst forms of the Protozoa. This method uses specific antibodies labeled with fluorescent dye to tag G. lamblia cysts, which are then viewed through an UV fluorescence microscope [15, 25, 26]. To use this method, it is first necessary to determine the antigen of G.

lamblia in order to make the antibody specific to the cyst membrane, although several commercial sources of antibodies for G. lamblia are already available. In practice, there is a slight possibility of cross-reactivity for the antibody because different organisms may share similar surface antigens [27]. Interference with the immunoassay signal may also arise from nonspecific binding of the antibody or autofluorescence from other microorganisms and the background [16-18]. While a number of commercially developed antibodies are highly specific to G. lamblia, it is impractical to deploy a large quantity of them for continuous field sensing. In practice, water samples need to be taken to a laboratory for the assay, which can delay the detection of cysts in time. At the same time, the viability of the cysts can not be determined unambiguously without additional staining or other procedure [20]. Therefore, the limitations of the current methods prompt a need to develop a detection method that passively senses the natural characteristics of this microorganism.

In this work, a fiber-optical fluorescence microscope is specifically designed to excite and collect the fluorescence from G. lamblia cysts. For the geometric convenience of the work, optical fibers will be used for the transmission of the laser excitation to the sample and for collecting the fluorescence light emitted and bringing it to a spectrometer detector. This approach is also in concert with a potential ultimate application of these techniques: namely the direct optical detection of microorganisms in reservoirs and other natural bodies of water.

Through this experimental setup, the laser-induced auto-fluorescence of G. lamblia cyst is extensively studied and compared with that from a few benign microorganisms such as Paramecium and Rotifer. The ONF of G. lamblia is found to have a distinctive

spectral shape under 401 nm excitation and a unique decay feature under 458 nm excitation compared to the other natural protozoa. Although the fluorescence microscope technique in this work is not in-situ yet, the result of this study on auto-fluorescence will facilitate the development of in-situ fluorescence probes for the detection of G. lamblia cysts.

1.2 Thesis Statement and Organization

This thesis will focus on examining stimulated ONF of natural microorganisms using visible light sources (lasers) as a source of excitation. The stimulated emission spectra obtained from G. lamblia cysts will be analyzed and compared with other microorganisms, such as G. muris, Paramecium, and Rotifer. As part of an effort seeking to determine root causes for the fluorescent characteristics of G. lamblia, the fluorescent properties of amino acids and coenzymes will be studied for fundamental causative features relating to G. lamblia's autofluorescence. The proposed work will examine untagged species of G. lamblia and other microorganisms as appropriate to the aim of this work. It will also seek to determine the optimal excitation source and wavelength that will assist in characterizing fluorescence excited from G. lamblia cysts. This optimal excitation condition would be investigated with a view to exciting uniquely characteristic optical natural fluorescence spectral features of G. lamblia cysts, enabling their detection with minimal interference from optical natural fluorescence of other waterborne microorganisms and particles.

The research part of this thesis will be presented in chapters 2 through 6. In chapter 2, the experimental setup that permits the successful investigation results is described.

Chapter 3 reports the laser induced ONF spectra of G. lamblia cysts. The ONF spectra of other microorganisms (Paramecium, Rotifer) in comparison with G. lamblia is reported in chapter 4. In chapter 5, the fluorescence of the aromatic amino acid L-tryptophan is discussed relating to the causes for the ONF of G. lamblia cysts. Finally, the fluorescence intensity from G. lamblia and other microorganisms as a function of excitation time in photobleaching is reported in chapter 6.

1.3 References

1. G.F. Craun, "Waterborne Outbreaks of Giardiasis, Current Statues," In: Giardia and Giardiasis, S. L. Erlandsen, and E. A. Meyer Eds. (Plenum Press, New York, 1984), pp. 243-261.
2. P. Willis and B. Hammond, "Advances in Giardia Research," The University of Calgary Press (1987).
3. G. J. Tortora, B. R. Funke, and C. L. Case, *Microbiology: An Introduction*, 4th ed. (Benjamin/Cumming, Redwood City, CA, 1992), pp. 313-319.
4. M. W. LeChevallier, W. D. Norton, and T. B. Atherholt, "Protozoa in open reservoirs," J. Am. Water Works Assoc. **89**, 84-96 (1997).
5. S. T. Bagley, M. T. Auer, D. A. Stern, and M. J. Babiera, "Sources and fate of Giardia Cysts and Cryptosporidium Oocysts in surface waters," J. Lake and Reserv. Manage. **14**, 379-392 (1998).
6. S. L. Erlandsen and E. A. Meyer, *Giardia And Giardiasis*, (Plenum press, 1984).
7. Lechevallie, M.W. ET AL., Giardia and Cryptosporidium in water Supplies, AWWARF, Denver, (1991).
8. D. A. Stern, "Monitoring for Cryptosporidium spp. and Giardia spp. and human enteric viruses in the watersheds of the New York City water supply system," http://www.epa.gov/owow/watershed/proceed/stern.html
9. G. Vesey, et al., "Appliction of Flow Cytometry Methods for the Routine Detection of Cryptosporidium and Giardia in Water," Cytometry.**16**, 1-6 (1994).
10. G. Vesey, et al., "Detection of Specific Microorganisms in Environmental Samples Using Flow Cytometry," Methods in Cell Biol. **42**, 489 (1994).

11. IC. Bacon, et al., "Quantitative Classification of Cryptosporidium Oocysts and Giardia Cysts in Water Using UV/VIS Spectroscopy," BIOS: Biomedical Optics Conference (1995).

12. K. Patten, et al., "Rapid Methods for On-line Detection of Cryptosporidium Oocysts and Giardia Cysts," Proc. AWWA WQTC, San Francisco, Calif (1994).

13. D. L. Cruz, A. Armah, and M. Sivaganesan, "Detection of Giardia and Cryptosporidium spp. in Source Water Samples by Commercial Enzyme Immunoassay Kits," Proc. AWWA WQTC, San Francisco, Calif (1994).

14. C. L. Mayer, and C. J. Palmer, "Evaluation of PCR, Nested PCR, and Fluorescent Antibodies for Detection of Giardia and Cryptospridium Species in wastewater," Appl. Envir. Microbiol. 62, 2081 (1996).

15. C. Water, P. Hibler, "An Overview of the Techniques Used for Detection of Giardia Cysts in Surface Water", Advances In Giardia Research, pp.197-204, 1988.

16. M. W. LeChevallier, ET AL. "Evaluation of the Immunofluorescence Procedure for Detection of Giardia Cysts and Cryptospordium Oocysts in Water." Appl. Envir. Microbiol. 61,690 (1995).

17. E. C. Nieminski, Frank W. Schaefer III, Jerry E. Ongerth, "Comparison of Two Methods for Detection of Giardia Cysts and Cryptosporiidium Oocysts in Water," Appl. And Envir. Micro. 61, 1714-1719 (1995).

18. "Development of Performance Evaluation Sample Preparation Protocols for Giardia Cysts and cryptosporidium Oocysts," EPA Contract No. 68-C3-0365. USEPA Water Docket (1996).

19. B. R. Dixon, M. Parenteau, C. Martineau, and J. Fournier, "A comparison of conventional microscopy, immunofluorescence microscopy and flow cytometry in the detection of Giardia lamblia cysts in beaver fecal samples," J. Immuno. Methods. **202**, 27-33 (1997).

20. L. Thiriat, F. Sidaner, and J. Schwartzbrod, "Determination of Giardia cyst viability in environmental and faecal samples by immunofluorescence, fluorogenic dye staining and differential interference contrast microscopy," Lett. Appl. Microbiol. **26**, 237-242 (1998).

21. H. A. Lindquist, A. dufour, L. Wymer, and F. Schaefer III, "Criteria for evaluation of proposed protozoan detection methods." Journal of Microbiology Methods. 37,33-43 (1999).

22. A. Ashendorff, M. Principe, A. Seeley, J. Laduca, L. beckhardt, W. Faber, and J. Mantus, " Watershed protection for new york city's supply," Journal AWWA. **89**,75-88 (1997).

23. G. F. Craun, " surface water supplies and health," Journal AWWA. **80**, 40-52 (1988).

24. R. Hoffman, J. Standridge, A. Prieve, J. Cucunato, and M. Bernhardt, " Using flow cytometry to detect protozoa," Journal AWWA. **89**, 104-111 (1997).

25. S. K. Stephen, J. L. Riggs, P. D. Dileanis, and T. J. Suk. "Isolation and detection of Giardia Cysts from water using direct immunofluorescence," Water resources bulletin, American water resources association. **22**, (1986).

26. J. L. Riggs, K. W. Dupuis, Koichi Nakamura, and David P. Spath, "Detection of Giardia lamblia by Immunofluorescence," Appl. And Envir. Micro. **45**, 698-700 (1983).

27. Walter Jakubowski, *Giardia methods workshop*, Denver, Colorado, 1-12 (1984).

28. W. Jakubowski, S. Boutros, W. Faber, R. Fayer, W. Ghiorse, M. LeChevallier, J. Rose, S. Schaub, A. Singh, and M. Stewart, "Environmental methods for Crypyosporifium," Journal AWWA. 107-121 (1996).

Chapter 2

Experimental Setup

2.1 Introduction

The chapter will focus on the experimental setups that are used to study the ONF of G. lamblia, other microorganisms, and amino acids.

2.2 Experimental Setup (1)

The schematic of the experimental setup used for studying ONF of G. lamblia cysts and other microorganisms is shown in Figure (2.1).

A CW Argon ion laser (Lexel model 95) has been used as an excitation source. This laser has a high power output and is ideal for research such as fluorescence spectroscopy. Its output is selectable at 458 nm, 476 nm, 488 nm, 496 nm, and 514 nm. The wavelength 458nm has been used to excite the fluorescence of G. lamblia cysts, because it induces the clearest ONF and least amount of noise among all the wavelengths.

In the setup, the laser output is low in height, so two plane mirrors are used to raise the laser beam. The reflected beam then goes through two equilateral dispersion prisms. The dispersion prism ensures that the spontaneous emission background from the laser (which may overlap with ONF) is minimized. Otherwise it would be mixed with the monochromatic excitation and contribute to the scattering noise. The laser beam is then reflected by a third plane mirror and enters a miniature fiber optical coupler. Inside the coupler, there is a small lens (dia. 5 mm, f.l. 10 mm) that focuses the laser into the core of one branch of a bifurcated multi-mode fiber (200 μm core, N.A. 0.22). Although the laser output is linearly polarized, the output from the fiber is unpolarized.

It is important to center the laser beam in the aperture of the fiber optical coupler, and to tilt the beam at the right angle with respect to the coupler to maximize the coupling efficiency. Because of its large core, the fiber can easily provide good coupling efficiency. The output of the optical fiber becomes a clean Gaussian beam, which corrects any spatial non-uniformity in the original laser beam profile. Sometimes, neutral density filters (ND 0.3) are used in front of the fiber optical coupler in order to attenuate the laser intensity at the fiber output.

The light exiting the fiber is sent into a Nikon microscope (Optiphot) through the epi-illumination port on the side of the microscope. The optics assembly of the illumination port is partially disassembled, leaving a single 100-mm focal length lens remaining inside the port. The excitation beam entering the microscope is first converged by this lens. An internal beam splitter window then reflects the collimated light downward along the optical axis of the microscope, with a reflection coefficient around 25%. The transmission spectrum of the beam splitter is showed in figure (2.2). The reflected light by the beam splitter is focused by the microscope objective lens on the microscope slide. The microscope objective lens used in most experiments has a power of 20X (Japanese standard JIS, f.l. 8.55 mm, w.d. 3 mm) and a numerical aperture (N.A.) of 0.40, which corresponds to a half angular aperture of the objective $\theta = 23.58°$.

The objective lens of different power, 20X (N.A. 0.4) and 5X (N.A. 0.1) often induce the same fluorescence spectra in shape; however, the intensity of the image increases with the power of the objective (lower N.A. means lower power). The standard objective used for the experiment is 20X. The targets that appear non-fluorescent with a power of

5X may appear weakly fluorescent with a power of 20X for the objective because 20X has a bigger N.A. of 0.4 and focuses the laser more tightly on the sample. Sometimes the objective of 5X is used in order to see the target in a small magnification.

The G. lamblia samples to be observed are prepared in a Fisher drop slide, which has a concavity of 0.5 mm depth and 18 mm diameter. The Fisher drop slide is covered with a slim cover glass (Fisher, premium cover glass, size 24 x 50mm). In addition, a flat glass microscope slide (plain Fisher 3x1x1mm) with the slim cover glass (Fisher) is used for the paramecium, rotifer samples to reduce the movement of the microorganisms.

The light emitted by the sample passes through the same objective lens of the microscope, transmits through the beam splitter, passes a prism in the microscope, and finally goes through a relay lens assembly to form a real image above the microscope. Before the image plane, the output light also goes through an optical long pass filter (Schott GG495, Schott OG 515, Corning 3-69 and Corning 3-72 filters for various laser wavelengths) that is placed in front of a detection fiber. The filter is necessary to ensure that the laser scattering signal does not swamp the detector for the relatively low-level fluorescence signal. The filter passes the fluorescence on the red side of the laser line and blocks unwanted laser scattering. The optical long pass filters match the proper excitation wavelength: corning 3-72 ~ 401 nm; GG 495 ~ 458 nm; Corning 3-69 or OG515 (better than 3-69) ~ 496 nm. The transmission spectra of these long pass filters (LPF) have been measured using the setup in Figure (2.5), and the results are shown in Figure (2.3). These are measured by using Ocean Optics white light source with ND3.0 attenuation. The setting for spectrometer channel is (6, 100) for (integration time (msec),

average number). Different LPF does change the shape of the spectra, but it does not change the decay (photo-bleaching) character of the microorganisms.

Another multi-mode fiber (Ocean Optics, 400 μm core, N.A. 0.22) is aligned above the photographic port of the microscope and is coaxial with the optical axis of the microscope to detect the emission light of the object. The real image mentioned above is sent into the core of this fiber. The other end of this collecting fiber is connected to an fiber optical spectrometer (Ocean Optics S2000), which is interfaced with a computer that has LabView software displaying the emission spectra integrated by the spectrometer's CCD array detector. The integration time typically used with the spectrometer is 4 second. The S2000 Spectrometer has high detection sensitivity (86 photon/count, 2.9 x 10^{-17} J/count, which is equivalent to 2.9 x 10^{-17} watts/count for 1-second integration). The spectrometer accepts light transmitted through multi-mode optical fiber and disperses it via a fixed grating across the CCD array, which is responsive from 187-879 nm (effective range).

The approximate FWHM optical resolution (OR) is related to the dispersion (D) and the resolution (R) of the spectrometer by

$$OR = D \times R.$$

The dispersion is calculated from the spectral range of the grating (S) and the number of detector elements (N):

$$D = \frac{S}{N}.$$

For the S2000 Spectrometer, the spectral range of the grating is 650 nm [1], the number of the detector elements is 2048 [1] and the resolution for a 25 μm slit is 4.2 pixels [1], so the calculated optical spectral resolution of the spectrometer is 1.3 nm

(FWHM). The acquired spectra were smoothed and the final spectral resolution is 16.6 nm.

A white light source (Ocean optics LS-1) is used to align both the excitation and collection fibers. A circular spot of size 25 μm representing the circle of illumination and another circular spot of size 40 μm representing the circle of collection are located at the center of the cross hairs in the microscope's field of view. The laser power coupled into the excitation fiber output was either 2.5 or 10 mW. The throughput of the microscope for the excitation is approximately 1%. Therefore, the direct excitation intensity on the slide sample is about 4-16 W/cm^2.

Before taking the measurements in the experimental setup, the microscope is first focused on an individual object (for example, a G. *lamblia* cyst) by adjusting the height of the stage that carries the slide (z-direction) and observing through the eyepiece. The excitation and collection fibers are then translated along their longitudinal axes until they form sharp images on the same plane as the object. The sharp images are viewed through the eyepiece as sharp circular reflections of the fiber's illumination by the glass slide. The two fibers are then translated along their transverse axes until their images overlap concentrically on the cross hairs of the field.

The image of the excitation and detection fibers on the cross hairs of the eyepiece of the microscope is shown in the following figure.

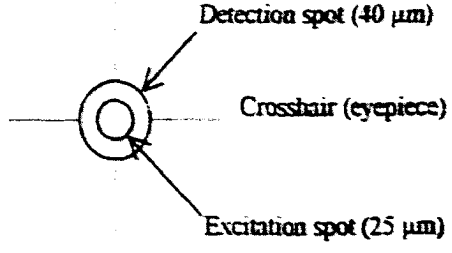

The target microorganisms are first translated away from the cross hair where the laser would be focused. The auto-fluorescence spectrum of the substrate (blank buffer solution or water) is then measured and saved as a background by choosing a store dark mode on the spectrometer software. The background spectrum is then automatically subtracted from the signal (by using Scope-dark mode). The microorganisms are then moved to center on the cross hair while the laser is blocked. Subsequently, the signal spectra are saved as soon as the laser is unblocked. The measurements are always taken in a dark room at room temperature.

2.3 Experimental setup (2)

The experimental setup used in studying ONF of G. lamblia and other microorganisms is schematically shown in Figure (2.4). A CW semiconductor laser (blue laser, Power technology, PPM04) has been used as an excitation source. The laser emits light of 401 nm from a 5-mW gallium nitride-based laser diode. The spectral line width is less than 1 nm. The experimental setup using the blue laser (figure 2. 4) is similar to the setup in figure (2.1) without using the two equilateral dispersion prisms.

2.4 Experimental setup (3)

A schematic display of the experimental setup (Ocean Optics FHS-UV) for measuring the transmission spectra of the long pass filters is shown in figure (2.5). The fibers are attached to two collimators, which have lenses inside (5-mm dia., f/2 optimized for UV-VIS). The two collimators are aligned so that the output light from one fiber is collimated by the first lens and properly focused into the other fiber by the second lens.

The filter being tested is inserted in the path of the collimated light between the two collimators. A Tungsten halogen white light source (Ocean Optics LS-1) is used. Its output runs continuously from 360nm to 2 μm, offering high color temperature and extremely efficient output. An ND 3.0 filter is often inserted in a slot in the white light source to reduce the power of the light and prevent the saturation of the spectrometer detector.

A fiber optic cuvette holder (Ocean optics CUV-ALL 4-way) is also used in the optical setup when it is necessary to transmit collimated light through samples contained in cuvette. The cuvette holder can accommodate a 1-cm cuvette and has four fiber optic collimators (one on each side) that are identical to those used in the filter transmission setup. Optical multi-mode fibers can be attached to these collimators to illuminate the sample and collect light from it. When combined with the spectrometer and light source, the CUV-ALL assemblies can measure transmission, fluorescence, and scattering.

The collimators are screwed into the four sides of the sample well of the cuvette holder. One the optical fiber is connected to one of the collimator and the light source, creating the illumination part of the optical setup. Another optical fiber is connected to the other collimator and to the spectrometer, creating the detection part of the optical setup. Without the collimators, the light out of the fiber would diverge faster than what is needed for efficient transmission and collection of the signal. These collimators have the advantage of higher collection efficiency and better spatial resolution as both the transmission and acceptance angles are easily optimized.

The measurement of the transmission spectrum is taken when the room light is off. Store dark function is used when the white light is blocked at the light source, then store

reference function is used when the white light is let to pass without obstruction to be saved as a background. Finally, the transmission mode is used to take the transmission measurement. Integration time and average number are properly selected to minimize the refreshing time of the program. In general, it is better to use a more sensitive spectrometer channel (such as the slave channel) so that a small integration time may be used to obtain a large signal. On the other hand, the average number can be set to be as large as possible in order to smoothen the signal.

2.5 Experimental setup (4)

A schematic display of the experimental setup for 90° detection in Figure (2.6) is used to measure the fluorescence of an amino acid solution. The blue diode laser and the Argon ion laser are used as excitation sources. The excitation light is reflected by a plane mirror (M), and then coupled through the optical fiber coupler (C) to the optical fiber that is 200 μm in core diameter. For the Argon ion laser, the two dispersion prisms always are used to the output beam. The other end of the fiber is connected to a collimator on the fiber optic cuvette holder, which holds a fluorescence/scattering cell (NSG type 23, 4 windows polished, path length 10 mm, outside dimension 12.5 mm sq. x 49.0 mm h.) containing a solution of the amino acid. The emitted light from the cell is detected at 90° angle by a second optical fiber (400 μm core) through another collimation lens. The other end of the collection fiber is connected to the spectrometer S2000, which is turn connected to the computer. No long pass filter is used here.

2.6 Experimental setup (5)

A Schematic display of the experimental setup for 180° detection in figure (2.7) is used to measure the fluorescence of an amino acid solution.

The light beam leaving the laser source (diode laser or Argon Ion laser) is reflected by a plane mirror and then coupled through optical fiber coupler to one leg of a bifurcated fiber optic probe. The output light of the fiber enters a thin cuvette that contains the sample and the fluorescence is collected by a second fiber (side by side with the first) in the same probe. This second fiber guides the fluorescence light to the other leg of the bifurcated fiber and then to the spectrometer S2000 that is connected to the computer.

2.7 Experimental setup (6)

A Schematic display of the experimental setup for 0° detection in figure (2.8) is used to measure transmission/absorption of the amino acid solution. The source of excitation is a Xenon flash lamp (Ocean Optics PX-1). The pulsed Xenon lamp is a high energy light source with a short arc flash lamp optimized for UV measurements from ~ 220 to 750 nm. It offers excellent pulse-to-pulse stability. The output light of the lamp enters a fiber of 400 μm core dia. The other end of the fiber is connected to a collimator on a long-path transmission cell (Ocean Optics 10cm cuvette sample holder). The collimated light first passes through an ND3 filter to reduce the output power of the source, then passes through a 10 cm cell, and finaliy goes to another collimated lens connected to a second multimode fiber with same diameter as the excitation fiber. The other end of the collection fiber is connected the spectrometer S2000 that is connected to the computer.

The Xenon lamp is also connected to the Spectrometer for its pulse repetition rate control.

2.8 Experimental Setup (7)

A Schematic display of the experimental setup for 90° detection in figure (2.9) is used to measure the fluorescence of the amino acid solution. The source of excitation is the Argon laser or the diode laser. The laser beam goes through the sample directly (without the fiber waveguide) and the fluorescence is collected by the fiber at 90° location through the long pass filter.

2.9 Experimental Setup (8)

A Schematic display of the experimental setup for 180° detection in figure (2.10) is used to measure the fluorescence of an amino acid solution.

The light beam leaving the laser source (diode laser or Argon Ion laser) is reflected by a plane mirror and then coupled through optical fiber coupler to one leg of a bifurcated fiber optic probe. For the Argon ion laser, the two dispersion prisms always are used to the output beam. The output light of the fiber enters a beaker that contains the sample and the fluorescence is collected by a second fiber (side by side with the first) in the same probe. This second fiber guides the fluorescence light to the other leg of the bifurcated fiber, which is connected to a collimation lens of a filter holder. After going through a long pass filter, the light goes through another collimation lens connected to the other end of the filter holder, which is connected through another fiber (400 μm core) to the spectrometer S2000 that is connected to the computer.

2.10 Material

The G. lamblia cysts introduced into the slide cavity for excitation and observation are normally prepared in a PBS solution (a phosphate buffer saline solution with penicillin, streptomycin, and gentamicin). The sources of the cysts are experimentally infected gerbils. The cysts are purified from feces by sucrose and Percoll density gradient centrifugation. The storage condition for the sample is 4 to 6 degrees Celsius (i.e. refrigerator temperature). Suspensions of live cysts expire 21 days after the date of shipment. It is obtained from Waterborne Inc. Paramecium and rotifer are cultured in spring water were obtained from North Carolina biological supplies. L-tryptophan and FAD (Flavin adenine dinucleotide) are obtained from Sigma-Aldrich.

2.11 Discussion:

It is important that the background signal of the sample is small in order to obtain clear fluorescence spectra of large amplitude (after to the subtraction of the background from the emission spectra). A large background will greatly reduce the signal to noise ratio of the fluorescence even with background subtraction. Note that when a shorter laser wavelength is applied, a stronger background from the autofluorescence of the sample substrate can occur. Therefore, for the 401 nm excitation wavelength, the background is higher than that from the 458 nm wavelength excitation.

When the white light and the fibers are used for the alignments, the fibers give several images that come from the front surface of the multi-mode fibers. These images can be explained by the Cloud theory.

The Cloud theory for the image of the fiber on the slide can be expressed as the following:

The reflections from planes above and below the focal plane create the cloudy (fuzzy) image, but the sharp image comes from the reflection from the plane of the focus.

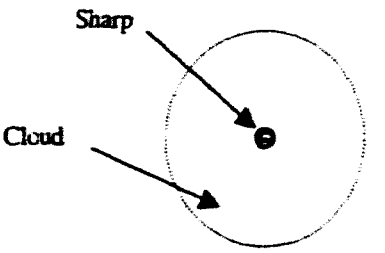

The cloud for the excitation fiber is about a factor of five larger than its sharp image, and the cloud for the collection fiber is about a factor of three larger than its sharp image. The size of the cloud also depends on the type of the microscope slide used in the experiment. Slides with wells (cavities) give larger cloud image than flat slides.

In order to minimize the background, the following steps must be followed:

On the microscope, use the objective lens of a power 5X to locate the protozoa (microorganisms) and a relatively clean background surrounding the protozoa. Then use the objective lens of 20 X and adjust the sample stage until the protozoa are on focus. Send white light into the two fibers. Look for their images on the focal plane of the protozoa. Move the fibers along their longitudinal axes. Multiple positions along these axes can be found that form a sharp image of the same size, accompanied by cloudy images of different sizes. Choose the position that gives the largest relative size in

cloudy image. This position spreads out the unwanted background fluorescence to a maximum degree and will give the minimum background in the collected signal.

The reason why there are bigger cloud images of the fiber on the well slide than the flat slide is that the light goes deeper from the plane of focus (POF) in well slide, which creates more cloudy image, as showed in the following figure.

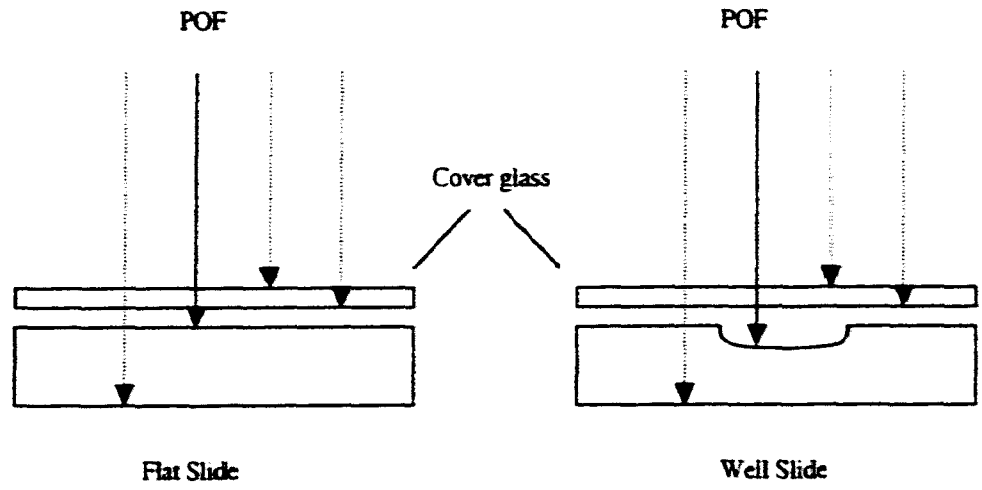

A light beam (white light or laser) is brought to a point of focus by the objective lens at the level labeled "plane of focus". The fluorescence is emitted by the specimen from the point of focus (solid rays) and passes back through the objective lens, through the beam splitter to the fiber and the detector (spectrometer). However, autofluorescence will also be emitted by the substrate background from planes above and below the plane of focus (dashed lines), but this light will be prevented from reaching the spectrometer by the detector fiber, which has a small core diameter. The more spreaded out the background image is, the less efficient the background can reach the spectrometer. Thus, only the light originating from the plane of focus is most effectively collected by the detector.

Note that G. lamblia (and other microorganisms) can sit at different depth in the well slide, which can make the focus of the microscope and the focus of the fibers difficult. Therefore, a piece of rock or plant is sometimes focused on as a reference for the plane of focus.

The microscope for the setup is designed to illuminate the sample with the excitation light (laser) and collect the emitted light while excluding the laser scattering by using long pass filters.

2.12 Conclusion

The experimental setup above has been used to study the optical natural fluorescence (ONF) of G. lamblia cysts and other microorganisms. The main components consist of optical multi-mode fibers used as waveguides for illumination and detection, a highly sensitive spectrometer, long pass filters, and suitable CW blue excitation sources.

2.13 References

1. Ocean Optics, Inc. http://www.OceanOptics.com/
2. R. Kingslake, Applied Optics and Optical Engineering, Vol. IV, Optical Instruments Part I, (Academic Press, New York/London, 1967).
3. R. Kingslake, "Applied Optics and Optical Engineering," III, Optical Components, (Academic Press, New York/London, 1965).
4. D. Malacara, Geometrical and Instrumental Optics, 25, methods of Experimental Physics, (Academic Press, Inc. Boston, 1988).

2.14 Figures

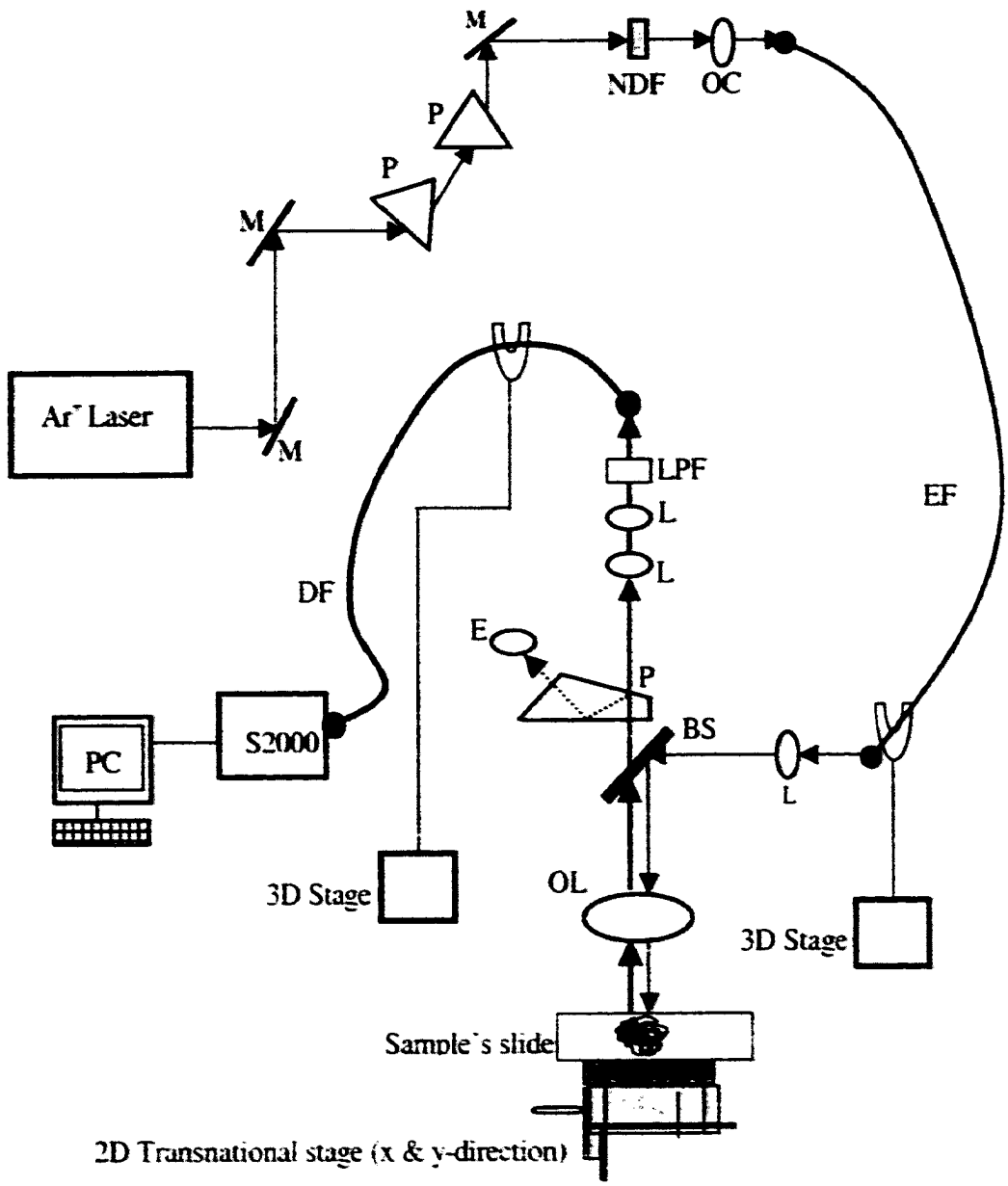

Fig. 2.1. Schematic display of the experimental setup: M, flat mirror; C, fiber coupler; EF, Excitation fiber; DF; Detection Fiber; L, lens; BS, beam splitter; OL, objective lens; E, eyepiece (ocular); LPF, long pass filter

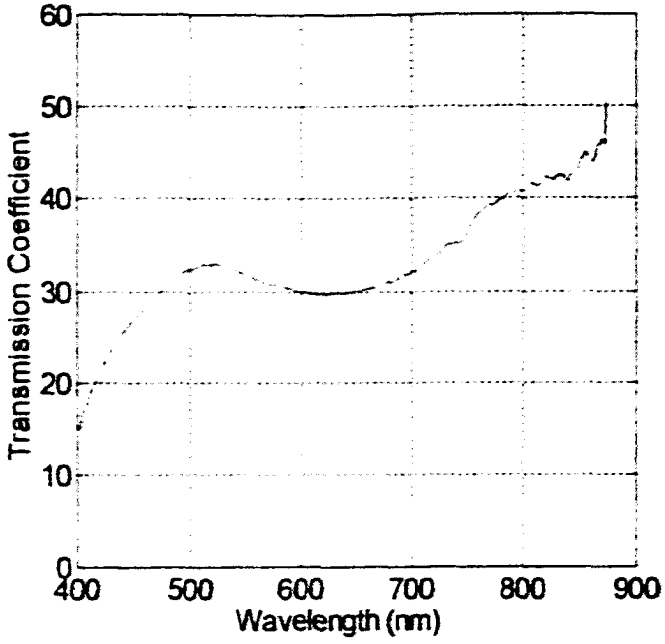

Fig. 2.2. Measured transmission of the Microscope Beam Splitter.

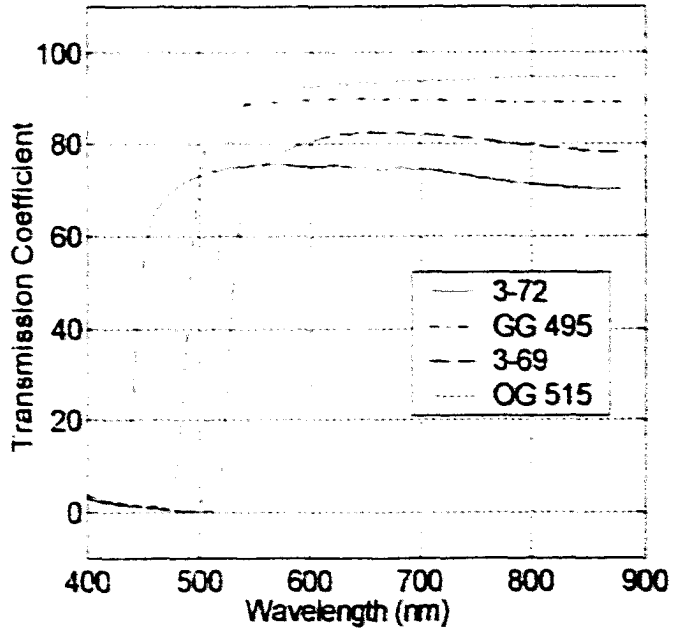

Fig. 2.3. Measured transmission spectra of the long pass filters Corning 3-72, Schott GG495, Corning 3-69, and Schott OG 515.

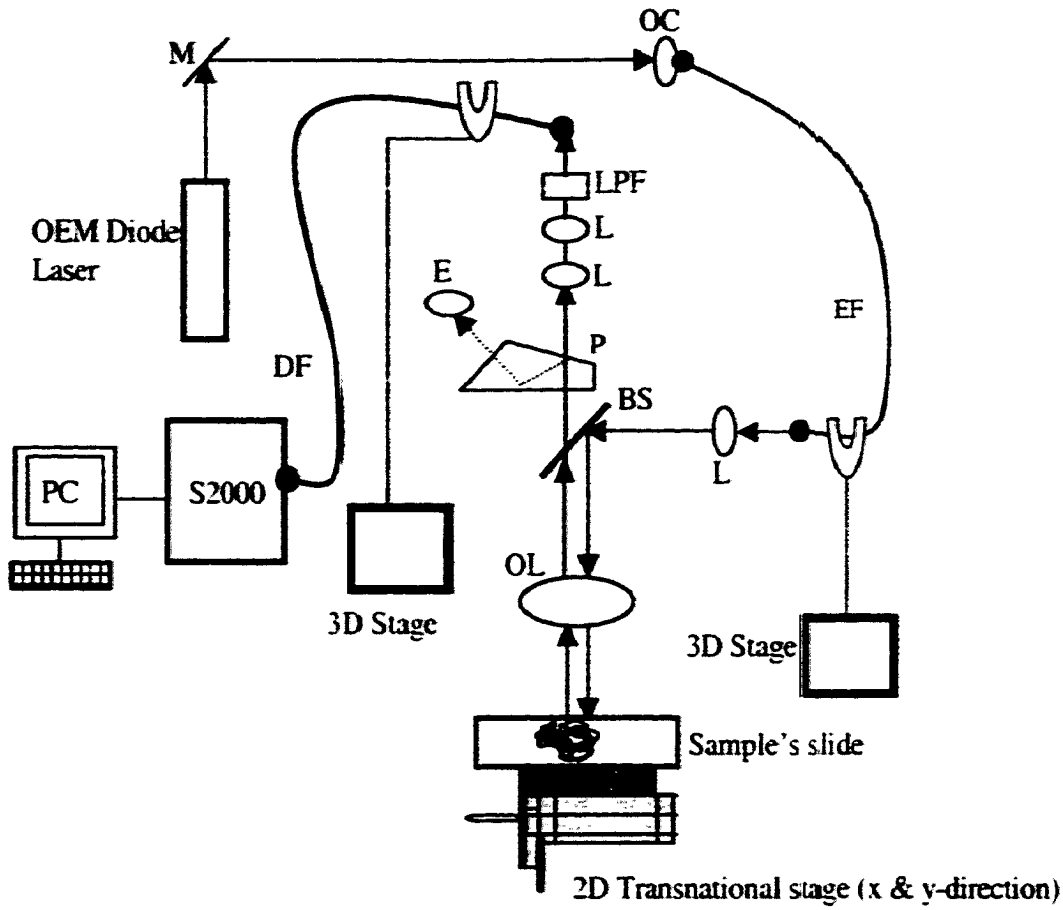

Fig. 2.4. Schematic display of the experimental setup: M, flat mirror; OC, fiber coupler; EF, Excitation fiber; DF, detection fiber; L, lens; BS, beam splitter; OL, objective lens; E, eyepiece (ocular); LPF, long pass filter.

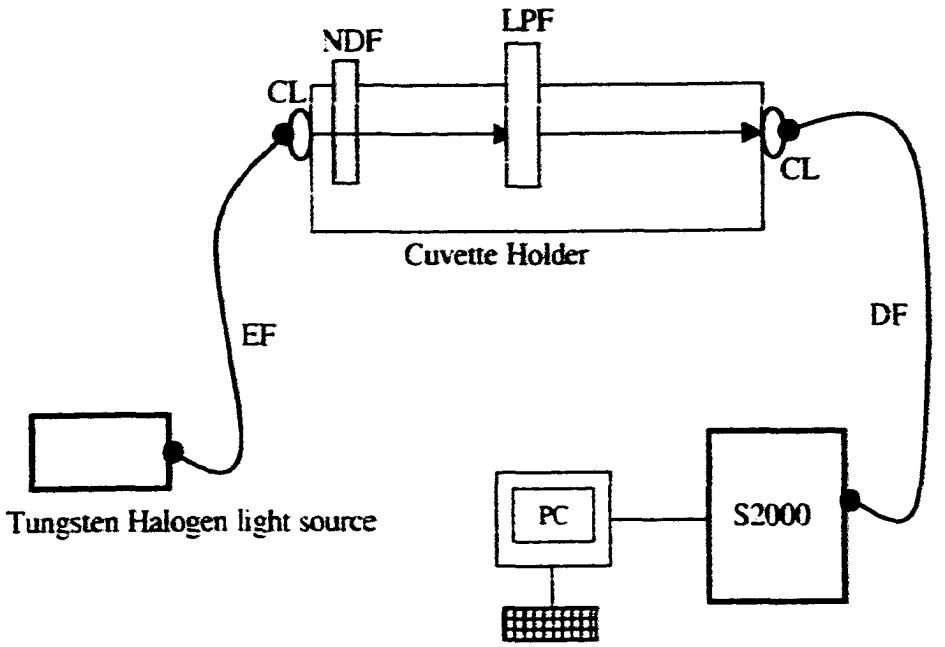

Fig. 2.5. Schematic display of the experimental setup for 0° detection: EF, Excitation fiber; DF, detection fiber S2000, Spectrometer; CL, collimating lens; NDF, natural density filter, using LPF, long pass filter.

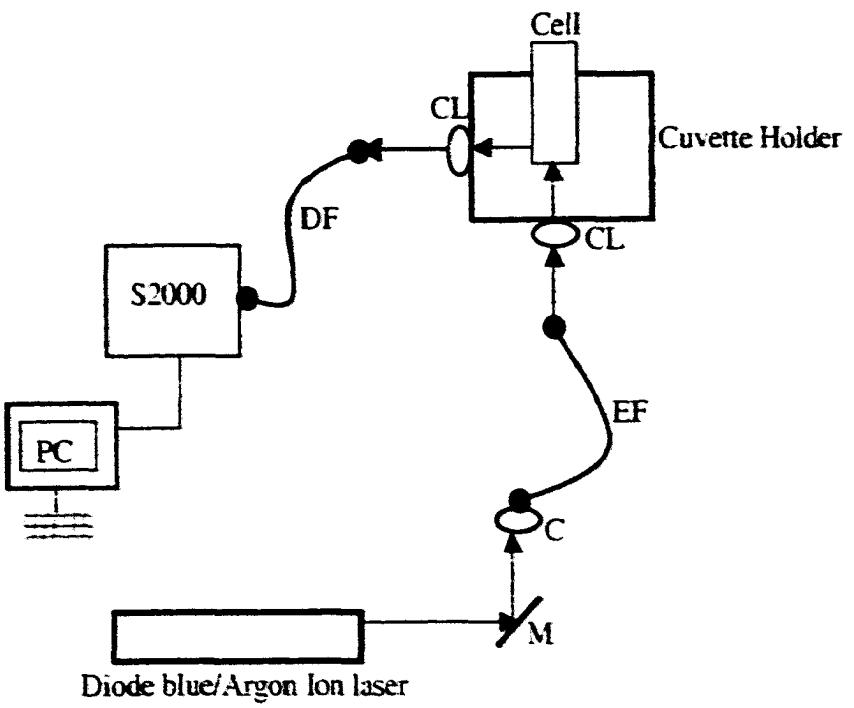

Fig. 2.6. Schematic display of the experimental setup for 90° detection: M, flat mirror; C, fiber coupler; EF, excitation fiber; DF, detection fiber; CL, collimating lens.

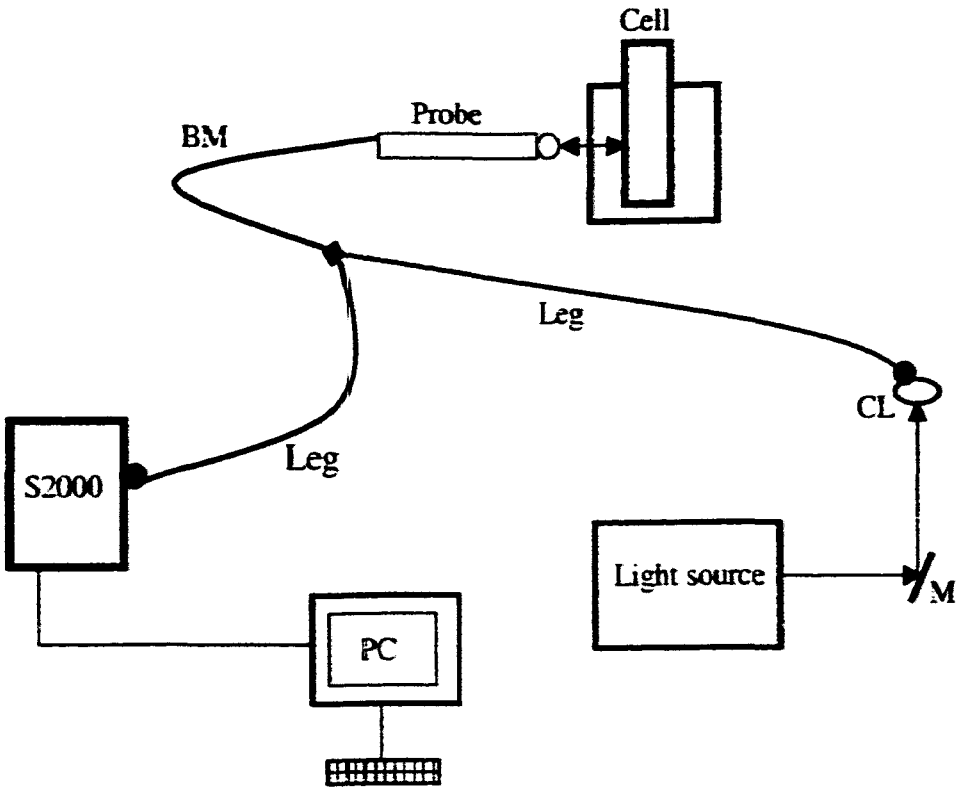

Fig. 2.7. Schematic display of the experimental setup for 180° detection: BM, bifurcated mixed optical fiber; M, flat mirror.

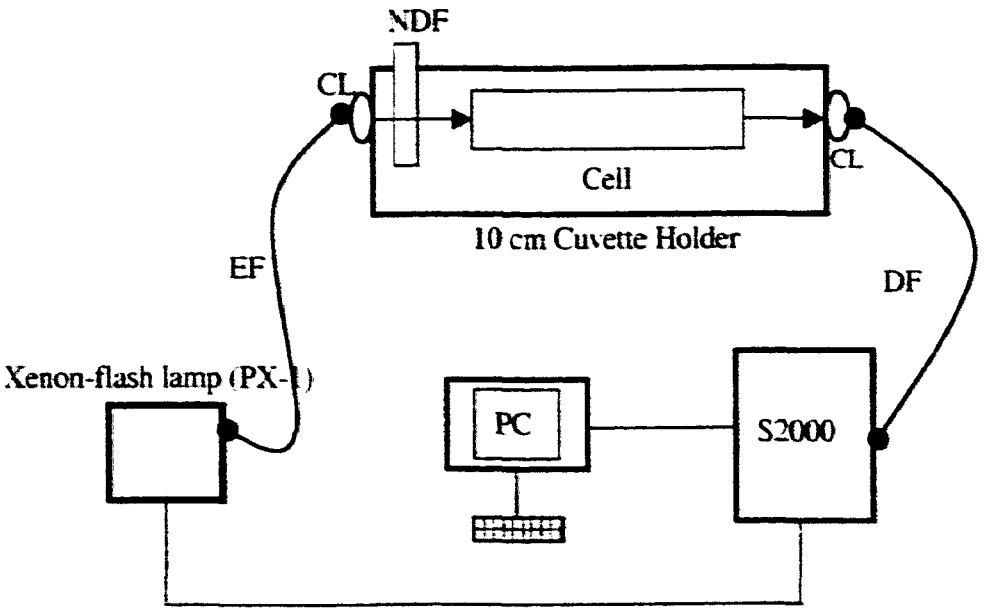

Fig. 2.8. Schematic display of the experimental setup for 0° detection: MMF, multi-mode fiber; S2000, Spectrometer; CL, collimating lens; using 10 cm cell.

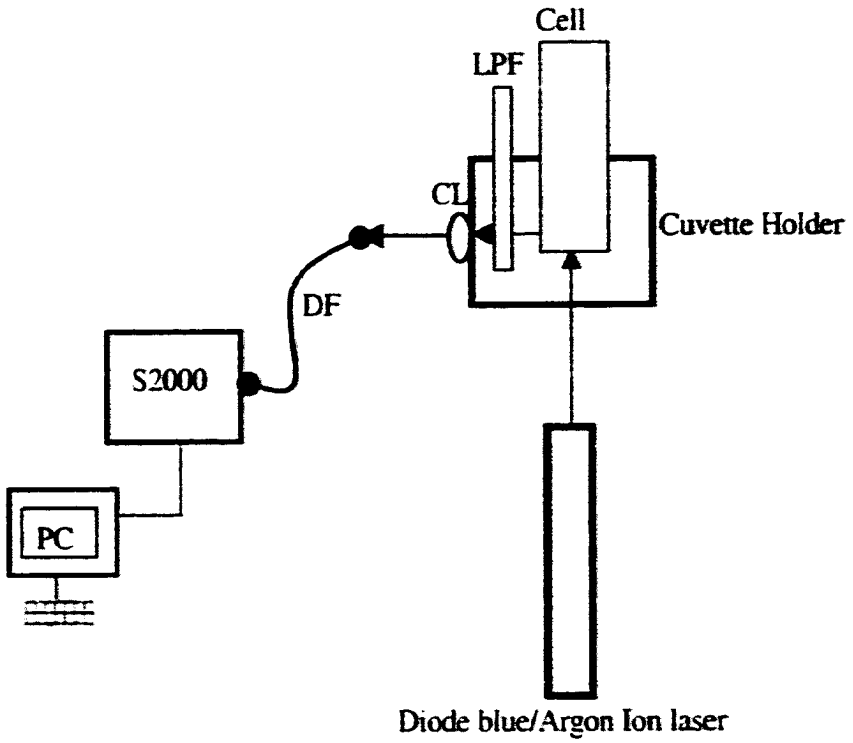

Fig. 2.9. Schematic display of the experimental setup for 90° detection: DF, detection fiber; CL, collimating lens; LPF, long pass filter.

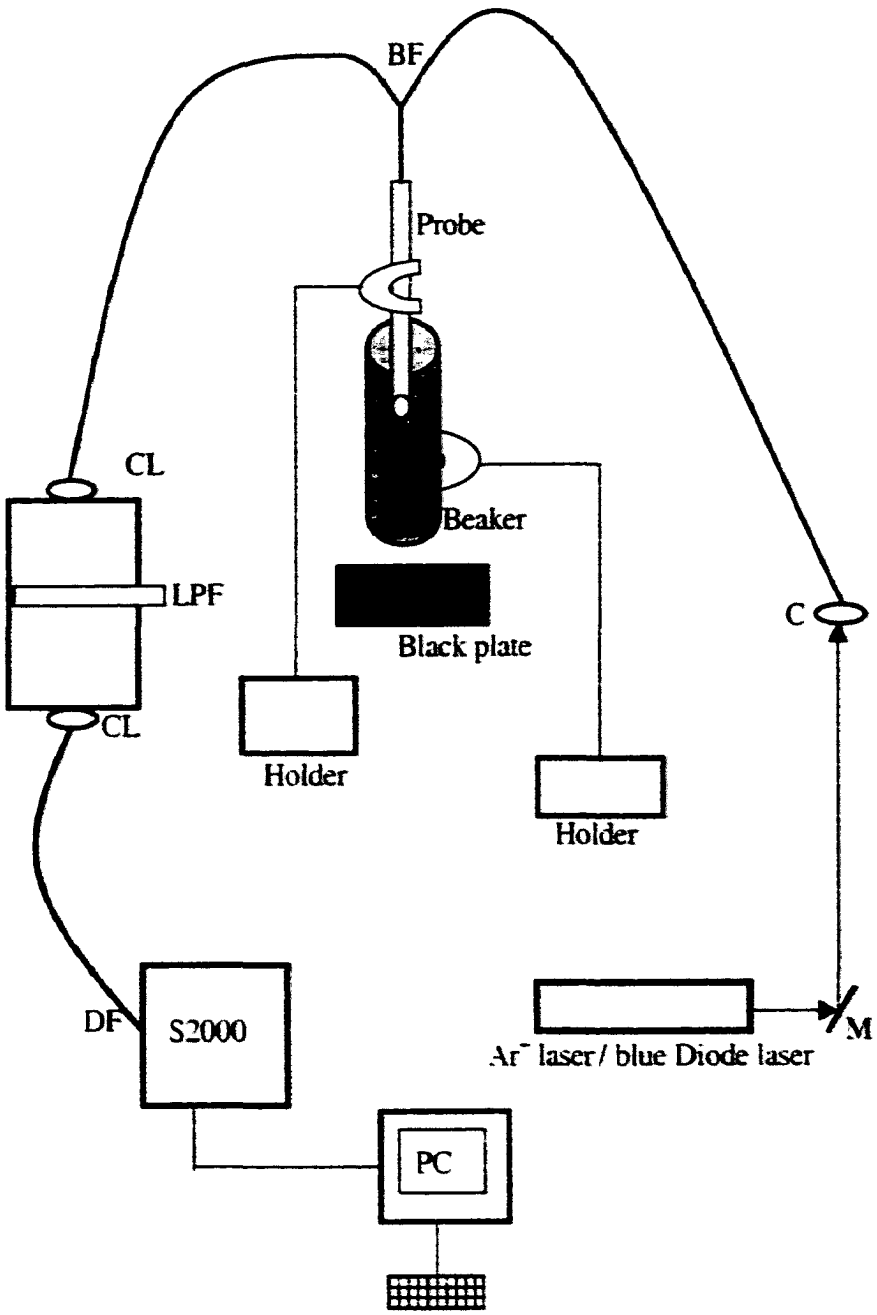

Fig. 2.10. Schematic display of the experimental setup for 180° detection: BM, bifurcated mixed optical fiber; M, flat mirror, CL, collimated lens, C, optical coupler, LPF, long pass filter, DF, detected fiber.

Chapter 3

A Study of Laser Induced- Optical Natural Fluorescence Spectroscopy of *Giardia lamblia* Cysts

3.1 Introduction

This chapter will concentrate on the autofluorescence spectra of *Giardia lamblia* cysts that were measured using the experimental setup mentioned in the previous chapter. The excitation wavelength was focused on the blue side in the visible range due to the observation that blue light excites stronger fluorescence from G. lamblia than green light and visible light experiences less absorption by water and glass than true UV.

Unless otherwise mentioned, the optical natural fluorescence (ONF) of G. lamblia refers to the data acquired from a cluster of cysts that were never exposed to laser before. The sample was always stored at refrigerator temperature and then prepared and tested at room temperature. The background emission by the medium in the sample under the same excitation condition as G. lamblia was always subtracted from the raw data from G. lamblia to produce the net ONF. This chapter and the rest of the thesis will not investigate the viability of G. lamblia.

3.2 Spectral Results and Discussion:

3.2.1 The ONF Spectra of a CLUSTER of G. lamblia Cysts Excited at 458 nm (Argon ion laser line)

The power of the laser coming out of the excitation fiber (Pf) was usually set at 10 mW. This power corresponded to an intensity of 16 W/cm^2 falling directly on the

microscope slide that carried the G. lamblia sample. A Schott GG495 long-pass filter was always used in front of the detection fiber to block laser scattering.

The raw ONF spectra of G. lamblia of the same age are first plotted (after smoothing) to check for the data's reproducibility. Once they are reproducible in shape, the raw data are first averaged before any further processing. The result is then smoothed (across a window of 8.5 nm) and normalized according to the primary fluorescence peak height. The average spectra of G. lamblia of different ages (and from different samples) are then compared to see if the age of the cysts affects the emission spectrum.

3.2.1.1 Pf = 10 mW

Figure (3.1) shows the ONF data from young G. lamblia that were 1, 4, and 5 days old respectively. The spectra overlap with each other in the major band, which peaks at 525 nm and has a full width half maximum (FWHM) of 75 nm. The negative peaks on the blue side in some of the spectra are caused by excessive subtraction of the laser scattering background.

Some additional peaks at 661 and 637 nm are believed to represent the fluorescence of pigments (such as chlorophyll) of algae impurity in the G. lamblia sample. These peaks are not an intrinsic part of G. lamblia's ONF because they are not reproducible in magnitude relative to each other and to the major band.

Figure (3.2) shows the ONF from slightly older G. lamblia that were 11, 12, 14, and 16 days old respectively. Likewise, figure (3.3) shows the ONF from G. lamblia that were 25 and 27 days old; figure (3.4), 40 and 44 days old; figure (3.5), 50 and 54 days old. Finally, figure (3.6) is from 60 and 111 days old samples.

Each figure above indicates that the ONF spectra of G. lamblia of a similar age are reproducible in shape under 458 nm excitation. Therefore, the spectra in each figure can be averaged to represent typical spectrum of G. lamblia in each age group. As a test, the average spectrum from very old cysts (60 to 111 days old) is compared with that from very young ones (1 to 5 days old) in figure (3.7). The result indicates that, although the two groups of cysts that are extremely different in age, their ONF spectra are very similar in shape. A similar conclusion may be drawn from G. lamblia of all other ages. Therefore, the age of the G. lamblia sample does not seem to have any effect on the ONF spectra shape. Consequently, the entire set of ONF spectra from G. lamblia of all age groups can be averaged, as shown in figure (3.8). The resulting spectrum has a full width half maximum (FWHM) of 83 nm and a primary peak at 519 nm.

Besides the age, the preparation condition for the sample was also varied to see its effect on the ONF of G. lamblia. Figure (3.9) shows a group of ONF spectra from G. lamblia cysts that were initially stored at refrigerator temperature until it was 45 days old, and then aged over night at room temperature. It is believed that room temperature condition can greatly quicken the aging of G. lamblia. During this aging process, the sample was kept wet. This figure shows that the ONF spectra from aged G. lamblia cysts also overlap with each other. An average of these spectra is then compared with that from a fresh sample, as shown in figure (3.10). The two spectra still overlap. This result confirms that the ONF spectral shape does not change even if the sample has aged enormously. In conclusion, the age of G. lamblia does not change its ONF spectrum.

3.2.1.2 Pf higher or lower than 10 mW

To find out whether the excitation intensity affects the spectral result of G. lamblia, the power of the laser out of the excitation fiber (Pf) was also varied. For example, figure (3.11), (3.12), and (3.13) show a group of ONF spectra from G. lamblia (1 day old) while the power out of the fiber was 20 mW, 5 mW, and 2.5 mW, respectively. Similar to the result obtained at 10 mW, each figure shows that the spectral shape is reproducible at a fixed excitation intensity. The average of the spectra at each excitation power is then taken and plotted together in figure (3.14). The result proves that the excitation intensity used in this experiment has no effect on the spectral shape of ONF of G. lamblia.

3.2.2 The ONF spectra of SINGLE G. lamblia cyst excited at 458 nm (Argon ion laser line)

The ONF spectra from single cyst are measured in the same manner as that from a cluster of cysts. Although it is easier to get higher emission intensity from a cluser of G. lamblia cysts, it is equally important to study the ONF from single G. lamblia cyst in order to estimate the detection limit of the experimental setup. The S/N ratio of a single cyst spectrum will serve this purpose. In addition, it is necessary to compare the spectral shape of single cyst with that of a cluster to ensure that the ONF spectrum shape does not depend on the number of cysts excited.

3.2.2.1 Pf = 10 mW

Figure (3.15) shows a group of ONF spectra from single young G. lamblia cyst that was 1 and 4 days old respectively. Like wise, figure (3.16) is for cyst that was 12 and 14

days old respectively; figure (3.17), 26 and 44 days old; figure (3.18), 60 and 111 days old. Each of these figures indicates that, similar to a cluster of cysts, single G. lamblia cyst at each age gives reproducible ONF in shape under 458 nm excitation.

The average spectra from single cyst that were 1 to 4 days old is compared with the average for 12 to 14 days old sample, as shown in figure (3.19). Likewise, the average for 1 to 4 days old cyst is compared with that for 60 to 111 days old, as shown in figure (3.20) These tests indicate that, like a cluster of cysts, single cyst emission is independent of age.

Consequently, the data from single G. lamblia cyst of all ages may be averaged together, as shown in figure (3.21). The resulting spectrum has a FWHM of 84 nm and a peak at 517 nm Compared to the average of ONF from a cluster of cysts, has a FWHM of 83 nm and a peak at 519 nm.

On the other hand, Figure (3.22) shows a group of ONF from single G. lamblia cyst that was stored at room temperature over night. This figure shows that the ONF of aged single cyst is also reproducible in shape. The average from aged cyst is then compared with the average from fresh cyst stored at refrigerator temperature, as shown in figure (3.23). Like that from a cluster of cysts, the spectral shape of ONF from a single G. lamblia cyst is not dependent on its age.

3.2.2.2 Pf = 2.5 mW

Figure (3.24) shows a group of ONF spectra of single G. lamblia cyst that was 58 days old. Because the spectra are reproducible in shape, they can be averaged together. This

average spectrum is then compared to the average spectrum from a cluster of G. lamblia cysts, as shown in figure (3.25).

3.2.3 The ONF spectra of a CLUSTER of G. lamblia cysts excited at 401 nm (blue diode laser)

The 401 nm emission of a blue diode laser was used to excite the ONF spectra from G. lamblia of different ages. The power out of the excitation fiber was 2.2-2.5 mW and the long pass filter used was Corning 3-72. The spectral data are processed in the same way as those obtained through 458 nm excitation.

Figure (3.26) shows a group of ONF spectra of G.lamblia cysts that were 32 and 36 days old. The spectrum has a FWHM of 79-nm approximately and a primary peak at 497 nm. The secondary peaks at 678 and 636 nm are again assigned to the pigments of algae impurity in the Giardia sample. These peaks basically agree with their counterparts at 661 and 637 nm in the data from 458 nm excitation. This figure shows that the ONF spectra of G. lamblia of the same age are reproducible in shape under 401 nm excitation. Thus these spectra can be averaged together.

Likewise, figure (3.27) shows a group of ONF spectra of G. lamblia cysts that are 27 days old. The spectra are again reproducible in shape. They can also be averaged together. Figure (3.28) then plots the average of the two sets of data together. Because the two average spectra agree in shape, all the raw data may be averaged, as shown in figure (3.29).

3.2.4 The ONF spectra of SINGLE G. lamblia cyst excited at 401 nm (blue diode laser)

Figure (3.30) shows a group of ONF spectra of single G. lamblia cyst that was 32 and 36 days old respectively. This spectrum shows that the ONF spectra of single G. lamblia of the same age are also reproducible in shape under 401 nm excitation. Thus these data can be averaged together.

Figure (3.31) shows a group of ONF spectra of single G. lamblia cyst that was 91 days old. These data are also reproducible in shape and can be averaged.

The average spectra of these two sets of data are then compared in figure (3.32). The result shows that the aging of single G. lamblia cyst does not change its ONF spectral shape under 401 nm excitation. This result is similar to the 458 nm excitation result. Because all of the single cyst data (from 401 nm excitation) overlap in shape, they can be averaged together, as shown in figure (3.33).

3.2.5 The ONF spectra of G. lamblia cysts excited at 496 nm (Argon ion laser line)

When the excitation wavelength was 496 nm, the power out of the excitation fiber was varied between 10 and 2.5 mW. The long pass filetr used was Schott OG 515.

The spectral data are processed in the same way as those obtained through 458 nm excitation.

In figure (3.34), a group of ONF spectra of G. lamblia under 496 nm excitation are plotted. The approximate age of the sample was 2 days. The power out of the fiber was also set at 10 mW. This spectrum shows that the ONF of G. lamblia is reproducible in shape under 496 nm excitation. Thus, all the data in figure (3.34) can be averaged. The

result is shown in figure (3.35). The average spectrum has a full width half maximum (FWHM) of 88 nm approximately and a primary peak at 646 nm. The secondary peaks appear at approximate 666 and 631 nm are also attributed to pigments of algae impurity in the G. lamblia cysts sample.

Under a lower excitation power of 2.5 mW, a group of ONF spectra of G. lamblia was measured and the data plotted in figure (3.36). The approximate age of the sample was 5 days. These data are again reproducible in shape. Thus they can be avearged and compared with the data obtained at higher excitation power. Figure (3.37) plots these averages together. The result shows that the excitation power does not affect the shape of ONF spectra under 496 nm excitation.

3.3 Miscellaneous results of the observed ONF spectra of G. lamblia cysts

Figure (3.38) compares the ONF spectra of G.lamblia cysts when the excitation wavelength is changed from 458 to 401 nm. The individual data have been divided by the transmission spectrum of the long pass filters respectively. Likewise, figure (3.39) compares the ONF spectra of G.lamblia cysts when the excitation wavelength is changed from 458 to 496 nm. Figure (3.40) shows all of three excitation (401, 458, and 496nm) wavelengths together. This figure proves that the ONF spectral peak of G.lamblia cysts shift to longer wavelength by increasing the excitation wavelength.

Some typical ONF data from a cluster of G. lamblia cysts, as well as their associated background spectra, are shown in figure (3.41) for two excitation wavelengths at 458nm and 496nm. This figure gives an example of the magnitude of G. lamblia fluorescence intensity compared to the sample background.

Figure (3.42) shows a group of background spectra of the G. lamblia sample at 458 nm excitation, when the power out of the excitation fiber was set at 10 mW. Figure (3.43) shows the ONF spectra of the background of G.lamblia cysts under 401 nm excitation with the power out of the excitation fiber at 2.2-2.5 mW.

The excitation power was changed to check the linearity of the fluorescence data. As shown in figure (3.44), the integrated fluorescence intensity of G. lamblia cysts is linear with respect to the laser power, which confirms that the excitation intensity used is low enough.

A pair of cross polarizers were used as an alternative method to reject laser scattering, which was assumed to be more polarized than the spontaneous emission of fluorescence. When one polarizer polarizes the laser output from the excitation fiber, another one was aligned at 90 degree in front of the collection fiber so that the laser scattering reaching the detector was minimized. The transmission spectrum of these linear polarizers was measured and shown in figure (3.45).

The ONF spectrum of G. lamblia obtained through the above method is then compared with that from the standard method (long pass filter), as shown in figure (3.46). This figure shows that, under 458 nm excitation, there is a reduction of the ONF intensity on the blue side of the spectrum by the long pass filter GG495. The distortion is noticeable, but insignificant for the shape of the spectrum.

3.4 Conclusion

This chapter reports the ONF spectra of G. lamblia excited and detected using the setups described in the previous chapter. The laser excitations used are of blue wavelength (458, and 401 nm). At 458 nm excitation, the peak of the ONF for G. lamblia cysts is located at 525 nm; at 401 nm excitation, the peak of the ONF is located at 496 nm approximately.

3.5 Figures

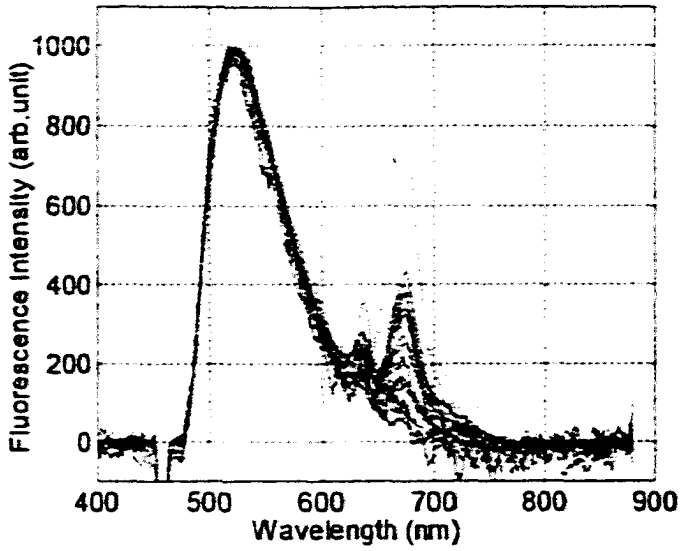

Fig. 3.1. Comparison of ONF spectra for G. lamblia of samples 1, 4, and 5 days old. Excitation wavelength is 458 nm and the power out of the excitation fiber is 10 mW.

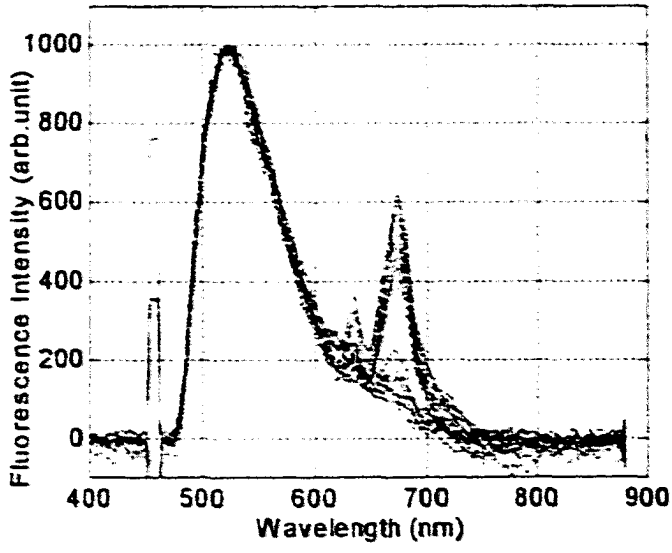

Fig. 3.2. Comparison of ONF spectra for G. lamblia of samples 11, 12, 14, and 16 days old. Excitation wavelength is 458 nm and the power out of the excitation fiber is 10 mW.

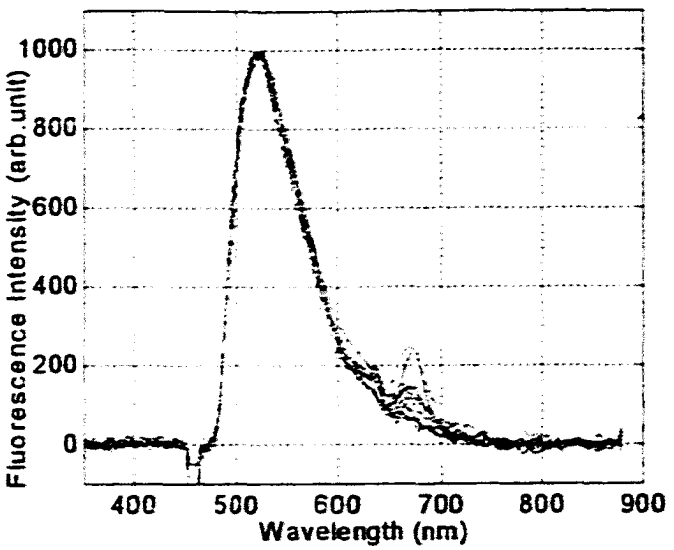

Fig. 3.3. Comparison of ONF spectra for G. lamblia of samples 25 and 27 days old. Excitation wavelength is 458 nm and the power out of the excitation fiber is 10 mW.

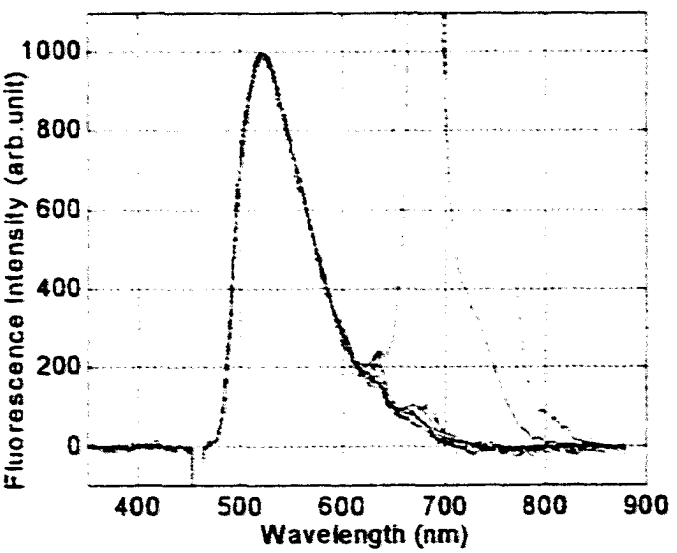

Fig. 3.4. Comparison of ONF spectra for G. lamblia of samples 40 and 44 days old. Excitation wavelength is 458 nm and the power out of the excitation fiber is 10 mW.

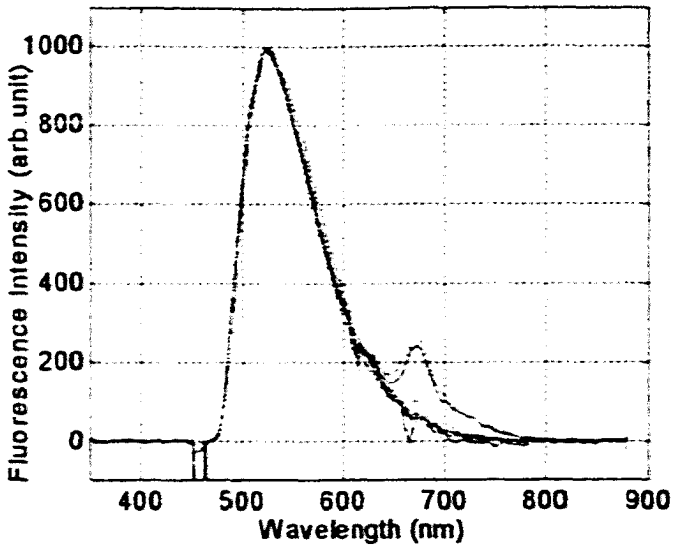

Fig. 3.5. Comparison of ONF spectra for G. lamblia of samples 50 and 54 days old. Excitation wavelength is 458 nm and the power out of the excitation fiber is 10 mW.

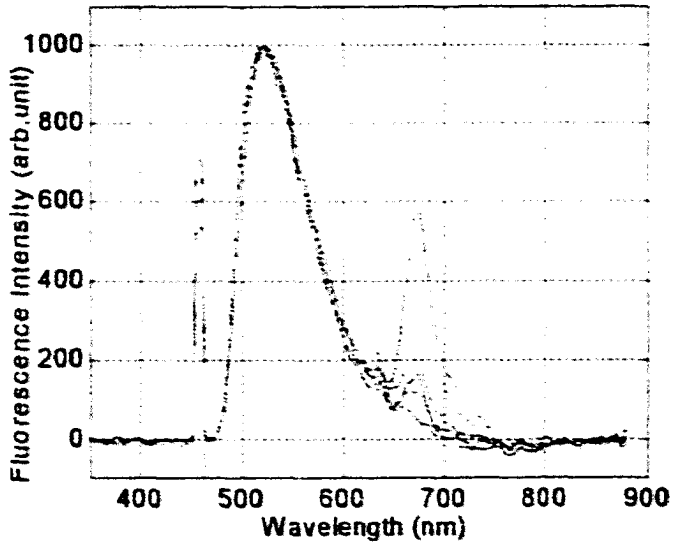

Fig. 3.6. Comparison of ONF spectra for G. lamblia of samples 60 and 111 days old. Excitation wavelength is 458 nm and the power out of the excitation fiber is 10 mW.

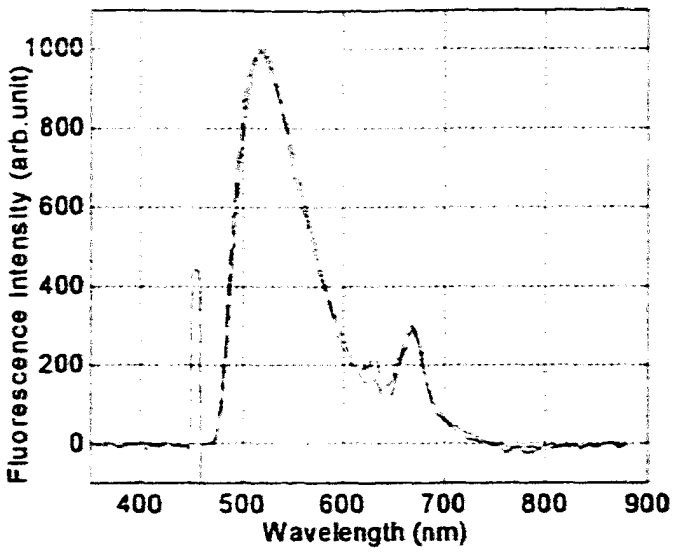

Fig. 3.7. Comparison of the averaged ONF spectra of G. lamblia for very young ones (1 to 5 days old) with very old ones (60 to 111 days old). Excitation wavelength is 458 nm and the power out of the excitation fiber is 10 mW.

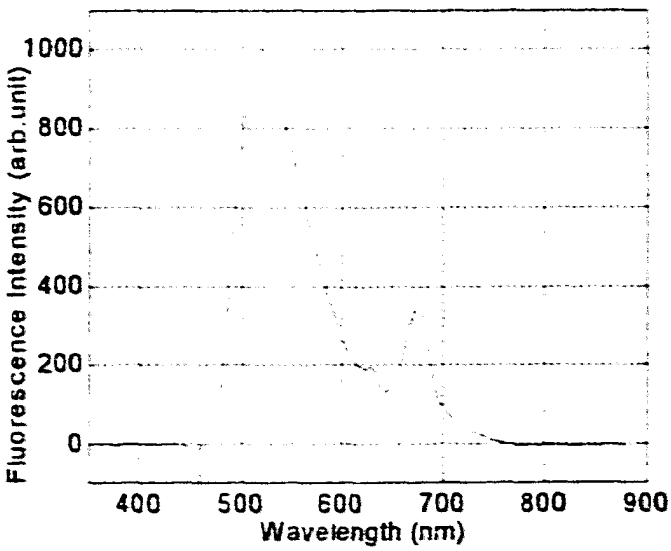

Fig. 3.8. An averaged ONF spectrum of G. lamblia for samples 1 to 111 days old. Excitation wavelength is 458 nm and the power out of the excitation fiber is 10 mW.

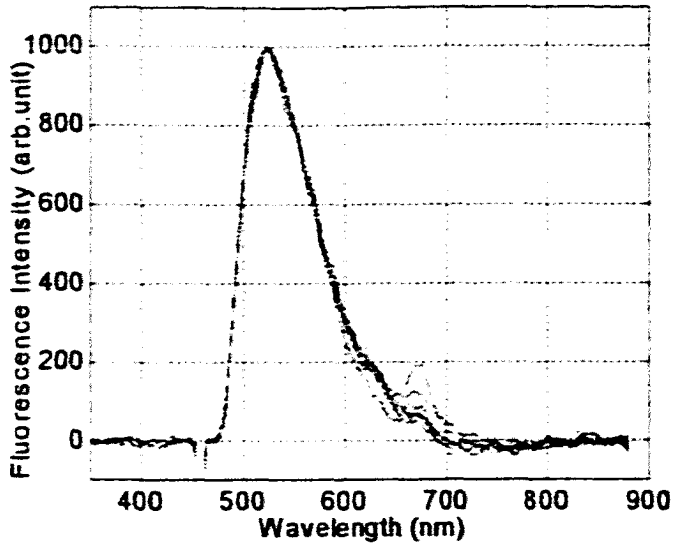

Fig. 3.9. Comparison of the ONF spectra of G. lamblia for samples stored at refrigerator temperature until it was 45 days old and then aged over night at room temperature. Excitation wavelength is 458 nm and the power out of the excitation fiber is 10 mW.

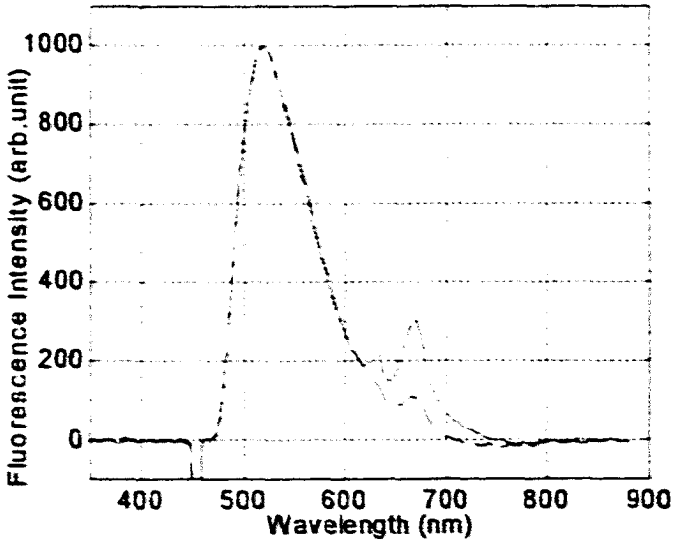

Fig. 3.10. Comparison of the averaged ONF spectra of G. lamblia for a fresh sample and a sample aged over night at room temperature. Excitation wavelength is 458 nm and the power out of the excitation fiber is 10 mW.

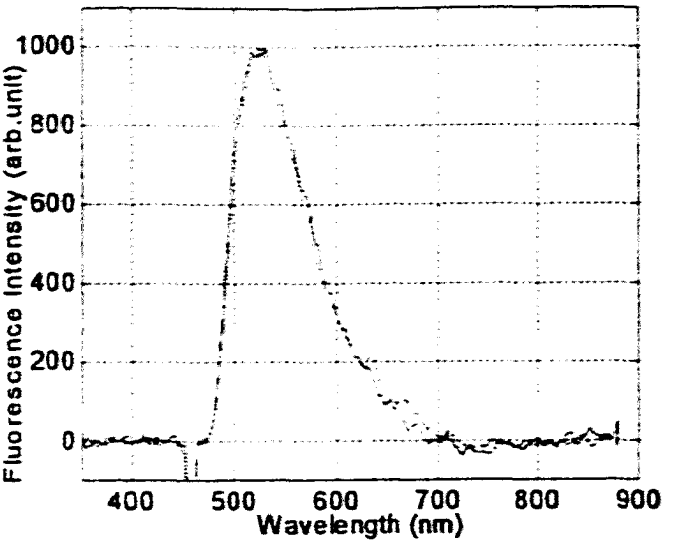

Figure 3.11. Comparison of the ONF spectra of G. lamblia of a sample 1 day old. Excitation wavelength is 458 nm and the power out of the excitation fiber is 20 mW.

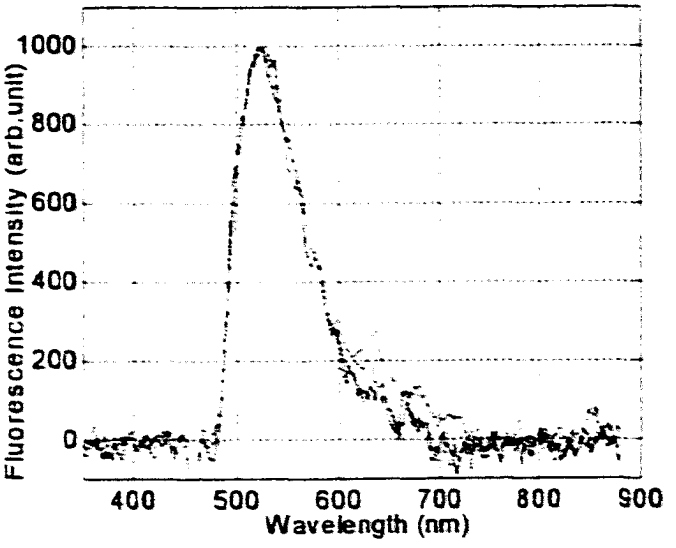

Fig. 3.12. Comparison of the ONF spectra of G. lamblia of a sample 1 day old. Excitation wavelength is 458 nm and the power out of the excitation fiber is 5 mW.

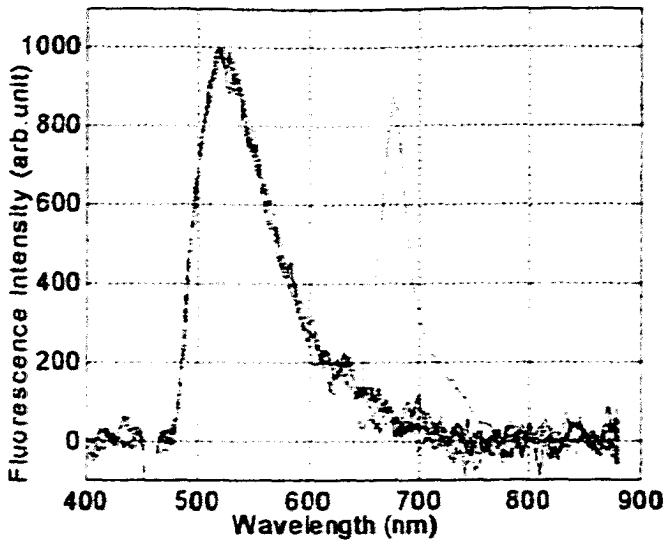

Fig. 3.13. Comparison of the ONF spectra of G. lamblia of sample 1 day old. Excitation wavelength is 458 nm and the power out of the excitation fiber is 2.5 mW.

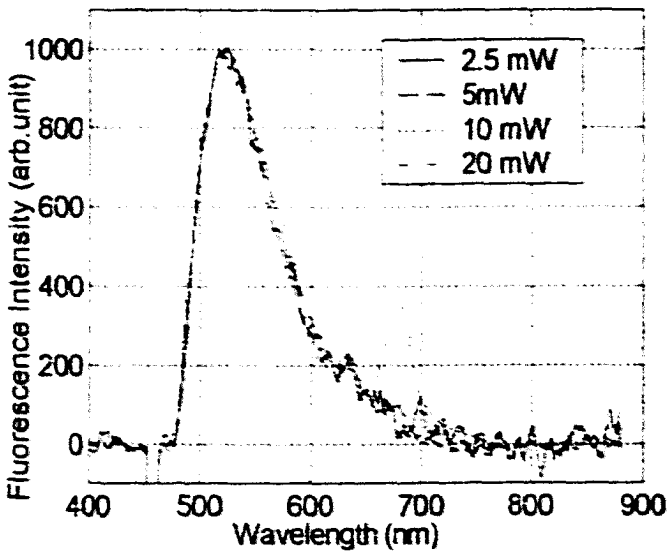

Fig. 3.14. Comparison of the averaged ONF spectra of G. lamblia. When the power out of the excitation fiber is 2.5 mW (solid), 5 mW (dash dot), 10 mW (dot), and 20 mW (dash) excited at 458 nm.

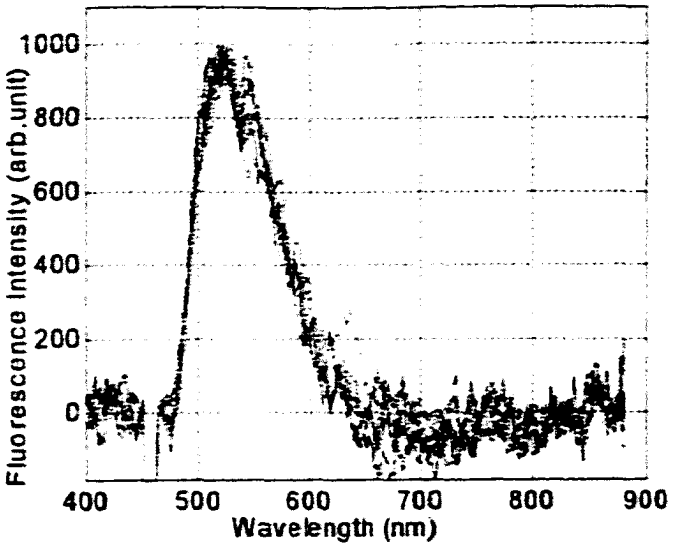

Fig. 3.15. Comparison of ONF spectra for single G. lamblia of samples 1 and 4 days old. Excitation wavelength is 458 nm and the power out of the excitation fiber is 10 mW.

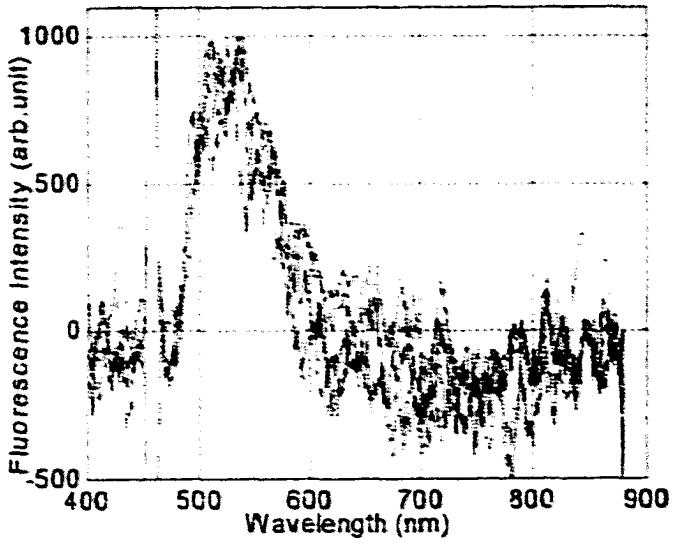

Fig. 3.16. Comparison of ONF spectra for single G. lamblia of samples 12 and 14 days old. Excitation wavelength is 458 nm and the power out of the excitation fiber is 10 mW.

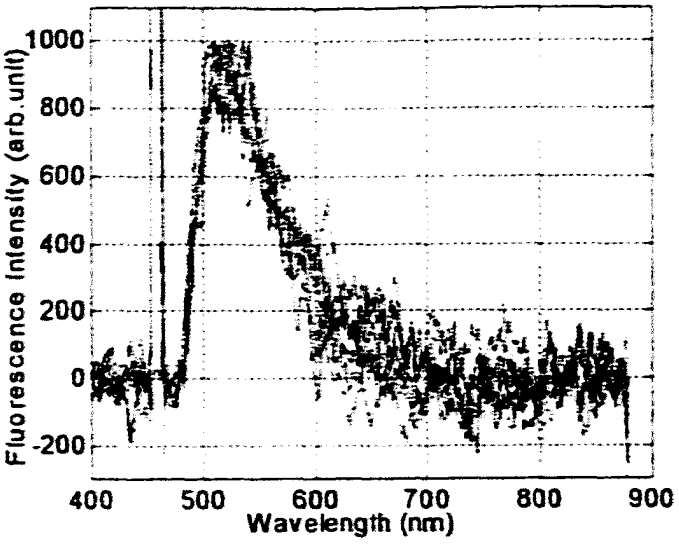

Fig. 3.17. Comparison of ONF spectra for single G. lamblia of samples 26 and 44 days old. Excitation wavelength is 458 nm and the power out of the excitation fiber is 10 mW.

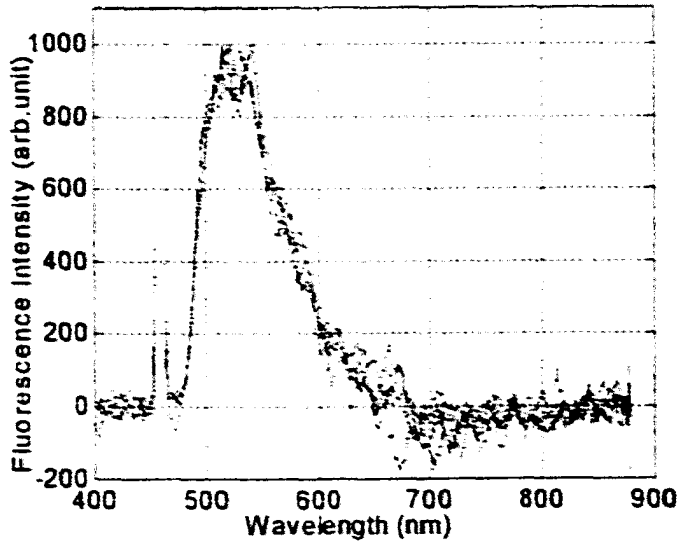

Fig. 3.18. Comparison of ONF spectra for single G. lamblia of samples 60 and 111 days old. Excitation wavelength is 458 nm and the power out of the excitation fiber is 10 mW.

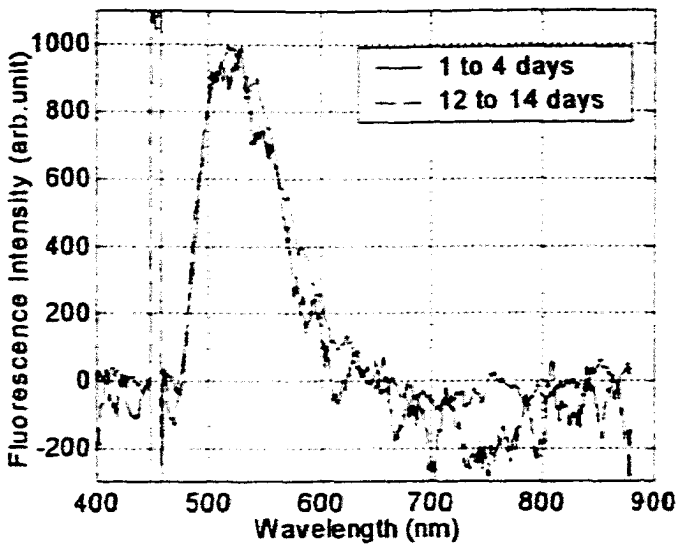

Fig. 3.19. Comparison of the averaged ONF spectra of single G. lamblia for sample 1 to 4 days old (solid) with other ones 12 to 14 days old (dash dot). Excitation wavelength is 458 nm and the power out of the excitation fiber is 10 mW.

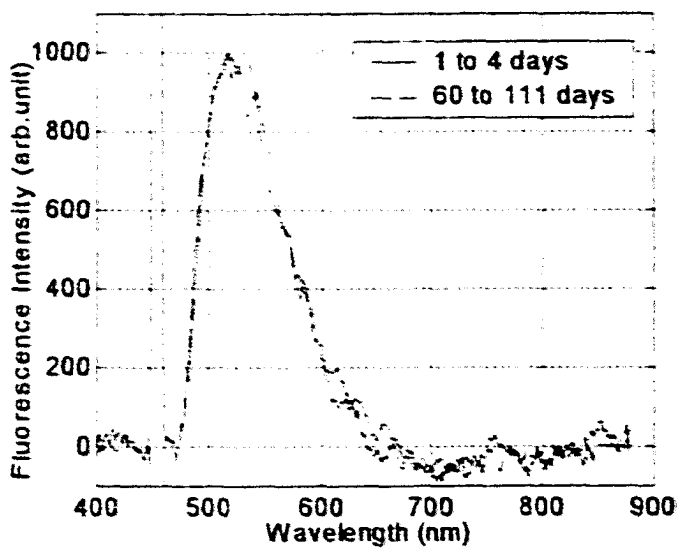

Fig. 3.20. Comparison of the averaged ONF spectra of single G. lamblia for samples 1 to 4 days old (solid) with other ones 60 to 111 days old (dash dot). Excitation wavelength is 458 nm and the power out of the excitation fiber is 10 mW.

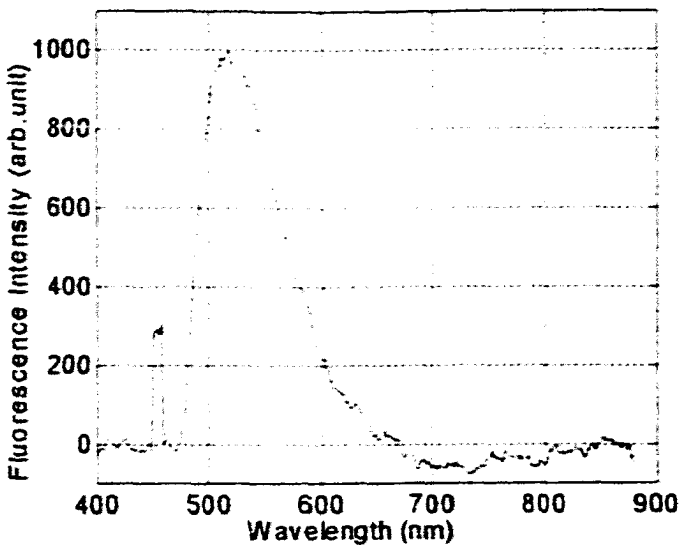

Fig. 3.21. An averaged ONF spectrum of single G. lamblia for samples 1 to 111 days old. Excitation wavelength is 458 nm and the power out of the excitation fiber is 10 mW.

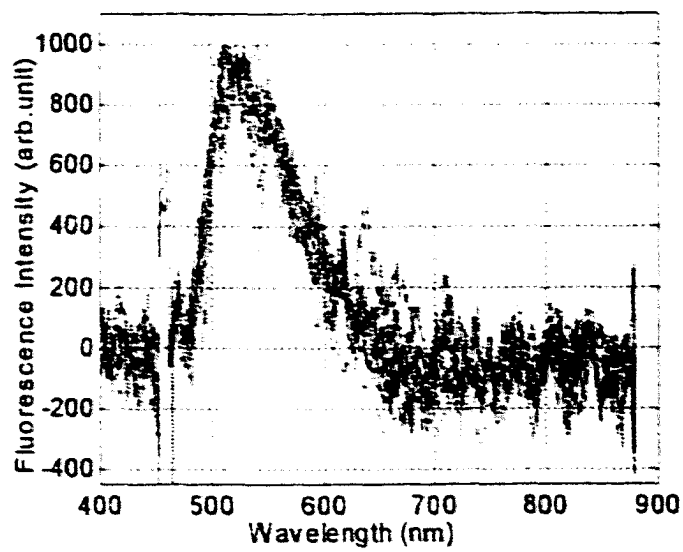

Fig. 3.22. Comparison of the ONF spectra of single G. lamblia for a sample aged over night at room temperature. Excitation wavelength is 458 nm and the power out of the excitation fiber is 10 mW.

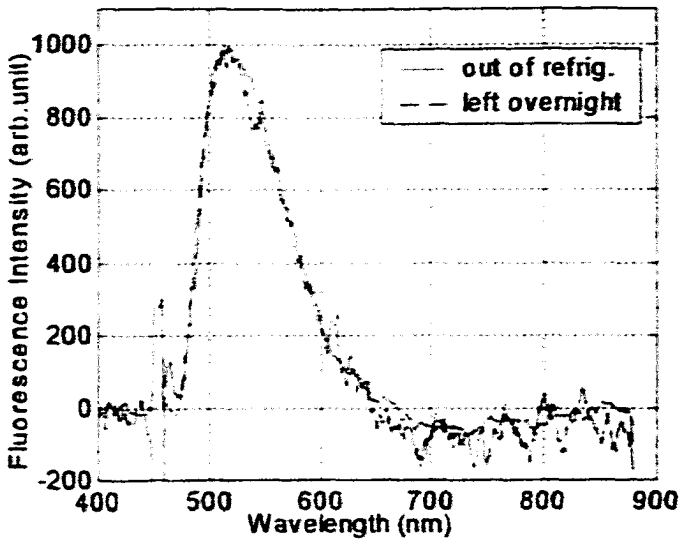

Fig. 3.23. Comparison of the averaged ONF spectra of single G. lamblia for a fresh sample (solid) and a sample aged over night at room temperature (dash dot). Excitation wavelength is 458 nm and the power out of the excitation fiber is 10 mW.

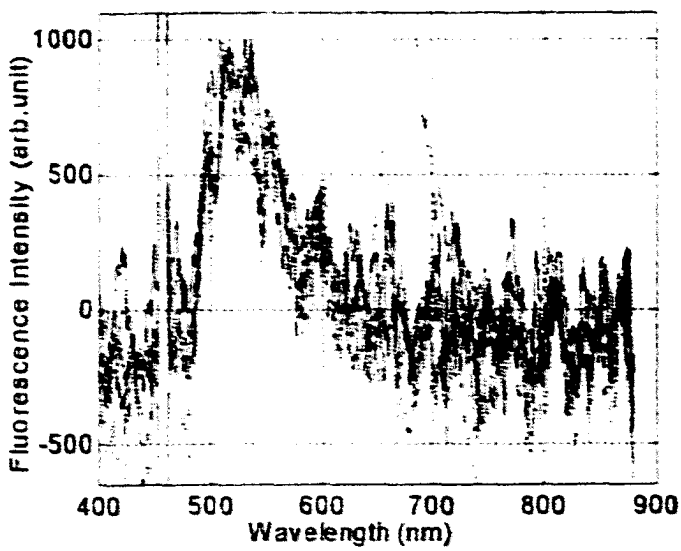

Fig. 3.24. Comparison of the ONF spectra of single G. lamblia. Excitation wavelength is 458 nm and the power out of the excitation fiber is 2.5 mW.

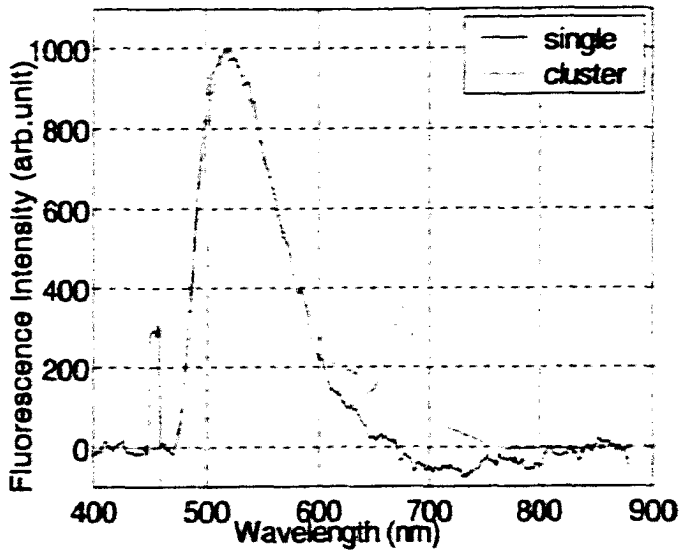

Fig. 3.25. Comparison of averaged ONF spectra of cluster G. lamblia (dash dot) and single G. lamblia (solid). Excitation wavelength is 458 nm and the power out of the excitation fiber is 10 mW.

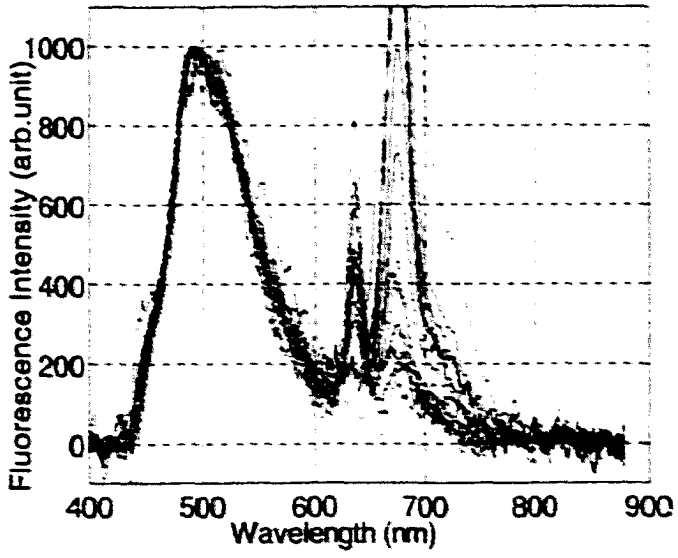

Fig. 3.26. Comparison of ONF spectra for G. lamblia of samples 32 to 36 days old. Excitation wavelength is 401 nm and the power out of the excitation fiber is 2.2- 2.5 mW.

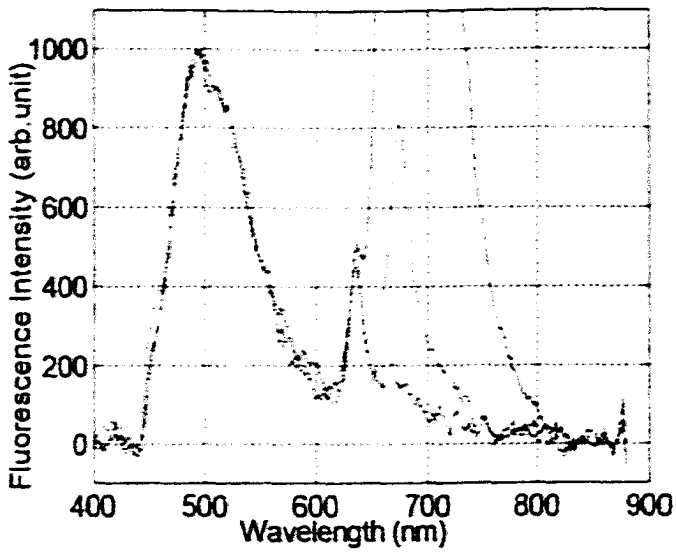

Fig. 3.27. Comparison of ONF spectra for G. lamblia of samples 27 days old. Excitation wavelength is 401 nm and the power out of the excitation fiber is 2.2-2.5 mW.

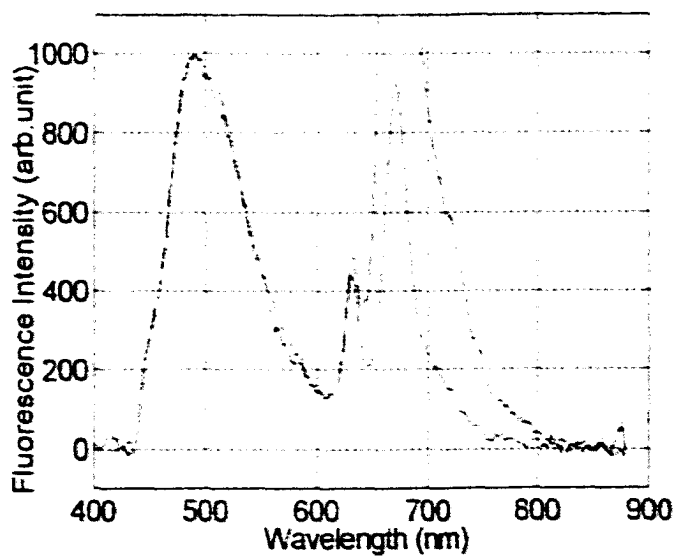

Fig. 3.28. Comparison of the averaged ONF spectra for G. lamblia of samples 32 and 36 days old (solid) and 27 days old (dash dot). Excitation wavelength is 401 nm and the power out of the excitation fiber is 2.2-2.5 mW.

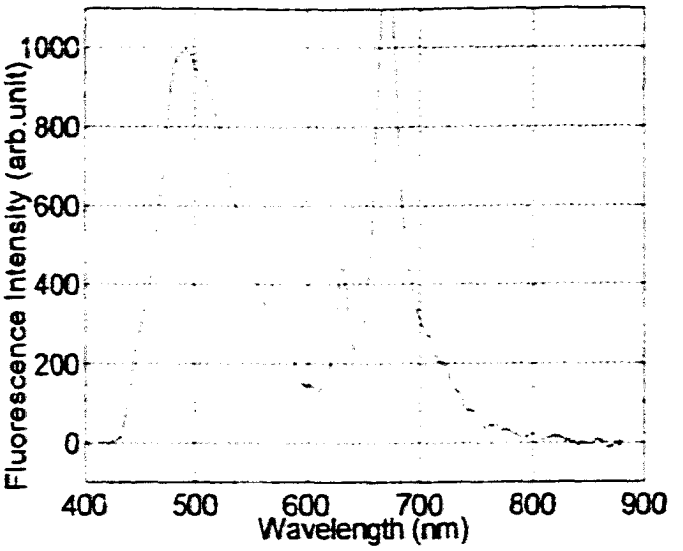

Fig. 3.29. Averaged ONF spectra for G. lamblia of samples 32 to 36 days old and 27 days old. Excitation wavelength is 401 nm and the power out of the excitation fiber is 2.2-2.5 mW.

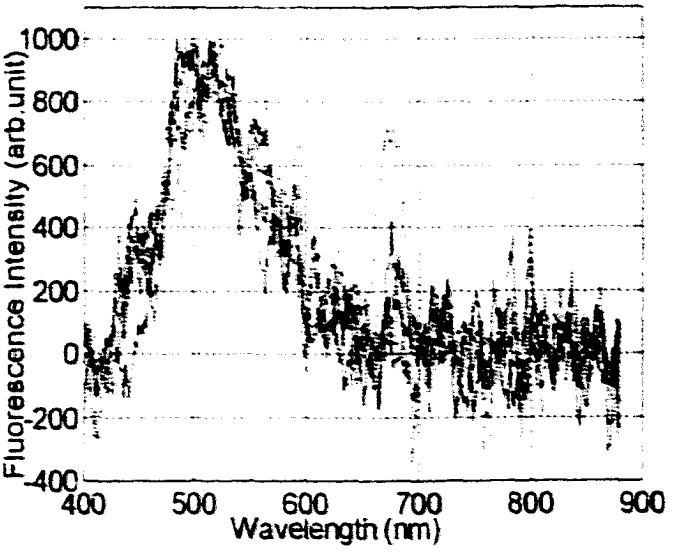

Fig. 3.30. Comparison of ONF spectra for single G. lamblia of samples 32 to 36 days old. Excitation wavelength is 401 nm and the power out of the excitation fiber is 2.2-2.5 mW.

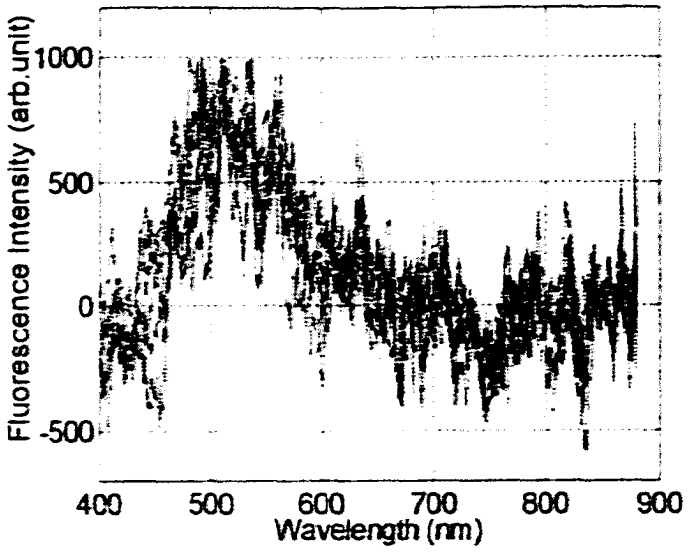

Fig. 3.31. Comparison of ONF spectra for single G. lamblia of samples 90 days old. Excitation wavelength is 401 nm and the power out of the excitation fiber is 2.2-2.5 mW.

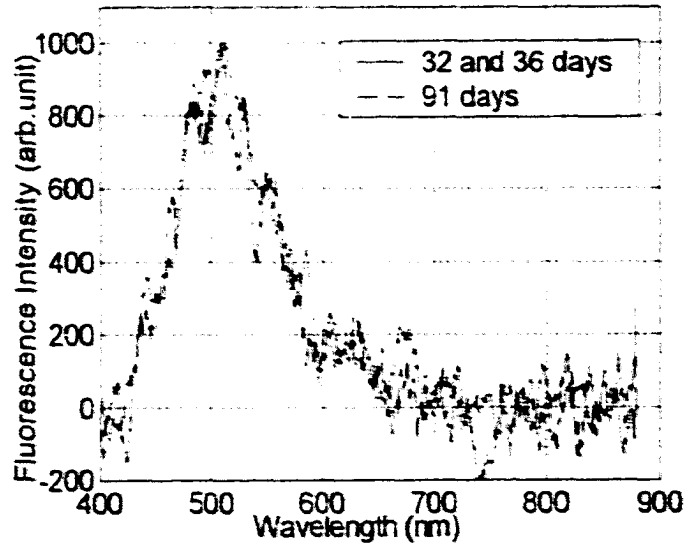

Fig. 3.32. Comparison of the averaged ONF spectra of single G. lamblia for sample 32 and 36 days old (solid) with other ones 91 days old (dash dot). Excitation wavelength is 401 nm and the power out of the excitation fiber is 2.2-2.5 mW.

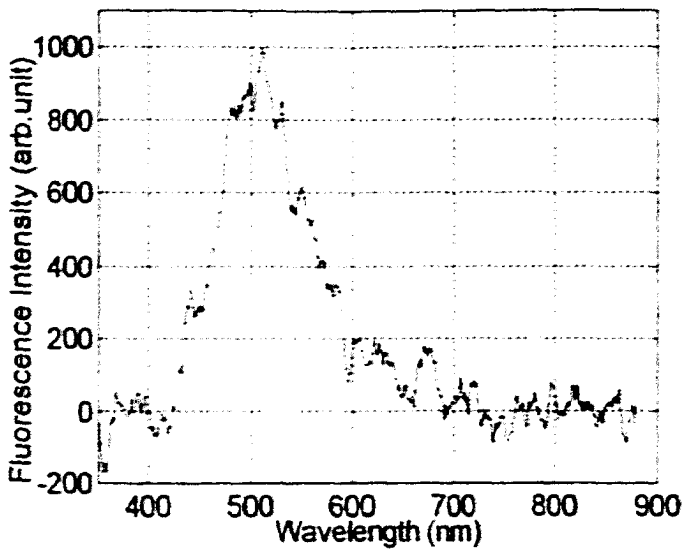

Fig. 3.33. An averaged ONF spectra of single G. lamblia for sample 32 and 36 days old with other ones 91 days old. Excitation wavelength is 401 nm and the power out of the excitation fiber is 2.2-2.5 mW.

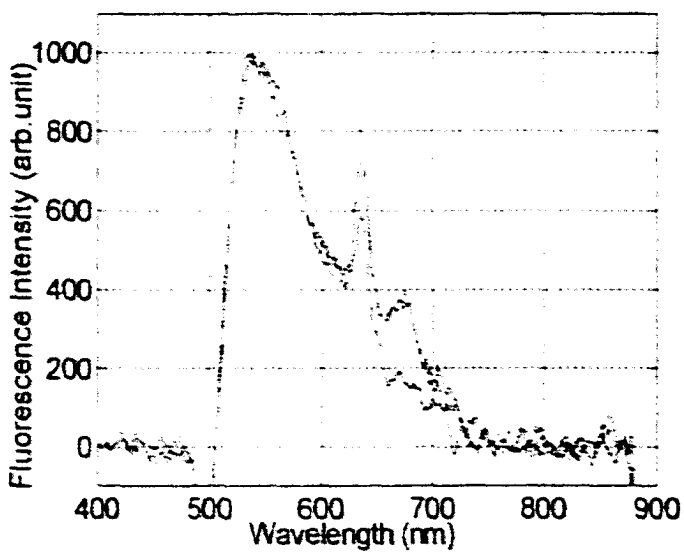

Fig. 3.34. Comparison of ONF spectra for G. lamblia of samples 2 days old. Excitation wavelength is 496 nm and the power out of the excitation fiber is 10 mW.

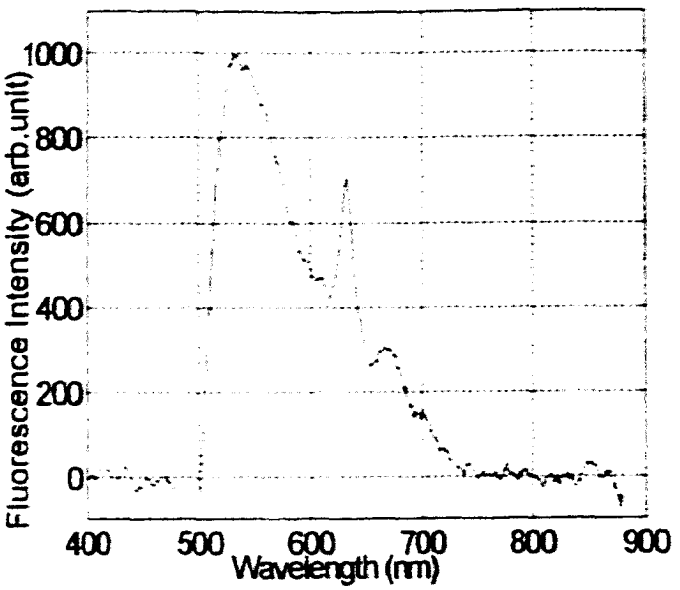

Fig. 3.35. An averaged ONF spectra for G. lamblia of samples 2 days old. Excitation wavelength is 496 nm and the power out of the excitation fiber is 10 mW.

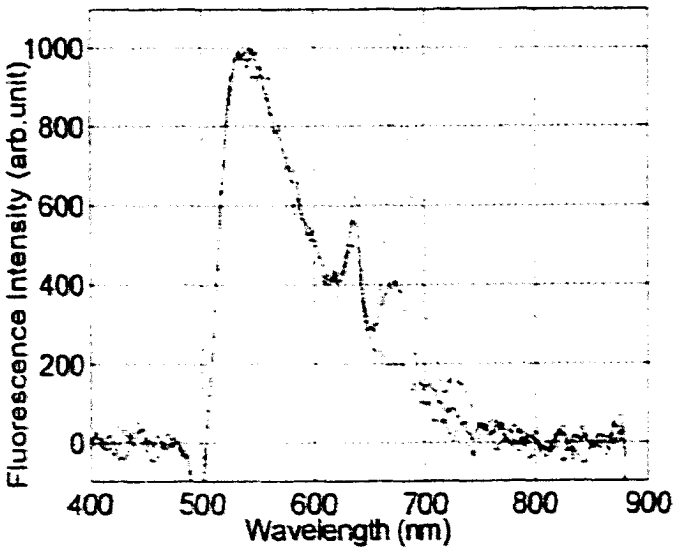

Fig. 3.36. Comparison of ONF spectra for G. lamblia of samples 5 days old. Excitation wavelength is 496 nm and the power out of the excitation fiber is 2.5 mW.

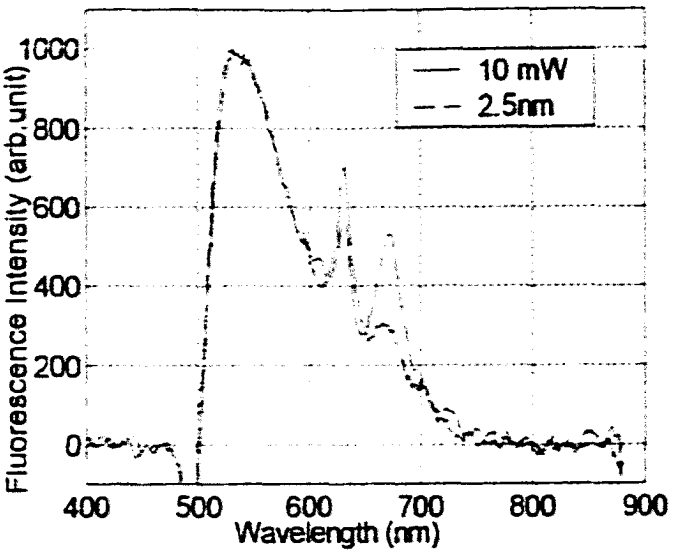

Fig. 3.37. Comparison of the averaged ONF spectra of G. lamblia. When the power out of the excitation fiber is 10 mW (solid) and 2.5 mW (dash) excited at 496 nm.

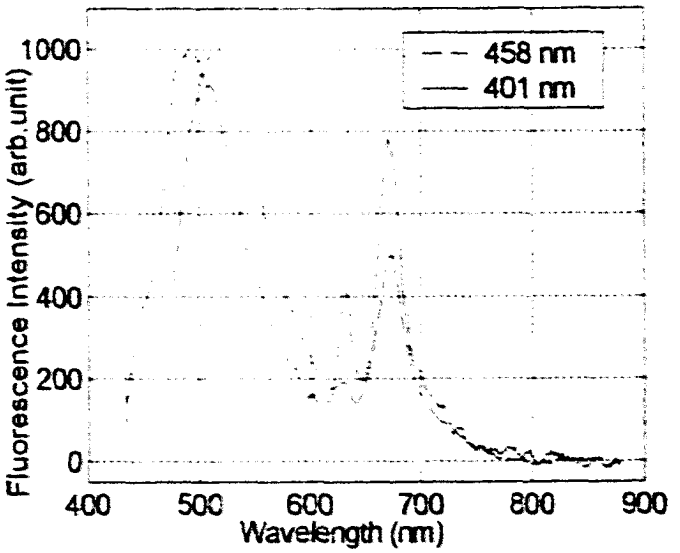

Fig. 3.38. Comparison of the ONF spectra of G. lamblia when the excitation wavelength changes from 458 nm (dash) to 401 nm (solid). The individual data have been divided by the transmission spectrum of the long pass filters respectively.

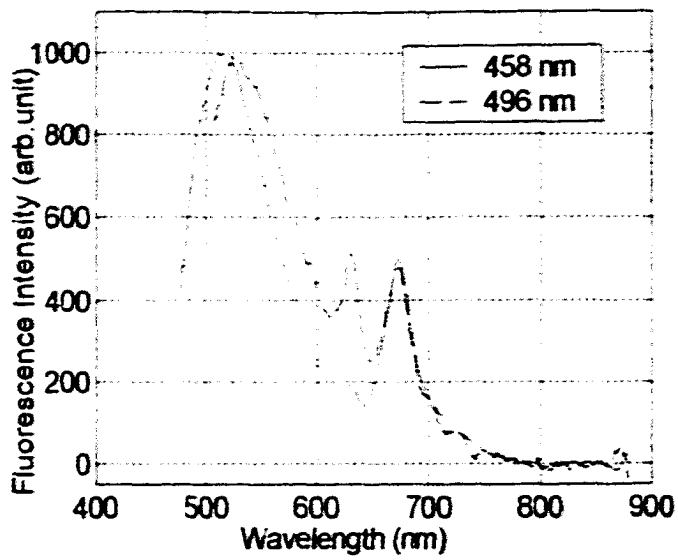

Fig. 3.39. Comparison of the ONF spectra of G. lamblia when the excitation wavelength changes from 458 nm (solid) to 496 nm (dash). The individual data have been divided by the transmission spectrum of the long pass filters respectively.

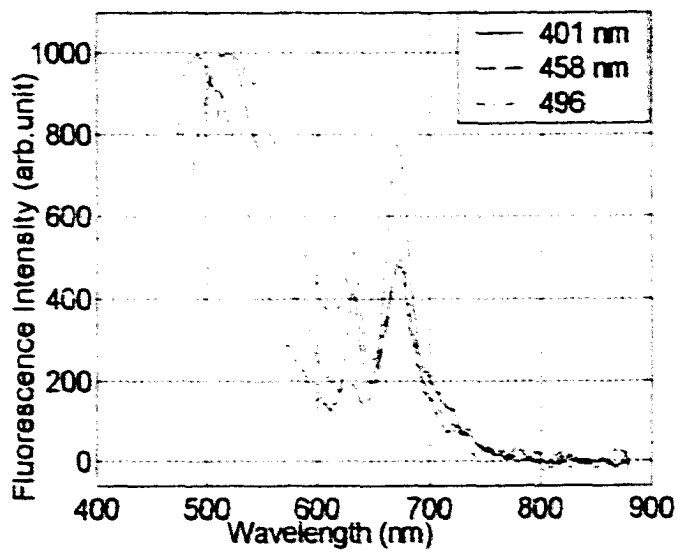

Fig. 3.40. Comparison of the ONF spectra of G. lamblia when the excitation wavelength 401 nm (solid), 458 nm (dash), and 496 nm (dash dot). The individual data have been divided by the transmission spectrum of the long pass filters respectively.

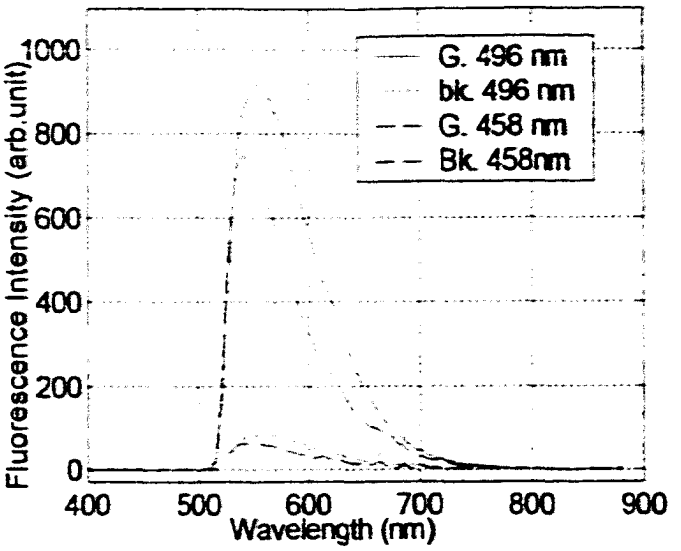

Fig. 3.41. Comparison of the ONF spectra of G. lamblia as well as their associated background spectra for two excitation wavelengths: 458 nm and 496 nm.

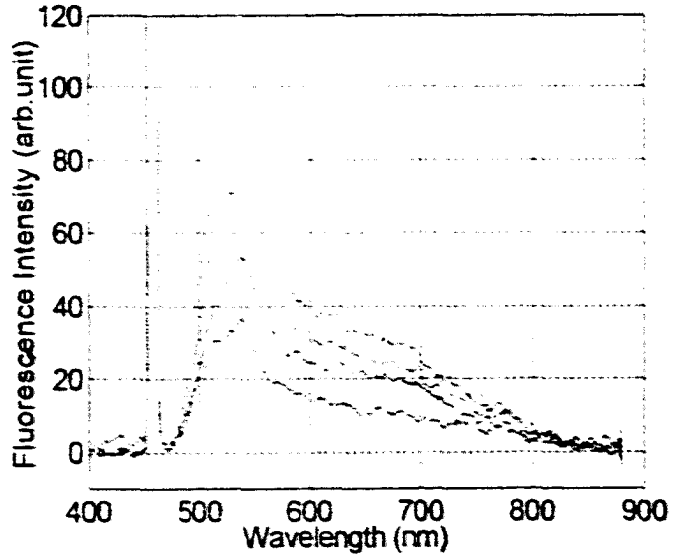

Fig. 3.42. A group of background spectra of G. lamblia sample at 458 nm excitation with power out of the excitation fiber is 10 mW.

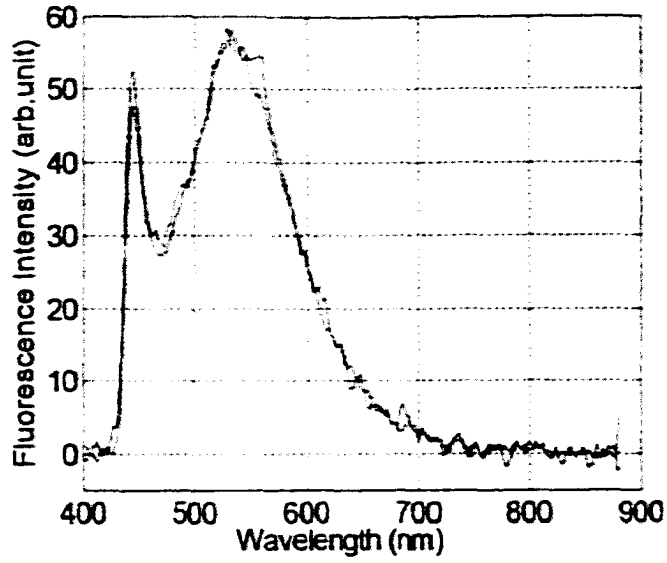

Fig. 3.43. Two background spectra of G. lamblia sample at 401 nm excitation with power out of the excitation fiber is 2.2-2.5 mW.

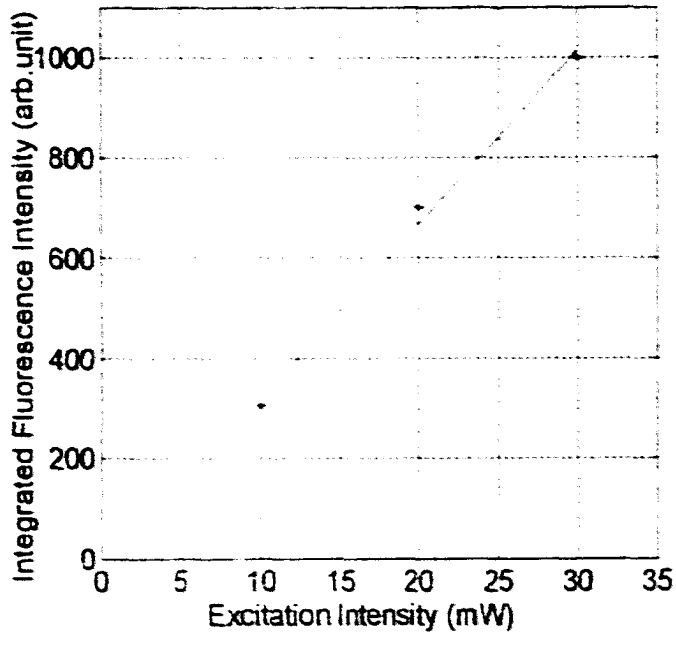

Fig. 3.44. Integrated ONF intensity of G. lamblia with respect to the laser power.

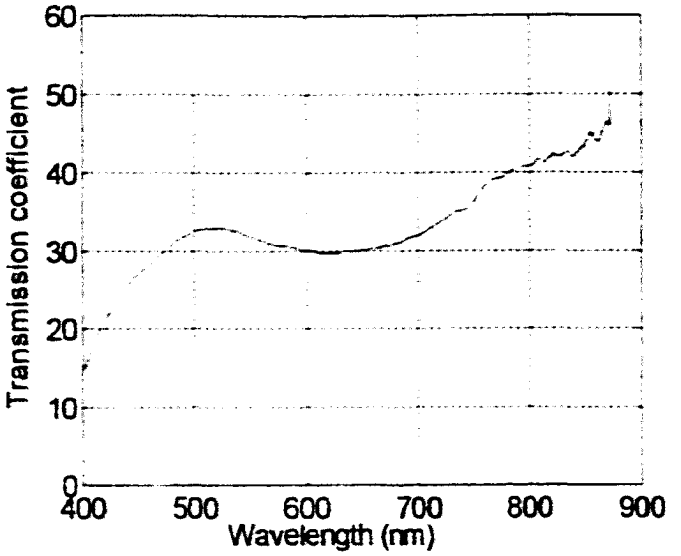

Fig. 3.45. Measured transmission spectrum of the linear polarizer.

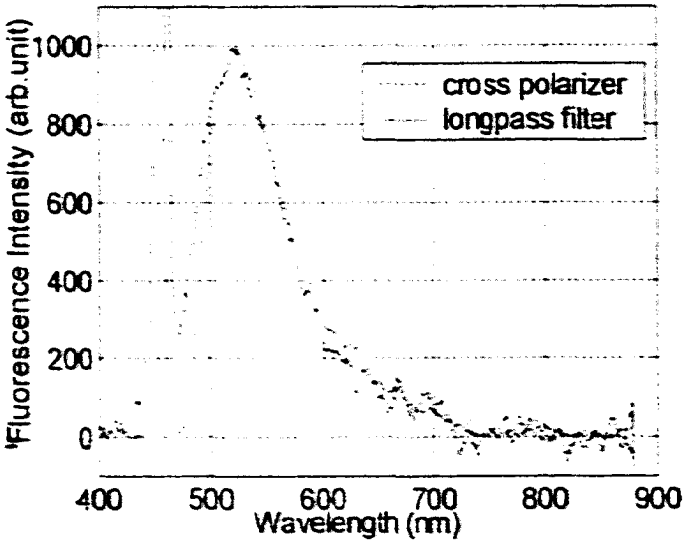

Fig. 3.46. Comparison of the ONF spectra of G. lamblia sample using cross polarizers method and the long pass filter method.

Chapter 4

Laser Induced Optical Natural Fluorescence Spectroscopy of *Giardia lamblia* Cysts Compared to Other Microorganisms

4.1 Introduction

ONF spectroscopy will be demonstrated to be an effective method for distinguishing *Giardia lamblia* from other waterborne microorganisms such as Paramecium (single cellular) and Rotifer (multi-cellular), as well as *Giardia muris* (another species of Giardia). The goal of the study is to find the characteristic ONF spectra for G. lamblia cysts in comparison to other microorganisms that exist in water. This thesis will not directly study the difference in the internal organization between G. lamblia cyst and the other microorganisms. Rather, through the ONF spectra of each microorganism at various excitation wavelengths, the differences between these microorganisms are reflected.

While the excitation wavelengths of 458 nm and 401 nm have been used to excite the fluorescence from these microorganisms, it is found that only 401 nm excitation is able to distinguish the ONF spectra of G. lamblia from the other microorganisms.

4.2 Spectral Results and Discussion:

4.2.1 Introduction to Paramecium

Paramecium is a small unicellular organism that is found commonly in natural water sources, such as lakes, ponds, and streams. It is 180-300 μm long, cylindrical-shaped

with a compact micronucleus and a rounded anterior [1]. Paramecium comes from commercial source as culture in spring water. They should not be stored at refrigerator temperature or exposed to direct sunlight. They should be kept at room temperature with sufficient oxygen above the water surface.

To prepare a sample, it is necessary to mount the Paramecium sample on a plane microscope slide that has no concavity in order to facilitate the drying of water from the sample. As water gradually dries, Paramecium slows down its motion. In the end, it completely stops. This is a good and critical moment to do ONF spectroscopy, for on one hand, Paramecium is fixed; on the other hand, immediately after it stops, Paramecium begins to lyse. As the body of Paramecium breaks down to many pieces, the ONF spectrum collected loses meaning.

4.2.2 ONF spectra of Paramecium at 458 nm excitation (Argon ion laser line)

The power of the laser coming out of the excitation fiber (Pf) was usually set at 10 mW. This power corresponded to an intensity of 16 W/cm^2 falling directly on the sample slide, if a 20X microscope objective is used. Sometimes, a smaller power of magnification such as 10X was used instead to excite a larger part of Paramecium's body. The intensity in that case was 4 W/cm^2. A Schott GG495 long-pass filter was always used in front of the detection fiber to block laser scattering.

The raw ONF spectra of Paramecium from the same sample, measured within a similar period of time, were first plotted (after smoothing) to check for the data's reproducibility. Once they are reproducible in shape, the raw data are first averaged before any further processing. The result is then smoothed (across a window of 8.5 nm) and normalized

according to the primary fluorescence peak height. The average spectra of Paramecium from different samples are then compared to see if they overlap.

4.2.2.1 Pf=10mW

Figure (4.1) shows the ONF data that was measured on several days from the same sample (#1) of Paramecium. The spectra overlap with each other in the major band, which peaks at 523 nm and has a full width half maximum (FWHM) of 73 nm. The negative peaks on the blue side of some of the spectra are caused by excessive subtraction of the laser scattering background.

Figure (4.2) shows the ONF data from Paramecium that was taken on several days from a different sample (#2) of Paramecium that was either newly acquired or recultured from old sample. Likewise, figure (4.3) (4.4), and (4.5) show the data from samples #3, 4, and 5 respectively.

Each figure above indicates that the ONF spectra of Paramecium from the same sample are reproducible in shape under 458 nm excitation. Therefore, the spectra in each figure can be averaged to represent typical spectrum of Paramecium of one sample. As a test, the average spectrums from sample #1 to #5 are compared in figure (4.6). The result indicates that the ONF spectra from different samples are also similar in shape. Consequently, the entire set of ONF spectra of Paramecium from samples #1-5 under 458 nm excitation can be averaged, as shown in figure (4.7). The resulting spectrum has a full width half maximum (FWHM) of 77 nm and a primary peak at 515 nm.

4.2.2.2 Pf = 2.5mW

To find out whether the excitation intensity affects the spectral result of Paramecium, the power of the laser out of the excitation fiber (Pf) was reduced. Figure (4.8) shows the ONF spectra from Paramecium when the power out of the excitation fiber was 2.5 mW. Because the spectra are reproducible in shape, they can be averaged together. This average spectrum is then compared to the average spectrum when the power out of the excitation fiber was 10 mW, as shown in figure (4.9). The result proves that the excitation intensity used in this experiment has no effect on the spectral shape of ONF of Paramecium.

4.2.2.3 Pf = 10mW using objective lens of power 10 X

Figure (4.10) shows the ONF data from Paramecium that was measured using 10X microscope objective (MO) lens. The figure indicates that the ONF spectra of Paramecium obtained through low power MO are also reproducible in shape. These spectra can then be averaged and compared to the average spectrum obtained through the 20 X objective lens. Figure (4.11) shows that the power of the MO does not make a difference in the ONF spectral shape. Therefore, although the 20X MO covers a relative small part of Paramecium's body, the resulting ONF is representative of the whole organism's emission under laser excitation.

4.2.3 ONF spectra of Paramecium at 401-nm excitation (blue diode laser)

The 401 nm emission of a blue diode laser was used to excite the ONF spectra from Paramecium. The power out of the excitation fiber was 2.2-2.5 mW and the long pass

filter used was Corning 3-72. The spectral data are processed in the same way as those obtained through 458 nm excitation.

Figure (4.12) shows the ONF data of Paramecium from the same sample (#4). The spectra overlap with each other in the major band, which peaks at 538 nm and has a full width half maximum (FWHM) of 95 nm. Likewise, Figure (4.13) shows the ONF data of Paramecium from a different sample (#5).

Each figure above indicates that the ONF spectra of Paramecium from the same sample are reproducible in shape under 401 nm excitation. Therefore, the spectra in each figure can be averaged to represent typical spectrum of Paramecium of one sample. The average spectrum from sample #4 and 5 are compared in figure (4.14). The result indicates that the ONF spectra from different samples are also similar in shape. Consequently, the entire set of ONF spectra of Paramecium from sample #4 and 5 under 401 nm excitation can be averaged, as shown in figure (4.15). The resulting spectrum has a full width half maximum (FWHM) of 97 nm and a primary peak at 533 nm.

4.2.4 ONF spectra of Paramecium at 496 nm excitation (Argon ion laser line)

When the excitation wavelength was 496 nm, the power out of the excitation fiber was 10 mW. The long pass filter used was Corning 3-69. The spectral data are processed in the same way as those obtained through 458 nm excitation.

Figure (4.16) shows the ONF data of Paramecium from sample #1, measured with 20 X objective lens. The spectra overlap with each other in the major band, which peaks at 546 nm and has a full width half maximum (FWHM) of 84 nm. Likewise, Figure (4.17) shows the ONF data of Paramecium from sample #3, measured with 10 X objective lens,

which covers a larger percentage of the Paramecium body. Each figure above indicates that the ONF spectra of Paramecium from the same sample are reproducible in shape under 496 nm excitation, when they are measured with a fixed objective lens power. Thus, the spectra in each figure can be averaged to represent typical spectrum of Paramecium from one sample. Furthermore, the average spectrum from sample #1 (20X) and #3 (10X) are compared with each other in figure (4.18). The result indicates that the ONF spectra are slightly different in shape when different percentage of the Paramecium body are excited; however, such a difference is not conclusive due to the small amount of data.

4.2.5 Comparing the ONF spectra of G. lamblia cysts (cluster) with Paramecium

Figure (4.19) compares the ONF spectra of G. lamblia with that of Paramecium when the excitation wavelength is 401 nm. When using 401 nm excitation, G. lamblia can be distinguished from Paramecium in the ONF spectra.

Figure (4.20) compares the ONF spectra of G. lamblia with the ONF of Paramecium when the excitation wavelength is 458 nm. When using 458 nm excitation, G. lamblia can not be distinguished from Paramecium because their ONF spectra are almost identical.

Figure (4.21) compares the ONF spectra of G. lamblia with the ONF of Paramecium when the excitation wavelength is 496 nm. When using 496 nm excitation, G. lamblia can not be distinguished from Paramecium because their ONF spectra are almost identical.

Figure (4.22) compares the ONF spectra of Paramecium when the excitation

wavelength is changed from 458 to 401 nm. The individual data have been divided by the transmission spectrum of the long pass filters respectively. The figure shows an interesting reverse shift of the ONF spectral band as the laser wavelength is shifted. Paramecium exhibits a 15 nm red shift when the laser is blue shifted by 57 nm from 458 to 401 nm, in contrast to the normal shift shown in G. lamblia.

Figure (4.23) compares the ONF spectra of Paramecium when the excitation wavelength is changed from 458 to 496 nm. This shows a weak shift or almost no shift compared to G. lamblia, which has a little shift.

4.2.6 Miscellaneous results of the observed ONF spectra of Paramecium

The background of the Paramecium sample can vary in the spectral intensity within the sample. Figure (4.24) shows a batch of background spectra of Paramecium in springwater at 458 nm excitation with the power out of the excitation fiber at 10 mW. This shows that the background intensity is better to be at a maximum range of 160 counts. Figure (4.25) shows a batch of background spectra of Paramecium sample at 401 nm excitation with power out of the excitation fiber at 2.2-2.5 mW. The intensity of the background and scattering are increased at 401 nm excitation wavelength compared to higher excitation wavelength.

4.2.7 Introduction to Rotifer

Rotifers are multi-cellular microorganisms that are typically 0.1 to 1mm long and are found in a variety of aquatic habitats [2]. Rotifers are very common in inland waters. In order to keep the Rotifer alive, the cultures should never be placed at refrigerator

temperature or in direct sunlight. They should be kept cool (20 to 22 C) with lids placed lightly over the storage jars. Rotifer cannot survive for long time because they increase rapidly and soon they exhaust their food supply. Therefore, most of the time they need to be cultured. They can be cultured on wheat medium with spring water in the same way as Paramecium.

4.2.8 ONF Spectra of Rotifer at 458 nm excitation (Argon ion laser line)

The ONF spectra of Rotifer were detected when its body stopped moving, after which the body did not lyse. The excitation was focused most of the time on the stomach of Rotifer. The power of the laser coming out of the excitation fiber (Pf) was usually set at 10 mW. A Schott GG495 long-pass filter was always used in front of the detection fiber to block laser scattering.

The raw ONF spectra of Rotifer from the same sample were plotted (after smoothing) to check for the data's reproducibility. Once they are reproducible in shape, the raw data are first averaged before any further processing. The result is then smoothed (across a window of 8.5 nm) and normalized according to the primary fluorescence peak height. The average spectra of Rotifer from different samples are then compared to see if they overlap.

Figure (4.26) shows the ONF data of Rotifer from sample A. The spectra overlap with each other in the major band, which peaks at 524 nm and has a full width half maximum (FWHM) of 85 nm. Because the spectra are reproducible in shape, they can be averaged together as in figure (4.27).

4.2.9 ONF Spectra of Rotifer at 401 nm Excitation (blue diode laser)

The 401 nm emission of a blue diode laser was used to excite the ONF spectra from Rotifer of different ages. The power out of the excitation fiber was 2.2-2.5 mW and the long pass filter used was Corning 3-72. The spectral data are processed in the same way as those obtained through 458 nm excitation.

Figure (4.28) shows the ONF data of Rotifer from sample B. The spectra overlap with each other in the major band, which peaks at 517 nm and has a full width half maximum (FWHM) of 107 nm. Likewise, Figure (4.29) shows the ONF data of Rotifer from sample B.

Each figure above indicates that the ONF spectra of Rotifer in the same sample are reproducible in shape under 401 nm excitation. Therefore, the spectra in each figure can be averaged to represent typical spectrum of Rotifer from one sample. The average spectrum from the two samples is then compared with each other in figure (4.30). The result indicates that the ONF spectra from different samples are also similar in shape. Consequently, the entire set of ONF spectra of Rotifer from sample A and B can be averaged, as shown in figure (4.31). The resulting spectrum has a full width half maximum (FWHM) of 95 nm and a primary peak at 515 nm.

4.2.10 ONF spectra of Rotifer at 496 nm excitation (Argon ion laser line)

When the excitation wavelength was 496 nm, the power out of the excitation fiber was 10 mW. The long pass filter used was Corning 3-69. The spectral data are processed in the same way as those obtained through 458 nm excitation.

Figure (4.32) shows the ONF data of Rotifer from sample D, measured using the

objective lens of power 10X. The spectrum has a peak at 546 nm and has a full width half maximum (FWHM) of 84 nm. Because there is only one spectrum shown here, the reproducibility of the data is uncertain.

4.2.11 Comparing the ONF spectra of G. lamblia cysts (cluster) with Rotifer

Figure (4.33) compares the ONF spectra of G. lamblia with that of Rotifer when the excitation wavelength is 401 nm. When using 401 nm excitation, G. lamblia can be distinguished from Rotifer in the ONF spectra.

Figure (4.34) compares the ONF spectra of G. lamblia with the ONF of Rotifer when the excitation wavelength is 458 nm. When using 458 nm excitation, G. lamblia cysts cannot be distinguished from Rotifer in the ONF spectra because the two are almost identical.

Figure (4.35) compares the ONF spectra of Rotifer when the excitation wavelength is changed from 458 to 401 nm. The individual data have been divided by the transmission spectrum of the long pass filters respectively. The figure indicates that the ONF spectra of Rotifer show a small shift (9 nm) when the laser wavelength is shifted; however, the spectrum is broader at 401 nm excitation compared to 458 nm: the FWHM is broadened to 106 nm, whereas G. lamblia maintains an 83 nm FWHM.

4.2.12 Miscellaneous results of the observed ONF spectra of Rotifer

Figure (4.36) shows a batch of background spectra of the Rotifer sample at 458 nm excitation with the power out of the excitation fiber at 10 mW. Figure (4.37)

the excitation fiber at 2.2-2.5 mW. The laser scattering and the background do increase at 401 nm excitation compared to other higher excitation wavelengths.

4.2.13 Introduction to *Giardia muris* cysts

Giardia muris is a flagellated intestinal protozoan [3]. The cyst is about 6 to 9 micrometers in diameter and 8 to 12 micrometers in length [4]. The excitation conditions for G. muris is the identical to that used for G. lamblia. The media of the sample is water, which is different from G. lamblia that was suspended in PBS solution.

4.2.14 ONF spectra of *Giardia muris cysts* (cluster) at 458 nm excitation (Argon ion laser line)

Figure (4.38) shows the ONF data from G. muris that were 1 day old . The spectra overlap with each other in the major band, which peaks at 516 nm and has a full width half maximum (FWHM) of 71 nm. Therefore, the spectra in the figure can be averaged to represent typical spectrum of G. muris under 458 nm excitation with the power out of the excitation fiber is 10 mW. This average is then compared with the ONF spectrum of G. lamblia as in figure (4.39). The figure indicates that two species of G. muris have similar ONF spectra in shape at 458 nm excitation. Further work is needed to confirm this result. In addition to the work at 458 nm, it is worthwhile using 401 nm to excite G. muris cysts to find out if its ONF differs from G. lamblia cysts.

4.2.15 ONF spectra of single *Giardia muris* cyst at 458 nm excitation (Argon ion laser line)

Figure (4.40) shows the ONF data from single G. muris that were 1 day old. The

from G. lamblia cysts.

4.2.15 ONF spectra of single *Giardia muris* cyst at 458 nm excitation (Argon ion laser line)

Figure (4.40) shows the ONF data from single G. muris that were 1 day old. The spectra overlap with each other in the major band, which peaks at 524 nm and has a full width half maximum (FWHM) of 77 nm. Therefore, the spectra in the figure can be averaged to represent typical spectrum of single G. muris. This average is then compared with the ONF spectrum of cluster of G. muris, as in figure (4.41). The result proves that the ONF spectra of single and cluster of G. muris overlap in shape under 458 nm excitation.

Furthermore, the data of single G. muris cyst is compared to that of single G. lamblia cyst, as in figure (4.42). The result shows that the ONF spectra of single cyst from the two species of Giardia are also similar to each other under 458 nm excitation.

4.2.16 Miscellaneous results of the observed ONF spectra of *Giardia muris* cysts

Figure (4.43) shows two background spectra of G. muris sample at 458 nm excitation with the power out of the excitation fiber at 10 mW. The background has low intensity compared to the cluster intensity.

4.3 Conclusion

When the excitation is blue-shifted to 401 nm, G. lamblia shows a unique fluorescence spectrum that differs from Paramecium and Rotifer in its peak position and spectral width, while at 458 nm excitation, all three microorganisms and G. muris show overlapping emission spectra.

4.4 References

1. Paramecium caudatum, Ehrenberg, 1838, http://www.microscopy-uk.org.uk/mag/articles/param1.html/.

2. Introduction to the Rotifera - Introduction to the Rotifera Rotifers: http://www.ucmp.berkeley.edu/phyla/rotifera/r

3. Summary-Parasites, DigestiveSystem (i) Giardiamuris. http://ourworld.compuserve.com/homepages/theb

4. Water filters & Giardia Distilled Wisdom, Alan Dove, Bill Tuthill, 1995. http://www.fc.net/~tdeagan/water/one.html

4.5 Figures

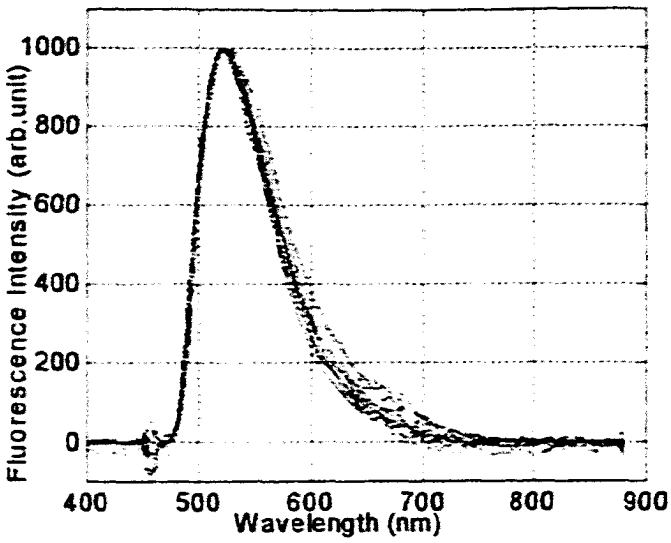

Fig. 4.1. Normalized the ONF spectra of Paramecium for sample #1. Excitation wavelength is 458 nm with power out of the excitation fiber 10 mW.

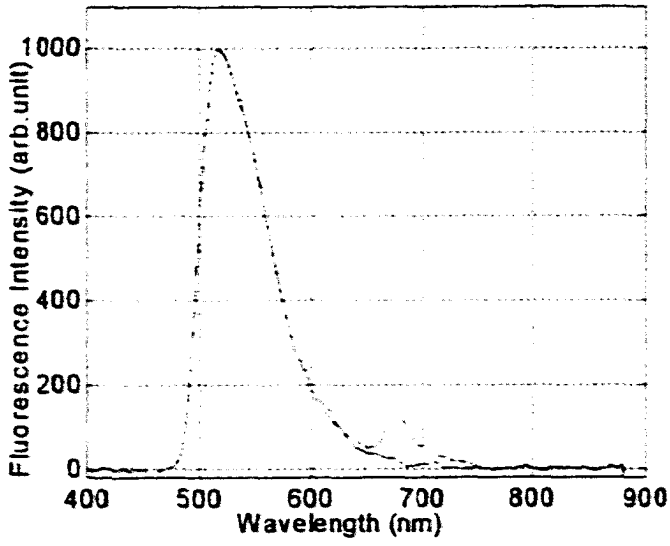

Fig. 4.2. Normalized the ONF spectra of Paramecium for sample #2. Excitation wavelength is 458 nm with power out of the excitation fiber 10 mW.

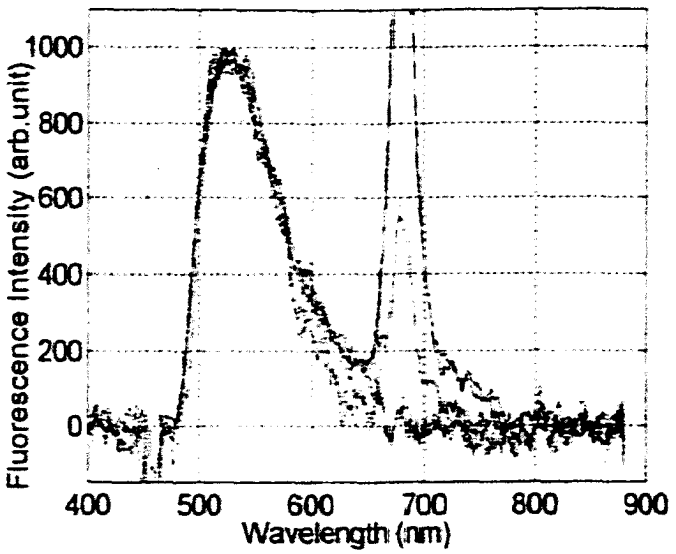

Fig. 4.3. Normalized the ONF spectra of Paramecium for sample #3. Excitation wavelength is 458 nm with power out of the excitation fiber 10 mW.

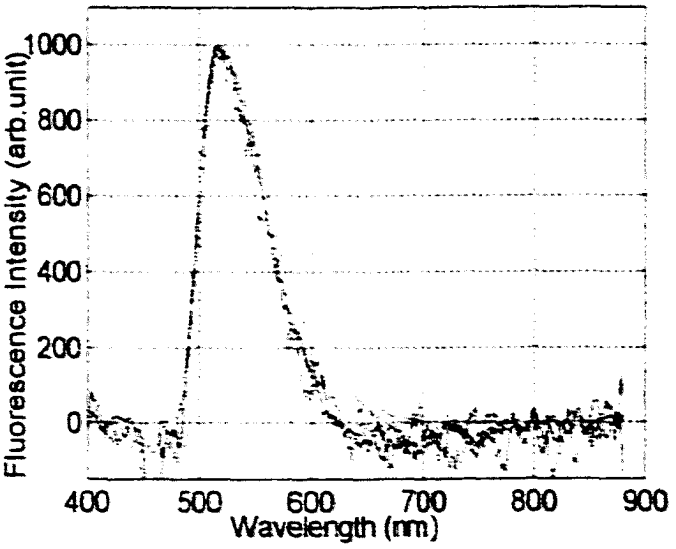

Fig. 4.4. Normalized the ONF spectra of Paramecium for sample #4. Excitation wavelength is 458 nm with power out of the excitation fiber 10 mW.

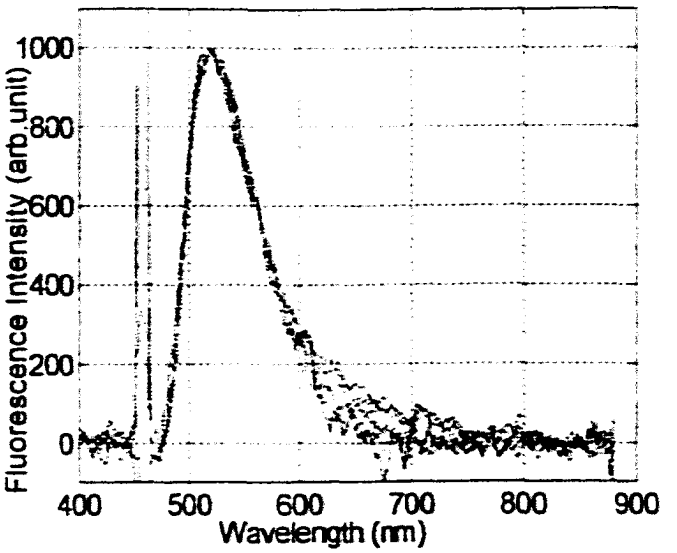

Fig. 4.5. Normalized the ONF spectra of Paramecium for sample #5. Excitation wavelength is 458 nm with power out of the excitation fiber 10 mW.

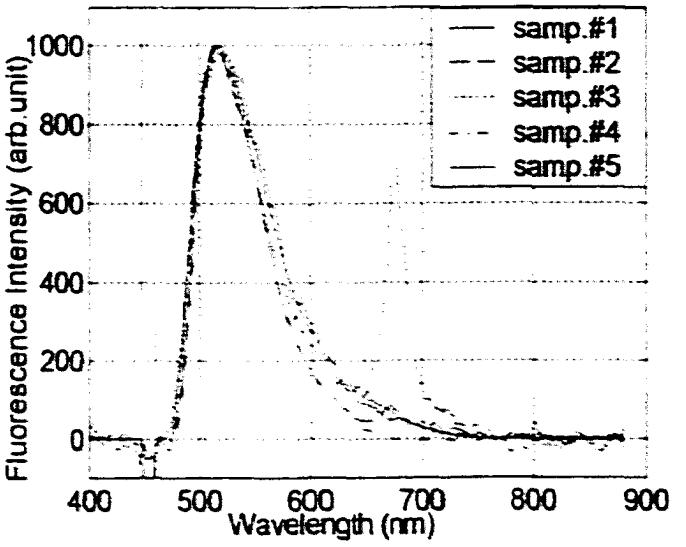

Fig. 4.6. Normalized the averaged ONF spectra of Paramecium for samples from #1 to #5. Excitation wavelength is 458 nm with power out of the excitation fiber 10 mW.

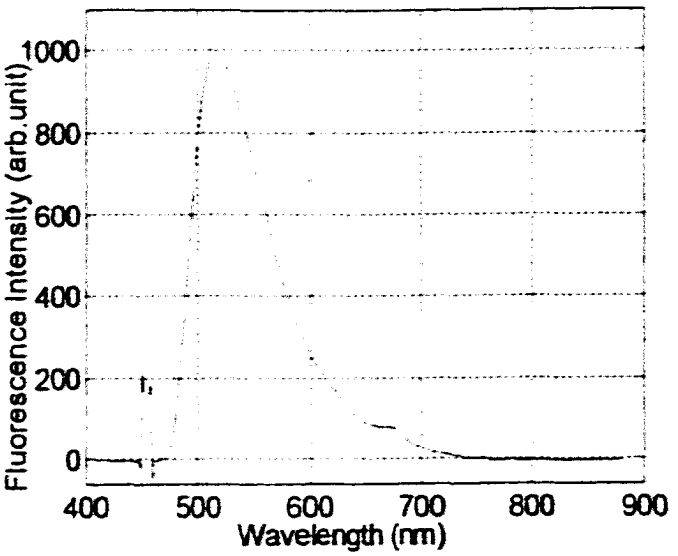

Fig. 4.7. Averaged of the ONF spectra of Paramecium for samples from #1 to #5. Excitation wavelength is 458 nm with power out of the excitation fiber 10 mW.

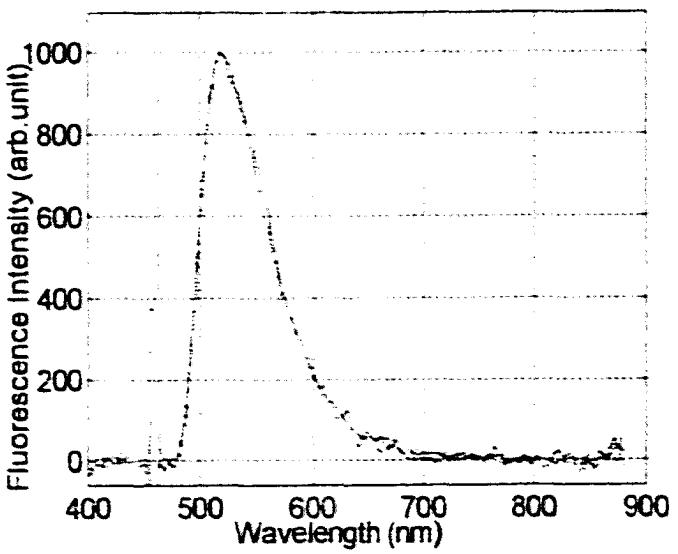

Fig. 4.8. Normalized the ONF spectra of Paramecium. Excitation wavelength is 458 nm with power out of the excitation fiber 2.5 mW.

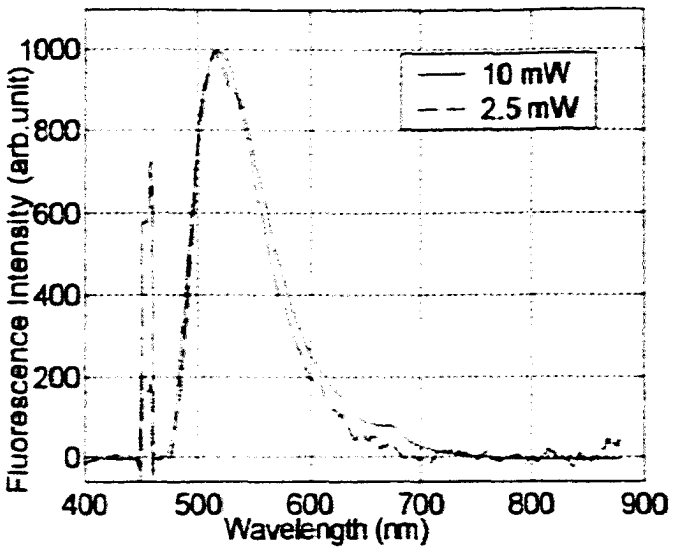

Fig. 4.9. Comparison the averaged ONF spectra of Paramecium at 458 nm excitation with power out of the excitation fiber 10 mW and 2.5 mW.

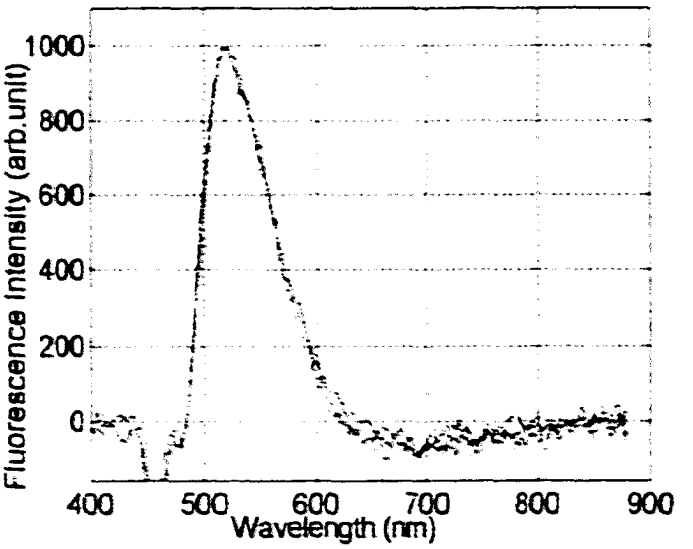

Fig. 4.10. Normalized the ONF spectra of Paramecium that was measured using 10X microscope objective lens, and the excitation wavelength is 458 nm with power out of the excitation fiber is 10 mW.

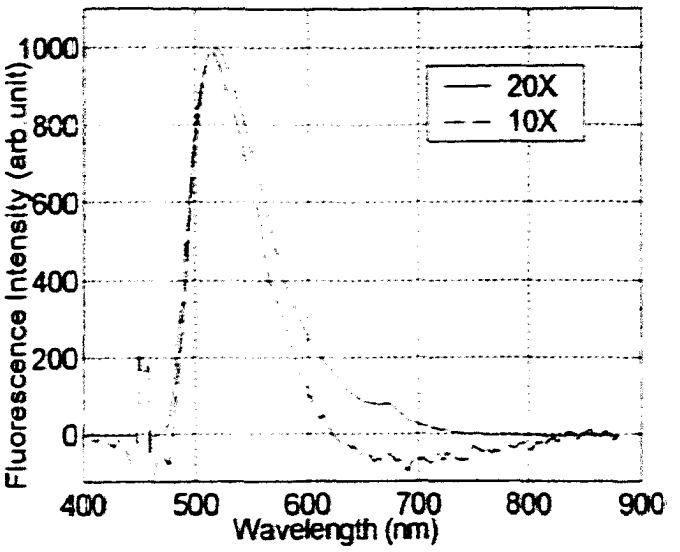

Fig. 4. 11. Comparison the averaged ONF spectra of Paramecium at 458 nm excitation with power out of the excitation fiber 10 mW, using 10X microscope objective lens, and 20X.

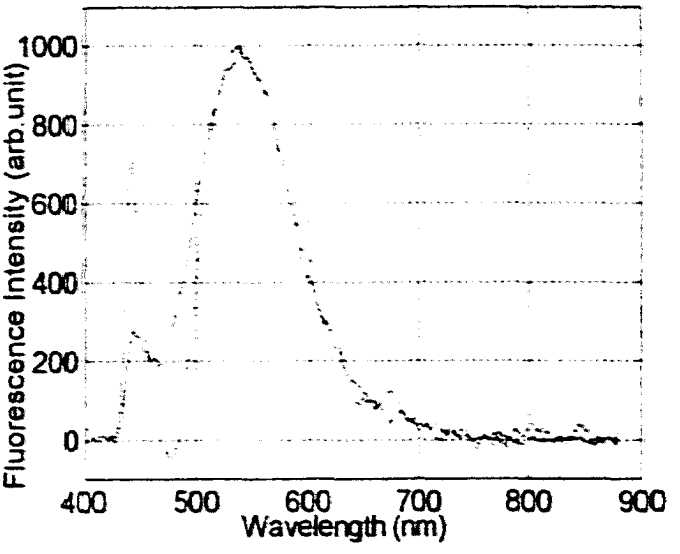

Fig. 4. 12. Normalized the ONF spectra of Paramecium for samples # 4. Excitation wavelength is 401 nm with power out of the excitation fiber 2.2-2.5 mW.

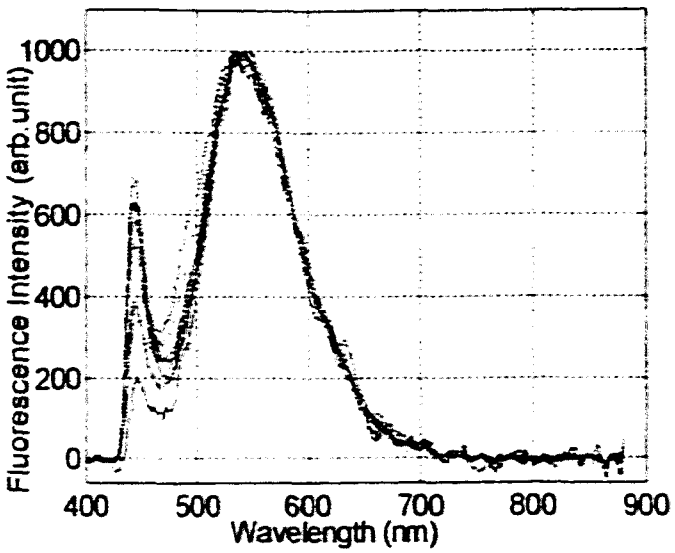

Fig. 4. 13. Normalized the ONF spectra of Paramecium for samples # 5. Excitation wavelength is 401 nm with power out of the excitation fiber 2.2-2.5 mW

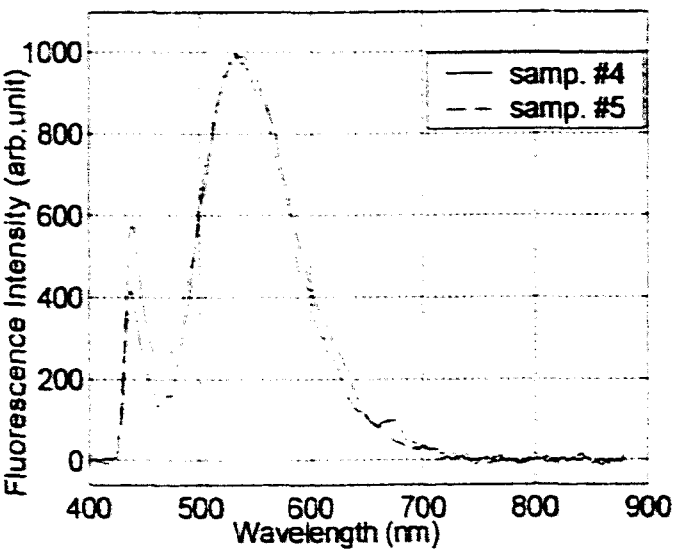

Fig. 4.14. Normalized the averaged ONF spectra of Paramecium for samples #4 and #5. Excitation wavelength is 401 nm with power out of the excitation fiber 2.2-2.5 mW

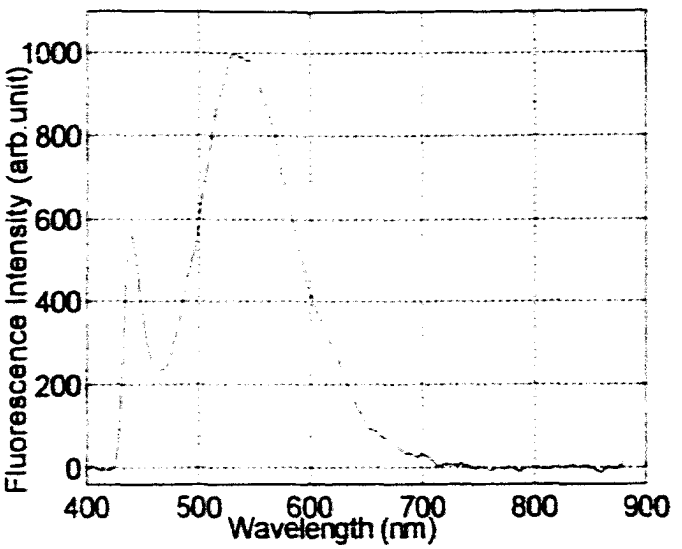

Fig. 4.15. Averaged ONF spectra of Paramecium for samples #4 and #5. Excitation wavelength is 401 nm with power out of the excitation fiber 2.2-2.5 mW.

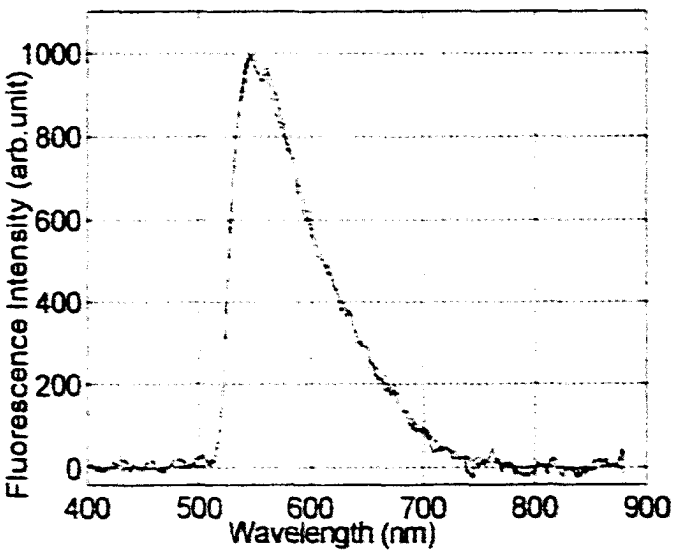

Fig. 4.16. Normalized the ONF spectra of Paramecium for samples # 1. Excitation wavelength is 496 nm with power out of the excitation fiber 10 mW.

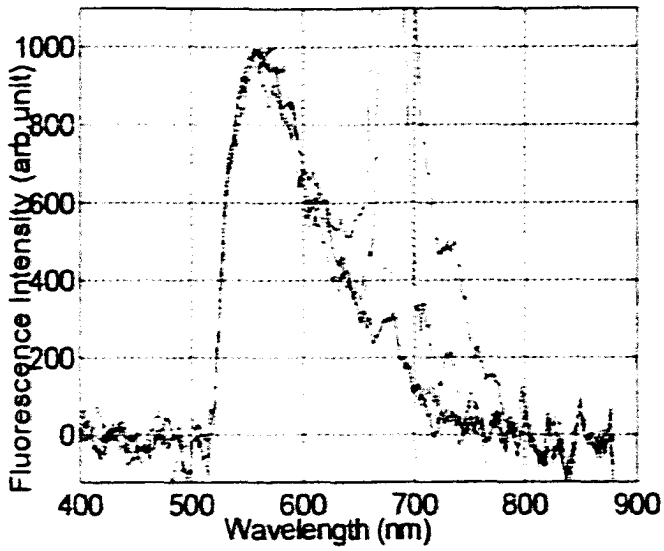

Fig. 4.17. Normalized the ONF spectra of Paramecium for samples # 3. Excitation wavelength is 496 nm with power out of the excitation fiber 10 mW. Using 10X objective lens.

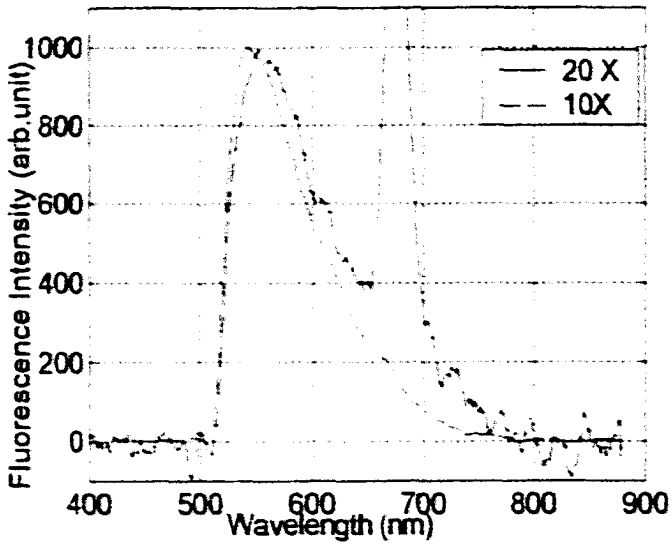

Fig. 4.18. Comparison the averaged ONF spectra of Paramecium at 496 nm excitation with power out of the excitation fiber 10 mW, using 10X microscope objective lens, and 20X.

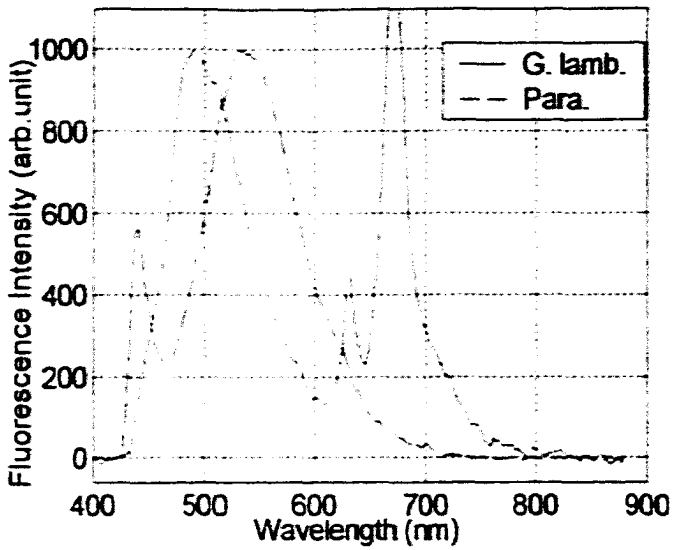

Fig. 4.19. Comparison of the averaged ONF spectrum of G. lamblia (solid) and Paramecium (dashdot), the excitation wavelength is 401 nm and the power out of the excitation fiber 2.2-2.5 mW.

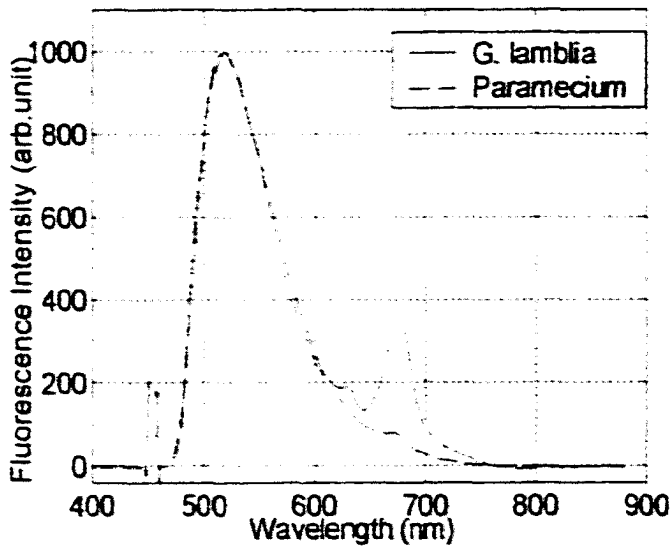

Fig. 4.20. Comparison of the averaged ONF spectrum of G. lamblia (solid) and Paramecium (dashdot), the excitation wavelength is 458 nm and the power out of the excitation fiber 10 mW.

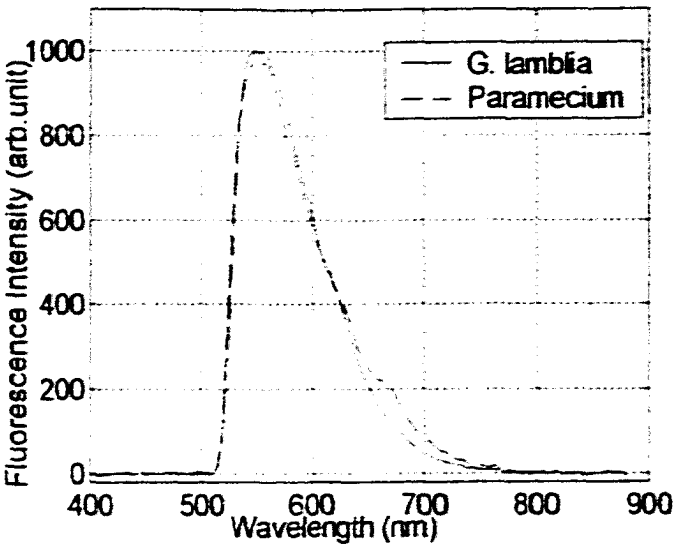

Fig. 4.21. Comparison of the averaged ONF spectrum of G. lamblia (solid) and Paramecium (dashdot), the excitation wavelength is 496 nm and the power out of the excitation fiber 10 mW.

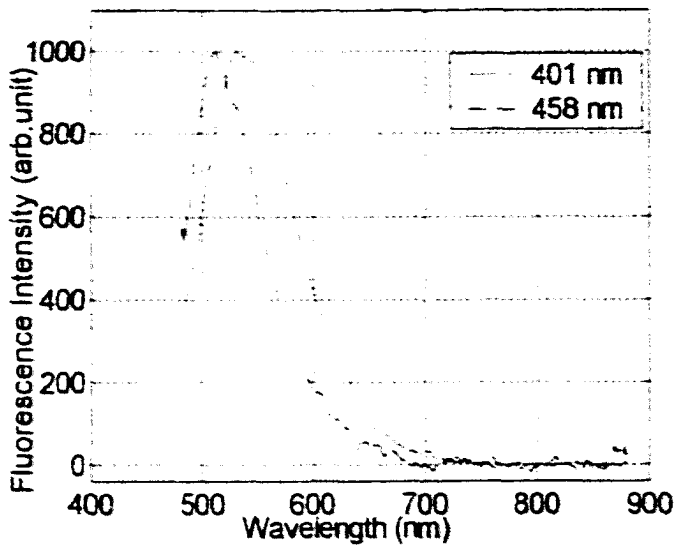

Fig. 4.22. Comparison of the ONF spectra of Paramecium when the excitation wavelength is changed from 458 (dashdot) to 401(solid) nm. The individual data have been divided by the transmission spectrum of the long pass filters respectively.

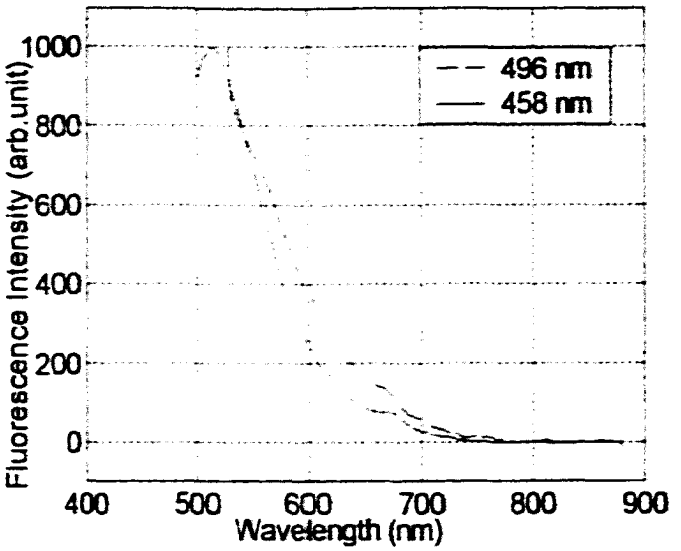

Fig. 4.23. Comparison of the ONF spectra of Paramecium when the excitation wavelength is changed from 458 (solid) to 496(dashdot) nm. The individual data have been divided by the transmission spectrum of the long pass filters respectively.

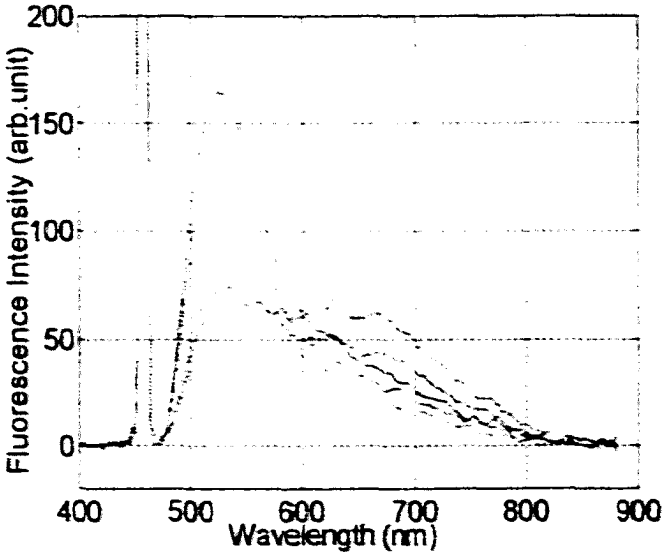

Fig. 4.24. A batch of background spectra of Paramecium in springwater at 458 nm excitation with the power out of the excitation fiber 10 mW.

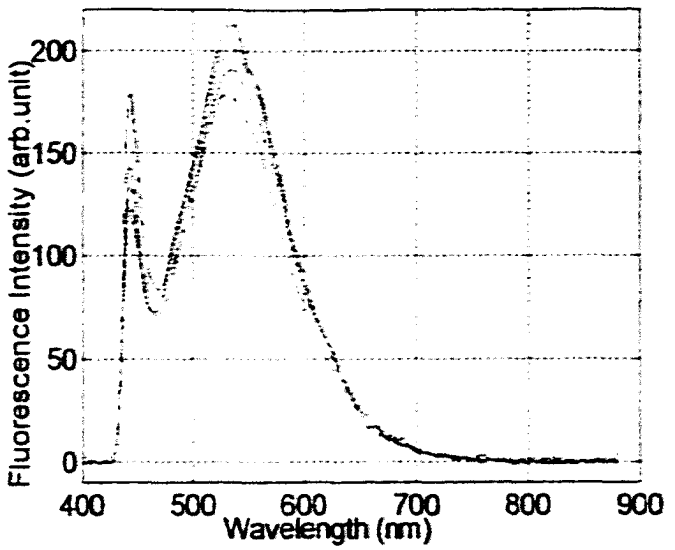

Fig. 4.25. A group of background spectra of Paramecium in springwater at 401 nm excitation with the power out of the excitation fiber 2.2-2.5 mW.

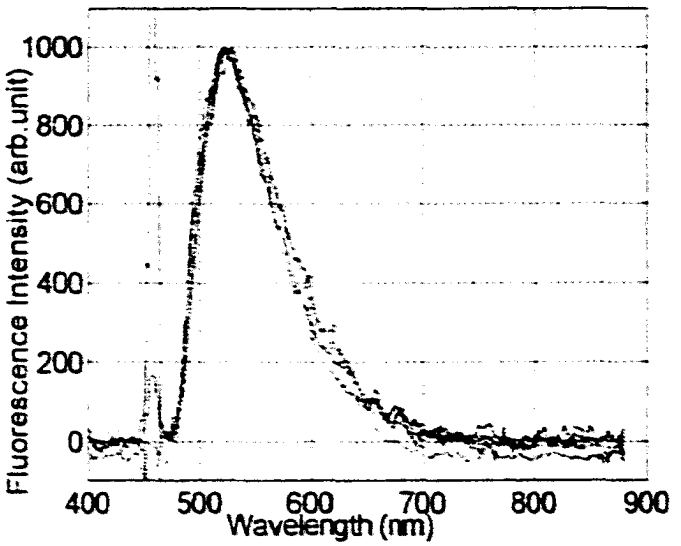

Fig. 4.26. Normalized the ONF spectra of Rotifer for sample A. Excitation wavelength is 458 nm with power out of the excitation fiber 10 mW.

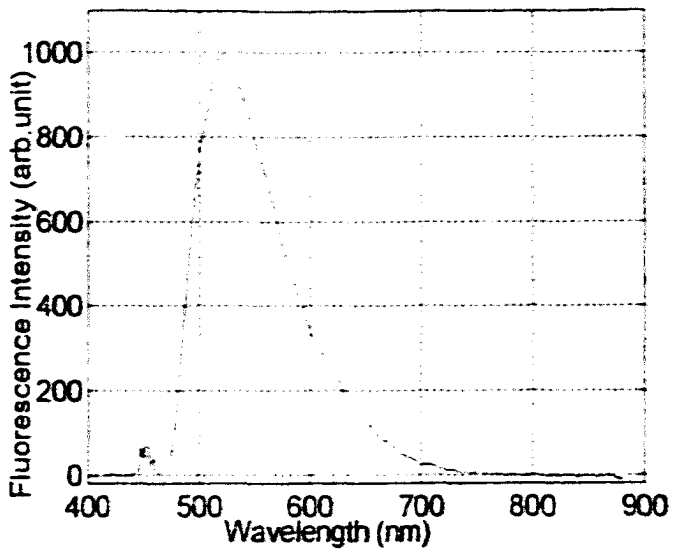

Fig. 4.27. Averaged ONF spectra of Rotifer for sample A. Excitation wavelength is 458 nm with power out of the excitation fiber 10 mW.

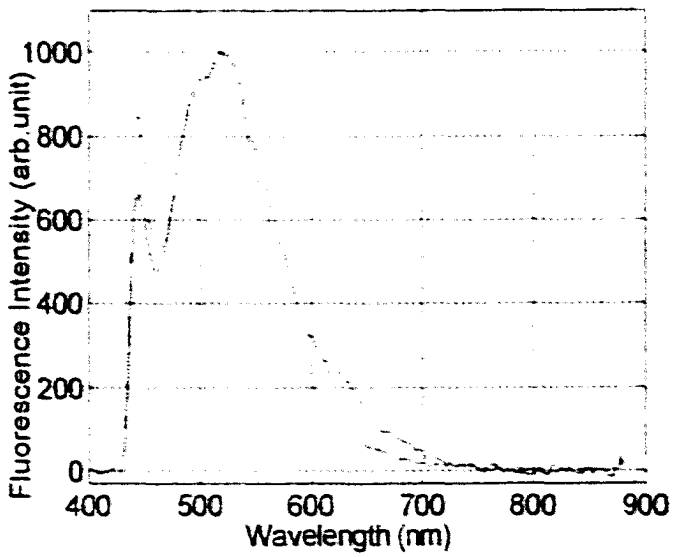

Fig. 4.28. Normalized the ONF spectra of Rotifer for sample B. Excitation wavelength is 401nm with power out of the excitation fiber 2.2-2.5 mW.

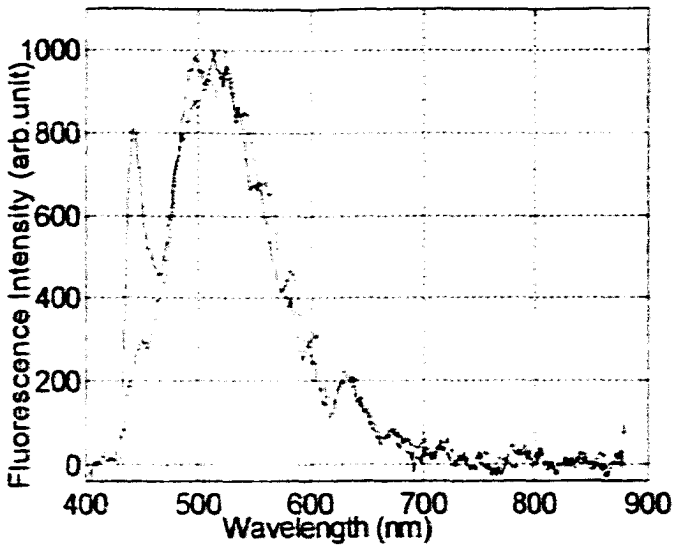

Fig. 4.29. Normalized the ONF spectra of Rotifer for sample B. Excitation wavelength is 401nm with power out of the excitation fiber 2.2-2.5 mW.

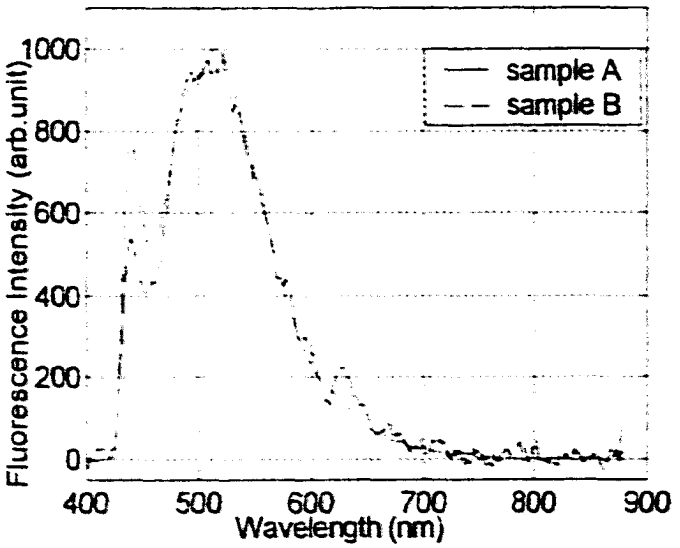

Fig. 4.30. Comparison of the averaged ONF spectra of Rotifer for sample A and B. Excitation wavelength is 401nm with power out of the excitation fiber 2.2-2.5 mW.

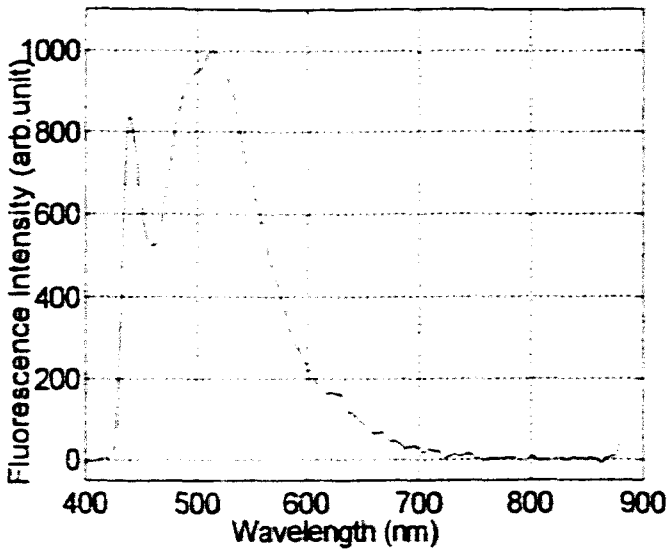

Fig. 4.31. Averaged ONF spectra of Rotifer for sample A and B. Excitation wavelength is 401nm with power out of the excitation fiber 2.2-2.5 mW.

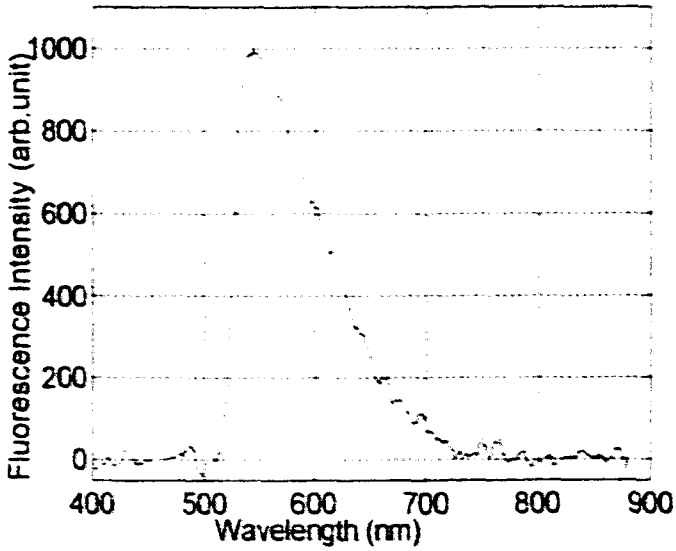

Fig. 4.32. The ONF spectra of Rotifer for sample D. Excitation wavelength is 496nm with power out of the excitation fiber 10 mW, using 10X objective lens.

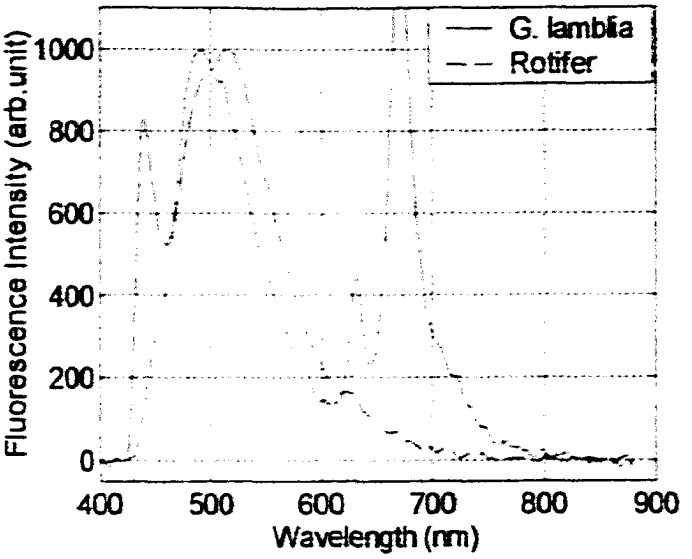

Fig. 4.33. Comparison of the averaged ONF spectrum of G. lamblia (solid) and Rotifer (dashdot), the excitation wavelength is 401 nm and the power out of the excitation fiber 2.2-2.5 mW._

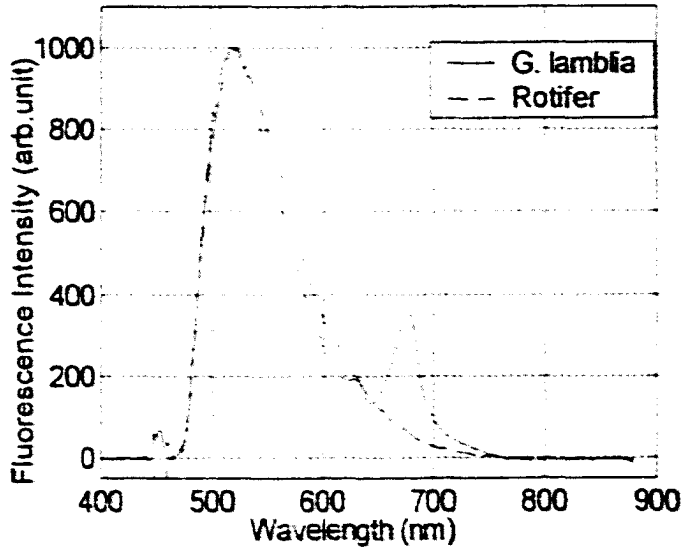

Fig. 4.34. Comparison of the averaged ONF spectrum of G. lamblia (solid) and Rotifer (dashdot), the excitation wavelength is 458 nm and the power out of the excitation fiber 10 mW._

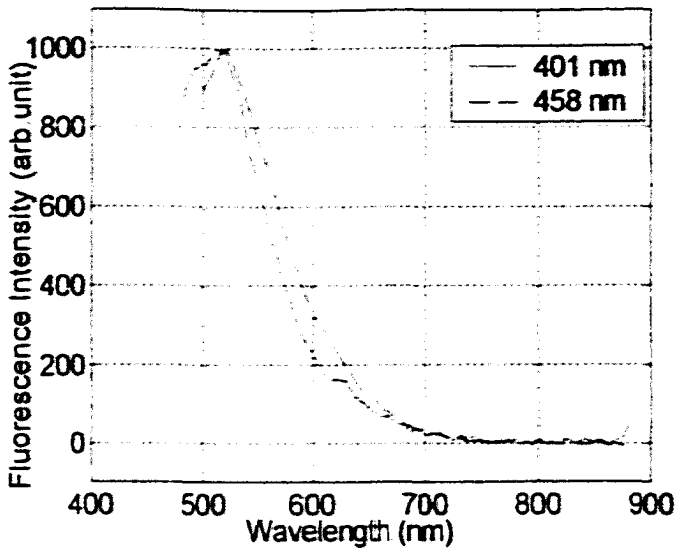

Fig. 4.35. Comparison of the ONF spectra of Rotifer when the excitation wavelength is changed from 458 (dashdot) to 401(solid) nm. The individual data have been divided by the transmission spectrum of the long pass filters respectively.

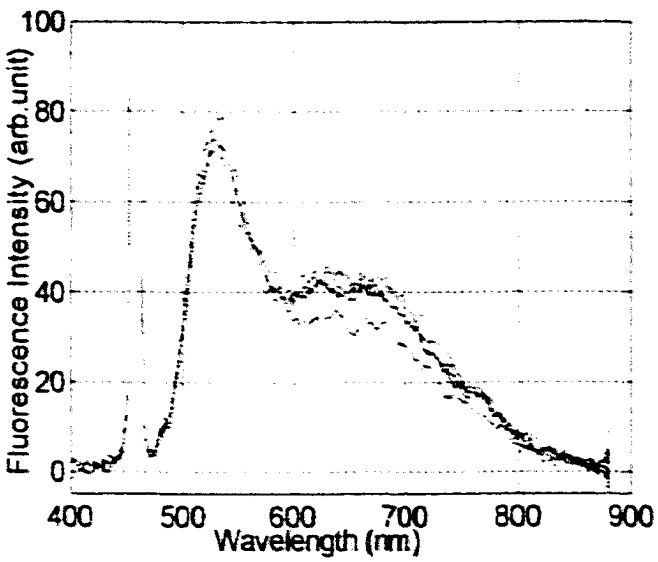

Fig. 4.36. A batch of background spectra of Rotifer in springwater at 458 nm excitation with the power out of the excitation fiber 10 mW.

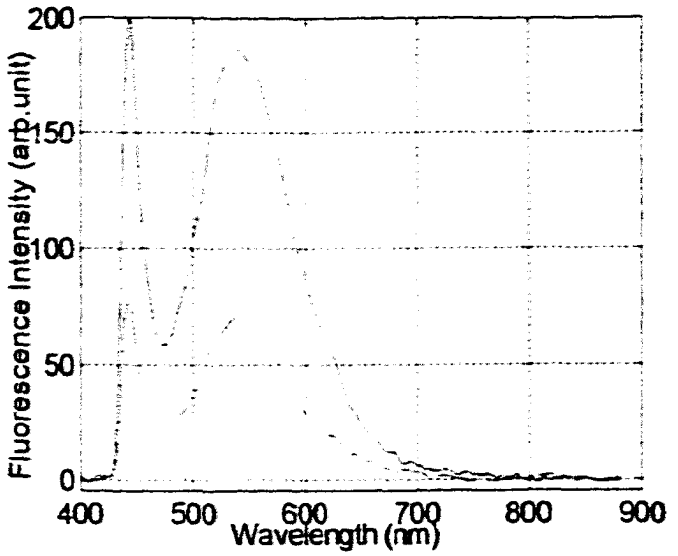

Fig. 4.37. Two of background spectra of Rotifer in springwater at 401 nm excitation with the power out of the excitation fiber 2.2-2.5 mW.

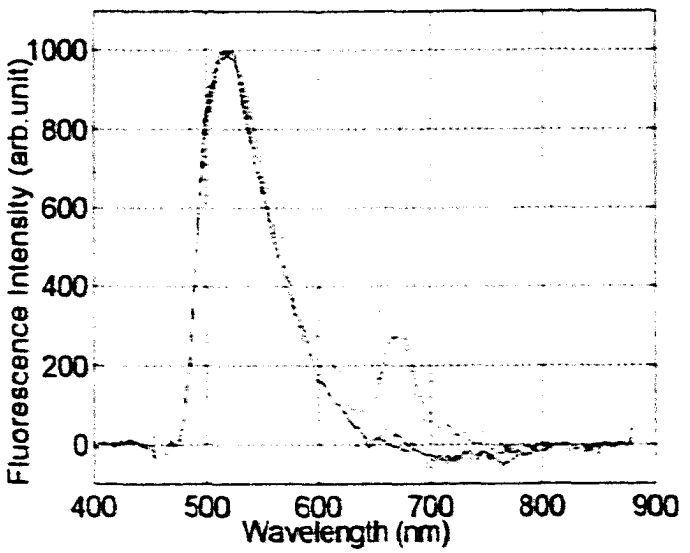

Fig. 4.38. Normalized the ONF spectra of G. muris for sample 1 days old. Excitation wavelength is 458 nm with power out of the excitation fiber 10 mW.

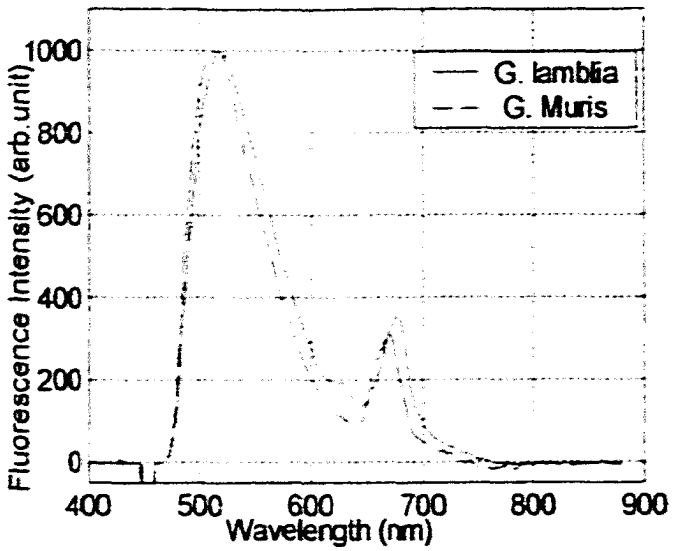

Fig. 4. 39. Comparison of the averaged ONF spectra between G. lamblia (solid) and G. muris (dashdot) at excitation wavelength 458 nm. and power out of the excitation fiber is 10 mW.

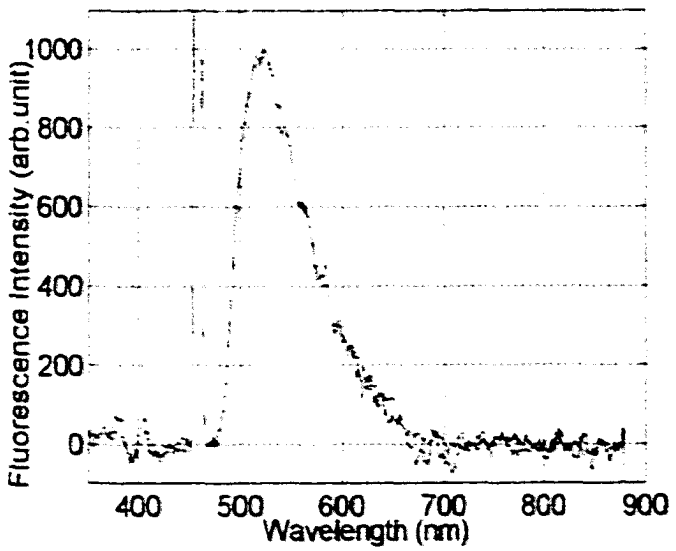

Fig. 4. 40. Normalized the ONF spectra of single G. muris for sample 1 days old. Excitation wavelength is 458 nm with power out of the excitation fiber 10 mW.

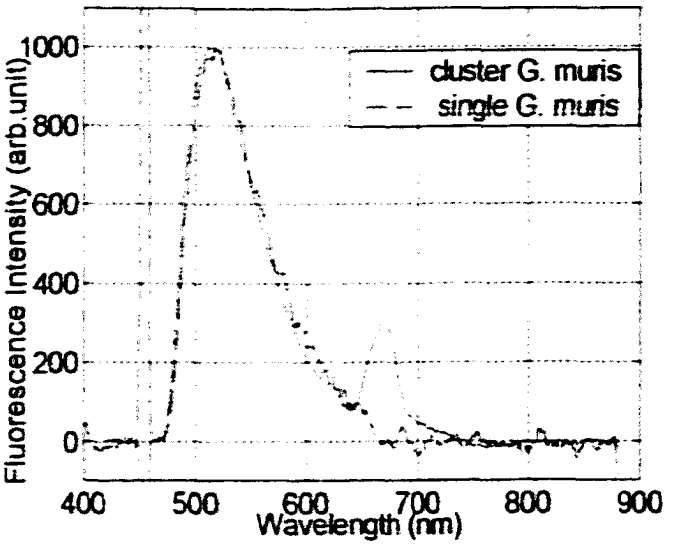

Fig. 4. 41. Comparison of the averaged ONF spectra between cluster of G. muris (solid) and single G. muris (dashdot) at excitation wavelength 458 nm, and power out of the excitation fiber is 10 mW.

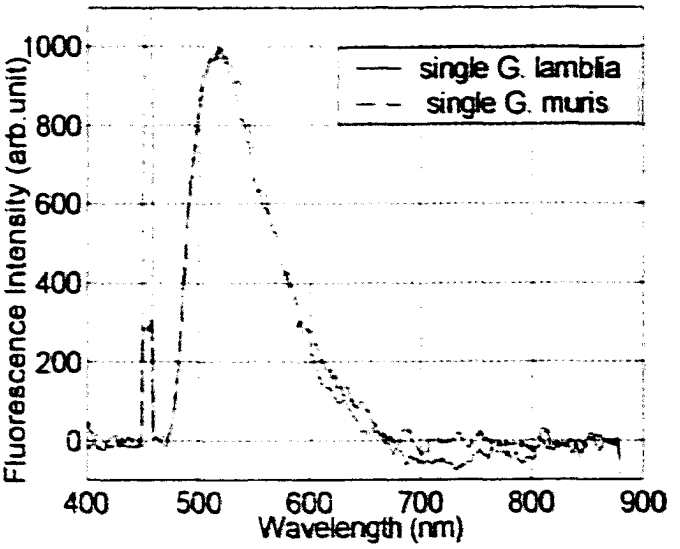

Fig. 4. 42. Comparison of the averaged ONF spectra between single G. lamblia (solid) and single G. muris (dashdot) at excitation wavelength 458 nm, and power out of the excitation fiber is 10 mW.

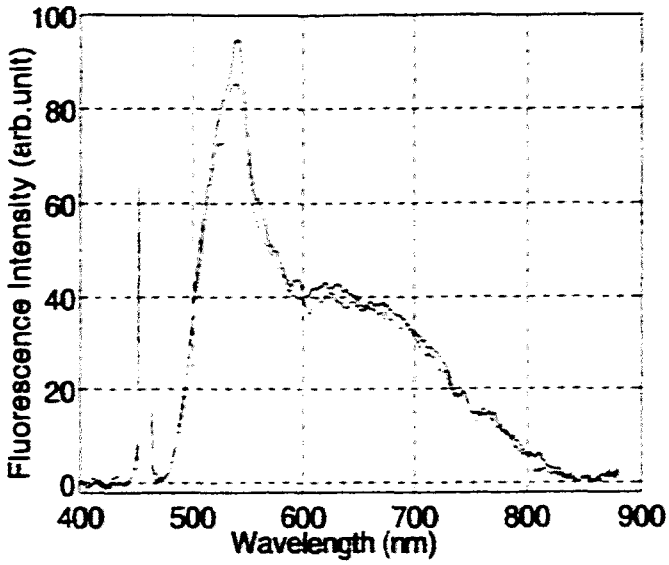

Fig. 4. 43. Two background spectra of G. muris sample excited at 458 nm wavelength and power out of the excitation fiber is 10 mW.

Chapter 5

The ONF spectrum of Giardia lamblia cysts compared to the fluorescence spectrum of Amino Acids

5.1 Introduction

It is observed that proteins play a significant and common role in the excited spectra obtainable from Giardia lamblia cysts. Proteins are the organic molecules that are essential ingredients in all aspects of the structure and function of microorganisms [4]. Proteins typically make up 50% or more of the cell's dry weight [1,19-21] and are composed of units of about 20 different amino acids, which are organic compounds that contain both the amino (_NH2) and carboxyl (_COOH) groups [2,19-21].

The general structural formula for an amino acid is

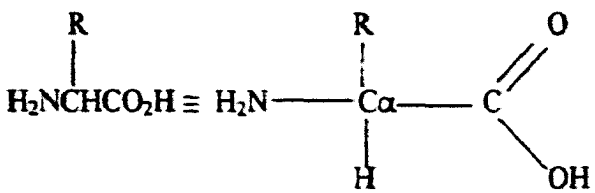

Cα is the alpha carbon atom in the center; R is a variable group that the molecules of the 20 standard amino acids different from one another; H2N is the amino group; COOH is the carboxyl group.

Most of these amino acids differ only in the nature of the *R* substituent. The standard amino acids are therefore classified on the basis of these *R* groups._Three natural amino

acid residues have the highest fluorescence efficiency [5], and they may contribute and play a key role in the cell fluorescence. They are: *L-tyrosine, L-tryptophan, and L-phenylalanine.* Most proteins are endowed with an intrinsic UV fluorescence property because they contain these aromatic amino acids that have absorption in the UV. The absorption of proteins at 280 nm is due to both tyrosine and tryptophan residues. At wavelengths longer than 295 nm, the absorption is due primarily to tryptophan [10].

L-Tryptophan is the most efficient fluorescent amino acid in proteins: It has the highest quantum yield of fluorescence. The L-tryptophan residues of proteins generally account for about 90% of the total fluorescence from proteins [10]. Thus, the fluorescence of most proteins is dominated by the tryptophan residues. On the other hand, tyrosine is highly fluorescent in solution, but its emission is generally weaker in proteins than tryptophan [10]. Furthermore, the quantum yield of phenylalanine in proteins is small, so the emission from this residue is rarely observed [10].

While the amino acids mentioned above are major contributors to cellular fluorescence, coenzymes derived from vitamins [14] such as FAD and NAD are also known to be strong fluorophores in cell [9,11,15-17,31,34]. Although their cellular concentrations are much lower than tryptophan [9], their fluorescence efficiency can be much higher.

5.2 The fluorescence of L-tryptophan solution compared to the ONF spectra of G. lamblia

Aqueous solution of the amino acid L-Tryptophan ($C_{11}H_{12}N_2O_2$, FW (formula weight): 204.2 g/mol) at the concentration of 12.5 and 25 mM was prepared in distilled

water. Like the excitation used for microorganisms, 401, 458, and 496 nm excitation were used to excite the tryptophan solution. The power of the excitation fiber was 2.5, 20, and 32 mW and Corning 3-72, Schott GG495, and OG515 were used respectively as long pass filters.

Figure (5.1) compares the smoothed ONF spectra of L-tryptophan when the excitation wavelength is changed from 458 to 401 nm. The individual data have been divided by the transmission spectrum of the long pass filters respectively. Likewise, figure (5.2) compares the ONF spectra of L-tryptophan when the excitation wavelength is changed from 458 to 496 nm. These figures show that the fluorescence spectrum of L-tryptophan shifts to the longer wavelength with increasing excitation wavelengths, which is similar to the ONF spectra of G. lamblia cysts. Figure (5.3) shows all of three excitation (401, 458, and 496nm) wavelength together.

The narrow peak at about 3150-3650 cm-1 from the excitation wavelength is attributed to the Raman peak of water, caused by the stretching vibration group of O-H [6]. Figure (5.4) compares the ONF spectra of G. lamblia with the fluorescence of L-tryptophan solution when the excitation wavelength is 401 nm. The longpass filter used for taking the two data were the same. The averaged baseline height between 200 and 300 nm is subtracted from the entire spectrum for L-tryptophan. Likewise, figure (5.5) compares the ONF spectra of G. lamblia with the fluorescence of L-tryptophan when the excitation wavelength is 458 nm, and figure (5.6) compares the two when the excitation wavelength is 496 nm. These figures show that the L-tryptophan fluorescence spectrum largely agrees with the ONF spectrum of G. lamblia cyst at all three excitation wavelengths.

5.3 The fluorescence of FAD (Flavin adenine dinucleotide) solution compared to the ONF spectra of G. lamblia

Aqueous solution of coenzyme FAD ($C_{27}H_{31}N_9O_{15}P_2Na_2$, FW (formula weight): 829.5 g/mol) at a concentration 5 to 10 μM was prepared in distilled water. The power out of the excitation fiber was 0.55, 1.25,1.25 mW for 401, 458, 496 nm excitation and Corning 3-72, Schott GG495, OG 515 long pass filters were used, respectively.

Figure (5.7) compares the smoothed fluorescence spectra of FAD when the excitation wavelength is changed from 458 to 401 nm. The individual data have been divided by the transmission spectrum of the long pass filters respectively. Likewise, figure (5.8) compares the ONF spectra of FAD when the excitation wavelength is changed from 458 to 496 nm. These figures show that the fluorescence of FAD does not shift with increasing excitation wavelength. Figure (5.9) shows all of three excitation (401, 458, and 496nm) wavelength together. This is clearly different from G. lamblia.

5.4 Discussions

At all three excitation wavelengths (401, 458, 496 nm), the fluorescence spectra of Giardia and tryptophan agree reasonably well (Fig. 5.4, 5.5, and 5.6). Like G. lamblia, tryptophan exhibits clear spectral shift when the laser excitation wavelength is changed (Fig.5.1-3). On the other hand, when the same excitations are applied to another major fluorescent molecule in cell, FAD, the results stand in sharp contrast to those from Giardia and L-trytophan (Fig.5.7-9). No spectral shifts are observed here when the laser excitation wavelength is changed.

The fluorescence of tryptophan has been extensive investigated under UV excitation [7-13,27-28,30]. However, as far as the author knows, there has not been any report on tryptophan fluorescence under visible excitation. The main reason for this is that the absorption bands of tryptophan are all located in the UV spectral range [7,30]. The study of the tryptophan molecule itself is naturally best undertaken with UV excitations. While excitation in the UV spectral range may be a better match to absorption bands of proteins and other constituents in microorganisms, the use of excitation sources in the visible for these experiments was dictated by the considerations of (i) availability; (ii) strong absorption of UV excitation inside the microscope optics; and (iii) strong absorption of UV excitation by water, which makes UV excitation impractical for potential remote sensing applications in natural water.

Although the visible excitations used to excite *Giardia* are far from the major absorption band of tryptophan, the concentration of the tryptophan sample in this work is high enough to allow the absorption edge to extend to 401 and 458 nm. At the same time, the concentration is kept low enough so that it does not exceed the average amino acid concentration in a cell, and fluorescence quenching does not occur [9].

When they are excited at 458 nm, *Giardia lamblia*, Paramecium, and Rotifer emit fluorescence of almost identical spectral shape that is similar to tryptophan in aqueous solution. This result suggests that the chromophores in these compounds that absorb long wavelength excitations are similar to each other. This result may be explained by the fact that the long wavelength excitation tends to excite a sub-ensemble of the chromophores (tryptophan) that are more homogeneous than the entire sample.

In contrast, when the excitation is blue-shifted to 401 nm, Giardia shows a unique fluorescence spectrum that differs from that of paramecium and rotifer in its peak position and spectral width, yet continues to match that of tryptophan. These results may be understood in the following context.

The major fluorescent molecules in cells can be divided into proteins and coenzymes. Tryptophan has been recognized as the major cause of natural fluorescence in proteins [7,9]. Thus, the predominant concentration of proteins in cell suggests that tryptophan plays an important role in cell fluorescence. Vitamin-derived coenzymes [15] such as FAD and NAD are also known to be strong fluorophores in cell [9,11,16-18]. And, although their cellular concentrations are typically much lower than tryptophan [9], their fluorescence efficiency can be much higher. However, the results presented in Fig.. show that induced fluorescence from FAD alone exhibits no spectral shift at different excitation wavelengths, implying homogeneous broadening of excited states at room temperature. These results therefore rule out the possibility of FAD and other coenzymes as the major cause of Giardia fluorescence since the latter shows distinct shifts with excitation wavelengths. The reason why these coenzymes are not causing Giardia fluorescence may have to do with the passive metabolism of Giardia cysts. Since these coenzymes are mainly involved in cellular metabolism [15], their concentration in Giardia can be expected to be relatively low.

The similarities of excited spectra observed for all three microorganisms and tryptophan for 458 nm excitation are in marked contrast to the match obtained for Giardia and tryptophan with 401 nm excitation and the differences observed for rotifer and paramecium. These differences may be due to the fact that compared to paramecium and

rotifer, Giardia is a much more primitive eukaryote [35], making it probable that at the shorter wavelength excitations the fluorophores in Giardia interact differently with their surroundings from those in paramecium and rotifer.

The unique properties of enzymes arise largely from their enormous structural and functional diversity that makes it possible to distinguish the ONF spectra of G. lamblia cysts from other microorganisms effectively. All these microorganisms, in response to their changing needs, have the activity of their enzymes increased, decreased, or even turned off entirely, which creates a different environment for the fluorophore (tryptophan) in a cell and affects the cellular fluorescence spectrum.

The results in this work show that FAD resembles organic dye molecules that are highly efficient in fluorescence. Like dyes at room temperature, the fluorescence of FAD shows no spectral shift at different excitation wavelengths because its absorption line is homogeneously broadened. This result rules out FAD as the major cause of G. lamblia fluorescence. The same conclusion may be drawn regarding other common coenzymes such as FMN, NAD, NADH, and the fluophore riboflavin itself. The reason why these coenzymes are not causing Giardia fluorescence may have to do with the passive metabolism of Giardia cysts. Since these coenzymes are mainly involved in active cellular metabolism [14], their concentration in Giardia can be expected to be insignificant.

Other evidence pointing to protein's role in G. lamblia fluorescence comes from a study of green fluorescent protein (GFP)[18,22-26,29], which shows a very similar temporal behavior in its emission intensity. While it is an interesting question, the exact

nature of the fluorophore (fluorescent material in the cell) responsible for Giardia cysts is beyond the scope of this work.

5.5 Conclusion

The fluorescence spectra of L-tryptophan shift to longer wavelength with increasing excitation wavelength. There is a great similarity between the spectra shape of L-tryptophan solution and that of G. lamblia cysts under visible laser excitations. This result supports the conjecture that L-tryptophan plays a predominant role in the ONF of G. lamblia cysts.

5.6 References

1. D. Alberts, J. Bray, M. Lewis, K. Raff, and J. D. Watson, Molecular Biology of the Cell, Second Ed.,(Garland Publishing, Inc. New York & London 1989).
2. K. Mathews, K. E. Van Holde, Biochemistry, (The Benjamin/Cummings Publishing Company, Inc. 1983).
3. L. J. Kleinsmith, and V. M. Kish, Principle of Cell and Molecular Biology, Second Ed., (HarperCollins College Publishers, 1995).
4. Branden and J. Tooze, Introduction to Protein Structure, Second Ed., (1999).
5. T. Timperman, K. E. Oldenburg, and J. V. Sweedler, "Native Fluorescence Detection and Spectral Differentiation of Peptides Containing Tryptophan and Tyrosine in Capillary Electrophoresis," Analytic Chemistry. 67. 3421-3426,1995.
6. Yariv, Amnon, Quantum Electronics, (John Wiley & Sons, Inc., New York, 1975).
7. E. A. Permyakov, Luminescence Spectroscopy of Protein (CRC, Boca Raton, FL, 1993).
8. R. Lakowicz, "On Spectral Relaxation in Proteins," Photochem. Photobiol. 72, 421-437 (2000).
9. S. V. Konev, Fluorescence and Phosphorescence of Proteins and Nucleic Acids (Plenum, New York, 1967).
10. R. Lakowicz, "Protein fluorescence," in Principles of Fluorescence Spectroscopy, 2nd ed., J. R. Lakowicz ed. (Kluwer/Plenum, New York, 1999).
11. R. R. Alfano and A. Katz, "Photonic pathology, fluorescence and raman spectroscopy for tissue diagnosis and characterization," in Analytical use of fluorescent probes in Oncology, Kohen and Hirschberg, eds. (Plenum, New York, 1996).

12. P. Demchenko, Ultraviolet Spectroscopy of Proteins (Springer, New York 1981).

13. E. D. Owen, "Principles of photochemical reactions," in Organic Compounds in Aquatic Environments, S. D. Faust and J. V. Hunter, eds. (Marcel Dekker, Inc. New York 1971).

14. L. J. Kleinsmith and V. M. Kish, Principles of cell and molecular biology, 2nd ed. (HarperCollins, New York, 1995).

15. M. Monici, R. Pratesi, P. A. Bernabei, R. Caporale, P. R. Ferrini, A. C. Croce, P. Balzarini, and G. Bottiroli, "Natural fluorescence of white blood cells: spectroscopic and imaging study," J. Photochem. Photobiol. **30**, 29-37 (1995).

16. M. Roederer and R. F. Murphy, "Cell-by-cell autofluorescence correction for low signal-to-noise systems: application to epidermal growth factor endocytosis by 3T3 fibroblasts," Cytometry. 7, 558-565 (1986).

17. C. Benson, R. A. Meyer, M. E. Zaruba, and G. M. McKhann, "Cellular autofluorescence - is it due to flavins," J. Histochem. Cytochem. 27, 44-48 (1979).

18. G. Cinelli, A. Ferrari, V. Pellegrini, M. Tyagi, M. Giacca, and F. Beltram, "The enhanced green fluorescent protein as a tool for the analysis of protein dynamics and localization: local fluorescence study at the single-molecule level," Photochem. Photobiol. 71, 771-776 (2000).

19. Encarta Learning Zone, Amino Acids, http://encarta.msn.com/find/Concise.asp?z

20. Encarta Learning Zone, Protein, http://encarta.msn.com/find/Concise.asp?ti

21. Amino acids, http://chemed.chem.purdue.edu/genchem/topicreview/bp/1biochem/amino2.html

22. T. Ha, Th. Enderle, D. F. Ogletree, D. S. Chemla, P. R. Selvin, and S. Weiss, "Probing the interaction between two single molecules: Fluorescence resonance energy between a single donor and a single acceptor," Proc. Natl. Acd. Sci. **93**, 6264-6268 (1996).

23. Erwin J. G. Peterman, Sophie Brasselet, and W. E. Moerner, " The fluorescence dynamic of single molecules of green fluorescent protein," J. Phys. Chem. A **103**, 10553-10560 (1999).

24. Mita Chattoraj, Brett A. king, Gerold U. Bublitz, and Steven G. Boxer, " Ultra-fast excited state dynamics in green fluorescence protein: Multiple states and proton transfer," Proc. Natl. Acad. Sci. **93**, 8362-8367 (1996).

25. Robert M. Dickson, Andrew B. Cubitt, Roger Y. Tsien, and W. E. Moerner, " On/off blinking and switching behavior of single molecules of green fluorescent protein," Nature **388**, 355-358 (1997).

26. T. M. H. Creemers, A. J. Lock, V. Subtramaniam, T. M. Jovin, and S. Volker, " Three photoconvertible forms of green fluorescent protein identified by spectral hole-burning," Nature Structural Biology **6**, 557-560 (1999).

27. Ling Zang and Michael A. J. Rodgers, " Formation of tryptophan radicals in irradiated aqueous solutions of hexachloroplatinate(IV): a flash photolysis study," Photochemistry and photobiology **70**, 565-567 (1999).

28. Christine Pokalsky, Peter Wick, Etti Harms, Fred E. Lytle, and Robert L. Van Etten, "Fluorescence resolution of the intrinsic tryptophan residues of bovine protein tyrosyl phosphatase," The Journal of Biological Chemistry. **270**, 3809-3815 (1995).

29. Alexander A. Voityuka, Maria-Elisabeth Michel-Beyerlea and Notker Rōscha, " Protonation effects on the chromophore of green fluorescent protein. Quantum chemical study of the absorption spectrum, " Chemical Physics Letters 272(3-4), 162-167 (1997).

30. B. Anfinsen, Jr., M. L. anson, Kenneth Bailey, and John T. Edsall, Advances in protein chemistry, Academic Press 17, (1962).

31. Douglas L. Heintzelman, Reuben Lotan, Rebecca R. Richards-Kortum," Characterization of the autofluorescence of polymorphonuclear leukocytes, mononuclear leukocytes and cervical epithelil cancer cells for improved spectroscopic discrimination of inflammation from dysplasia," Photochemistry and Photobiology. 71,327-332 (1999).

32. Brockhinke, R. Plessow, P. Dittrich, K. Kohse-Hoinghaus," Analysis of the local conformation of proteins with two-dimensional fluorescence techniques," Appl. Phys. B71, 755-763 (2000).

33. T. Timperman, K. E. Oldenburg, and J. V. Sweedler, "Native fluorescence detection and spectral differentiation of peptide containing tryptophan and tyrosine in capillary electrophoresis," Anal. Chem. 67, 3421-3426 (1995).

34. J. E. Aubin, " autofluorescecne of visible culture Mammalian cells," The Journal of Histochemistry and Cytochemistry. 27, 36-43 (1979).

35. J. Soltys, Giardia lamblia: cell biology and microscopy of one of the most primitive eukaryotes,http://www.geocities.com/CollegePark/Lab/4551/

5.7 Figures

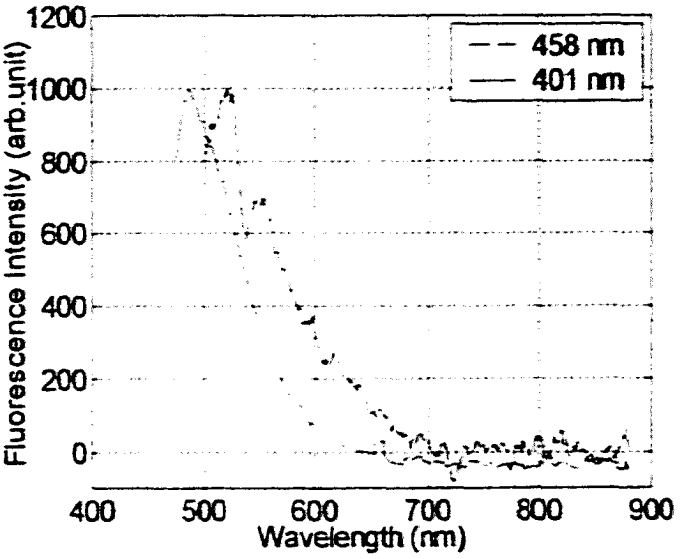

Fig. 5.1. Comparison of the ONF spectra of L-tryptophan when the excitation wavelength is changed from 458 to 401 nm.

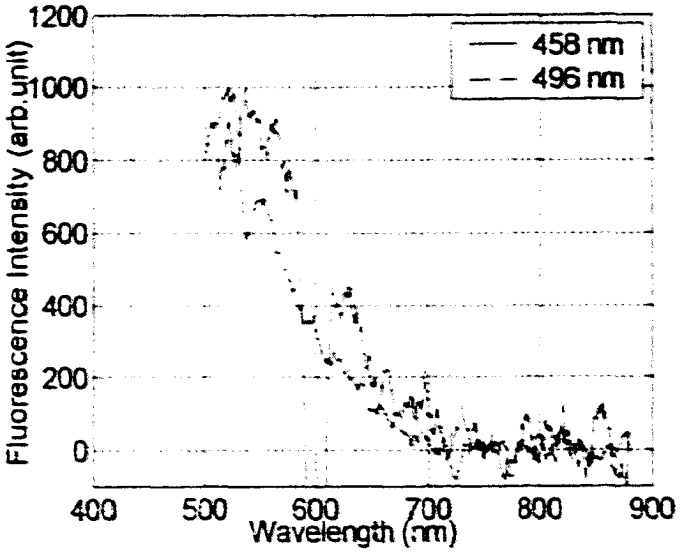

Fig. 5.2. Comparison of the ONF spectra of L-tryptophan when the excitation wavelength is changed from 458 to 496 nm.

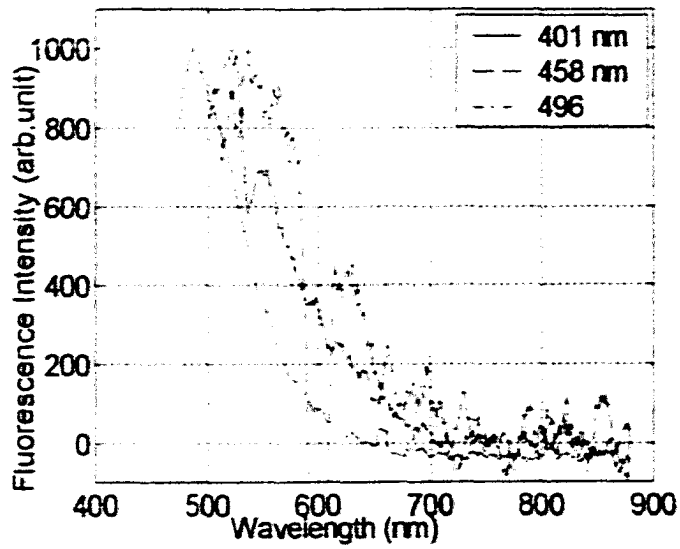

Fig. 5.3. Comparison of the ONF spectra of L-tryptophan when the excitation wavelength is changed from 401,458, and 496 nm.

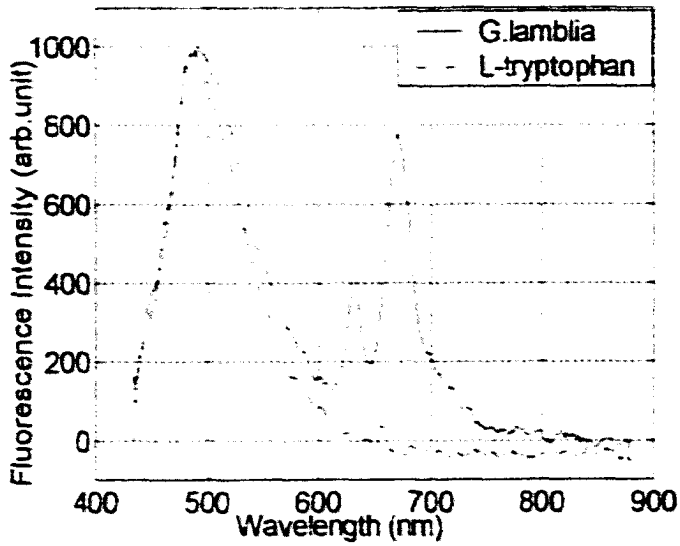

Fig. 5.4. Comparison of the ONF spectra G.lamblia and L-tryptophan when the excitation wavelength is 401nm.

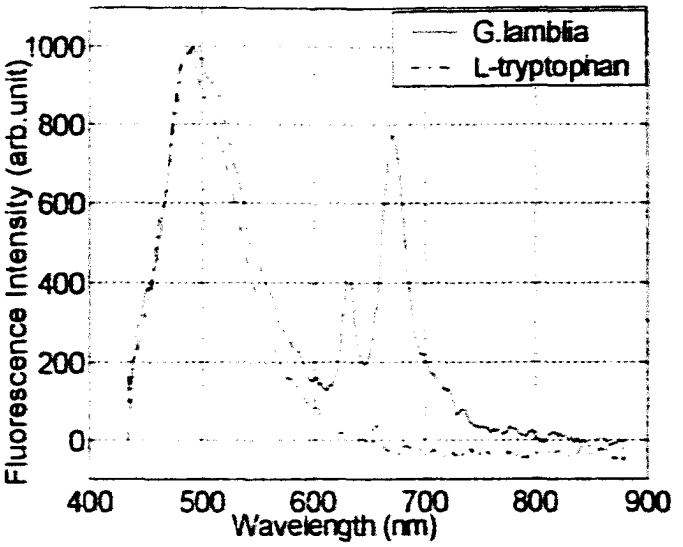

Fig. 5.5. Comparison of the ONF spectra G.lamblia and L-tryptophan when the excitation wavelength is 458 nm.

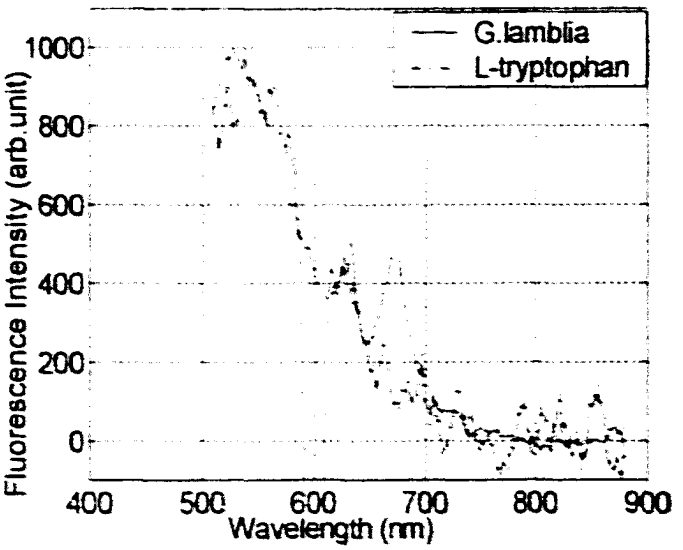

Fig. 5.6. Comparison of the ONF spectra G.lamblia and L-tryptophan when the excitation wavelength is 496 nm.

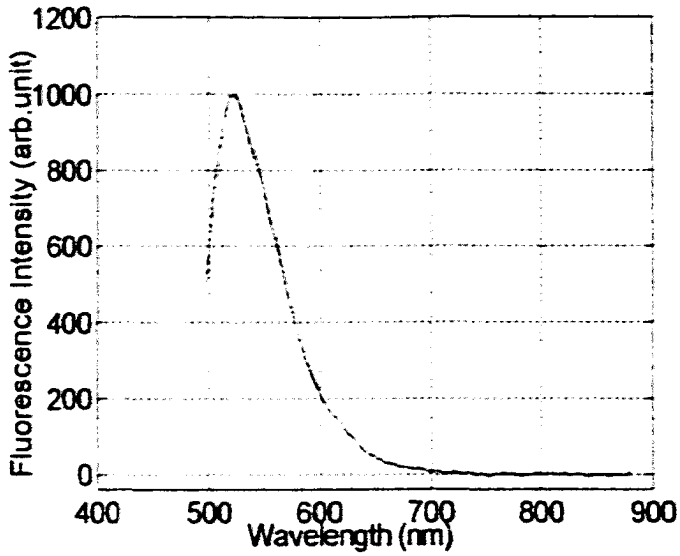

Fig. 5.7. Comparison of the ONF spectra of FAD when the excitation wavelength is changed from 458 to 401 nm.

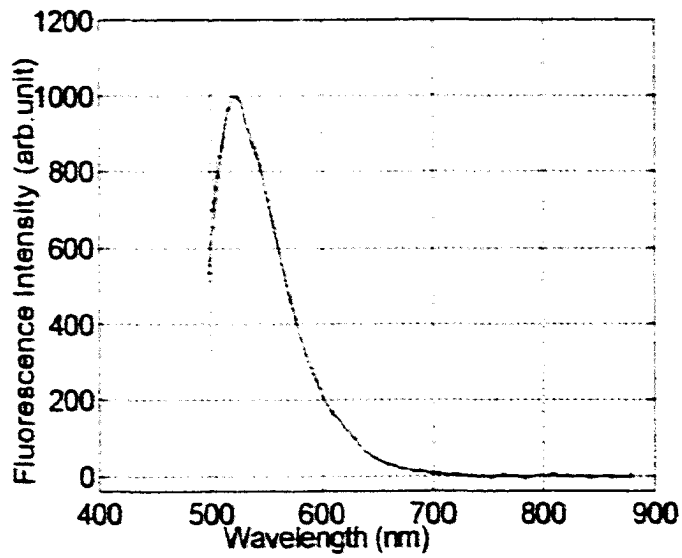

Fig. 5.8. Comparison of the ONF spectra of FAD when the excitation wavelength is changed from 458 to 496 nm.

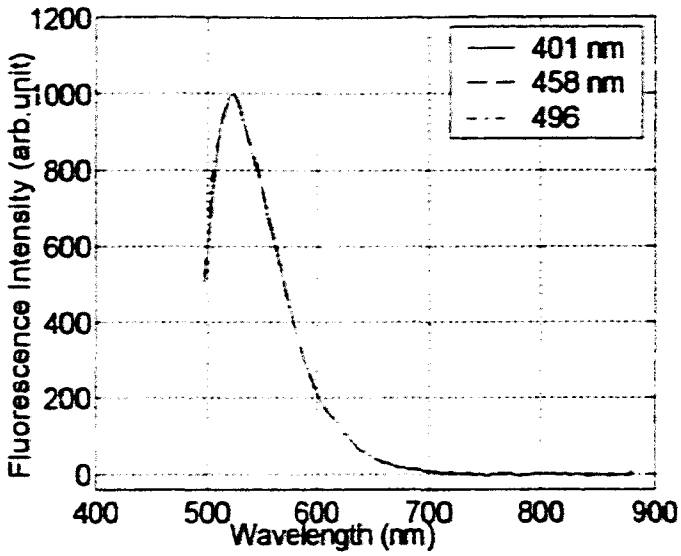

Fig. 5.9. Comparison of the ONF spectra of FAD when the excitation wavelength is changed from 401,458, and 496 nm.

Chapter 6

A study of the integrated fluorescence intensity from G. lamblia cysts and other microorganisms as a function of time under continuous excitation

6.1 Introduction

This Chapter will concentrate on the fluorescence intensity of the microorganisms versus time under continuous laser excitation. The characteristic decay of the intensity as a function of excitation time can be used to help distinguish G. lamblia cysts from other microorganisms.

6.2 The integrated fluorescence intensity as a function of excitation time for a CLUSTER of G. lamblia cysts excited at 458 nm (Argon ion laser line)

6.2.1 Pf = 10 mW

The 458 nm emission of the Argon ion laser was used to excite the ONF from G. lamblia of different ages. The power of the laser coming out of the excitation fiber (Pf) was usually set at 10 mW. This power corresponded to an intensity of 16 W/cm^2 falling directly on the microscope slide that carried the G. lamblia cysts sample.

The following figures plot the integrated fluorescence intensity (IFI) as a function of the excitation time. Each curve stands for one continuous excitation of a fixed sample and is normalized according to the maximum intensity, which usually occur during the first few seconds upon initiation of excitation.

Figure (6.1) shows a batch of IFI decay from G. lamblia that were 4 days old. The total lengths of the excitation were 120, 184, 192, and 356 seconds respectively. Each data point corresponds to an integration time of approximately 4 seconds. This figure shows a reproducible decay of IFI for G.lamblia cysts. Likewise, Figure (6.2) shows a batch of IFI decay from G. lamblia that were 60 days and 111 days old. The total lengths of excitation time are 180, 128, 80, 200, 240, 220, 152, and 220 seconds. This figure again shows a reproducible decay of IFI for G.lamblia cysts under 458 nm excitation.

Therefore, the decay in each figure can be averaged to represent typical decay of G. lamblia in each age group. The average decay from very old cysts (60 to 111 days old) is compared with that from very young ones (4 days old) in figure (6.3). The result indicates that, although the two groups of cysts that are extremely different in age, their decay are very similar in shape.

More data were taken to verify the reproducibility of the decay of IFI from G. lamblia cysts. Figure (6.4) shows a group of IFI decay from G. lamblia that were 47 days and 50 days old, where each data point corresponds to an integration time of approximately 5 seconds. The total lengths of the excitation were 475 and 435 seconds respectively. The decay is reproducible too. Likewise, figure (6.5) shows the IFI decay from a sample that were 5 days old, and the total lengths of the excitation were 100 seconds, which also overlap with each other. Therefore, the decay in each figure can be averaged to represent typical decay of G. lamblia in each age group. The average decay from old cysts (47 to 50 days old) is compared with that from very young ones (5 days old) in figure (6.6). These results confirm that the age of the G. lamblia sample does not have any apparent effect on the decay of the IFI.

6.2.2 Pf = 2.5 mW

In addition to the 10 mW power used above, G. lamblia cysts were also excited at lower excitation power of 2.5 mW out of the excitation fiber. Figure (6.7) shows a batch of IFI decay from a sample that were 1 to 5 days old under such low power excitation, where each data point corresponds to an integration time of approximately 4 seconds. This figure show that the IFI decay of G. lamblia also decays under lower power excitation and the decay is reproducible in general. The variation among these decays is small enough to allow an average of all the data.

6.3 The IFI as a function of excitation time for SINGLE G. lamblia cyst excited at 458 nm (Argon ion laser line)

The laser power out of the excitation fiber is 10 mW for this experiment. Lower excitation power was not used because the emission intensity of single cyst under 2.5 mW excitation was too low to be detectable.

Figure (6.8) shows a decay of IFI decay from single G. lamblia that were19 days old, where each data point corresponds to an integration time of 4 seconds. This figure shows that slower decay and more fluctuations compared to the IFI from a cluster of G. lamblia cysts. It may be that due to the bleaching of the cell exceeded to the background surrounded it.

6.4 The IFI as a function of excitation time for a CLUSTER of G. lamblia cysts excited at 401 nm (blue diode laser)

The 401 nm emission of a blue diode laser was used to study the ONF decay from G. lamblia. The power out of the excitation fiber was 2.2-2.5 mW. This corresponds to an excitation intensity of 4 W/cm^2.

Figure (6.9) shows the IFI decay from G. lamblia that were 2 days and 5 days old, and the integration time for each data point was 4 seconds. Likewise, figure (6.10) shows the IFI decay from G. lamblia that were 32 days old. The variation among the data is small enough to allow an average of the IFI decay that represents typical decay of G. lamblia in each age group. The average decay from old cysts (32 days old) is compared with that from young ones (2 to 5 days old) in figure (6.11).

The result indicates that, although the two groups of cysts that are different in age, their decay are similar in general.

6.5 The IFI as a function of excitation time for SINGLE G. lamblia cyst excited at 401 nm (blue diode laser)

The 401 nm emission of a blue diode laser was used to study the ONF decay from single G. lamblia. The power out of the excitation fiber was 2.2-2.5 mW.

Figure (6.12) shows the IFI decay from single G. lamblia cyst that was 36 days old, where the integration time for each data point was 4 seconds. The decay appears to be slower compared to that for a cluster of cysts at 401 nm excitation; however, further work is needed to confirm this result.

6.6 The IFI as a function of excitation time for Cluster of G. lamblia cysts excited at 496 nm (Argon ion laser line)

When the excitation wavelength was 496 nm, the power out of the excitation fiber was varied between 10 and 2.5 mW. The integration time for each data point is 4 seconds. Figure (6.13) shows a batch of IFI decay of G. lamblia sample that were 2 days old, measured with the power out of the excitation fiber at 10 mW. The variation among the data is small enough to allow an average of the IFI, as in figure (6.14). Likewise, figure (6.15) shows a batch of IFI decay of G. lamblia that were 5 days old, measured with the power out of the excitation fiber at 2.5 mW.

6.7 The IFI as a function of excitation time for Paramecium excited at 458 nm

The excitation condition for Paramecium under 458 nm is similar to that used fo G. lamblia. The power out of the excitation power was set at 10 mW. Where each data point corresponds to an integration time of approximately 5 seconds.

Figure (6.16) shows a batch of decays of IFI decay from Paramecium of sample # 1. The variation between the decays is much larger compared to that for G. lamblia.

6.8 The IFI as a function of excitation time for Paramecium excited at 401 nm

The excitation condition for Paramecium under 401 nm excitation is similar to that used fo G. lamblia. The power out of the excitation power was set at 2.2-2.5 mW. Where each data point corresponds to an integration time of approximately 4 seconds.

Figure (6.17) shows a batch of IFI decay for Paramecium of sample #2. In contrast to the data at 458 nm and those for G. lamblia, the IFI data for Paramecium under 401 nm

excitation do not show a monotonic decay. This may due to the 401 nm effecting on the internal structure of paramecium decay.

6.9 The IFI as a function of excitation time for Rotifer excited at 458 nm

The excitation condition for Rotifer under 458 nm is similar to that used for G. lamblia. The power out of the excitation power was set at 10 mW.

Figure (6.18) shows the IFI decay for Rotifer of sample A, measured using the objective lens of 20X. The integration time for each data point is 5 seconds. On the other hand, figure (6.19) shows a decay of Rotifer of sample A measured with objective lens of 10 X. The power out of the excitation power was set at 10 mW. The integration time for each data point is 4 seconds. By changing the integration time and the objective lens it may have an effect of the bleaching of the microorganism.

6.10 The IFI as a function of excitation time for Rotifer excited at 401 nm

The excitation condition for Rotifer under 401 nm excitation is similar to that used fo G. lamblia. The power out of the excitation power was set at 2.2-2.5 mW. Where each data point corresponds to an integration time of approximately 4 seconds.

Figure (6.20) shows a batch of IFI decay for Rotifer of sample B. In contrast to the data at 458 nm and 401nm those for G. lamblia, the IFI data for Rotifer under 401 nm excitation show a monotonic decay. It may be that due to the bleaching of the cell exceeded to the background surrounded it.

6.11 The IFI as a function of excitation time for Rotifer excited at 496 nm

The excitation condition for Rotifer under 496 nm excitation is similar to that used fo G. lamblia. The power out of the excitation power was set at 10 mW. Where each data point corresponds to an integration time of approximately 4 seconds.

Figure (6.21) shows the IFI decay for Rotifer of sample A measured with the objective lens of 10 X. This figure shows a non-monotonic decay compared to the G. lamblia.

6.12 The IFI as a function of excitation time for a CLUSTER G. muris excited at 458 nm

The excitation condition for G.muris under 458 nm excitation is similar to that used fo G. lamblia. Figure (6.22) shows a batch of IFI decay for a cluster of G. muris cysts that were 1 day old, under 458 nm excitation, measured with the laser power out of the excitation fiber at 10 mW. The integration time for each data point was 4 seconds. The variation among the data is larger compared to G. lamblia.

6.13 The IFI as a function of excitation time for single G. Muris excited at 458 nm

Figure (6.23) shows a batch of IFI decay for single G. muris cyst that were 1 day old, under 458 nm excitation, measured with the laser power out of the excitation fiber at 10 mW. The integration time for each data point was 4 seconds. The variation among the data is similar compared to single G. lamblia cyst under 458 nm excitation.

6.14 Comparison of the decays of IFI for Giardia lamblia cysts excited at different wavelengths

Figure (6.24) shows that the averaged IFI decay for G. lamblia cysts (cluster) excited at different wavelengths (401 nm, 458 nm, and 496 nm) and collected with the same integration time of 4 seconds. The laser power out of the excitation fiber is fixed at 2.5 mW. The figure shows that 401 nm excitation induces the slowest decay in IFI from G. lamblia cysts compared to 458 nm and 496 nm under the same excitation intensity.

Figure (6.25) shows the averaged IFI decay for G. lamblia excited at 458 nm with different excitation power (2.5 mW and 10 mW out of the excitation fiber). The integration time was fixed to be 4 second. The decay (photobleaching) of the IFI for G. lamblia is faster when the excitation intensity is higher.

6.15 The recovery of IFI for G. lamblia during relaxation between excitations

Figure (6.26) shows that the IFI decay for G. lamblia under 458 nm excitation, measured with the laser power out of the excitation fiber at 10 mW. The integration time was 5 seconds. The excitation was interrupted during the photobleaching in order to investigate the effect of recovery of fluophores. Likewise, figure (6.27) shows the ONF spectral recovery shape for the data in figure (6.26).

The initial excitation lasted for 65 seconds; the laser was blocked and the G. lamblia cysts were allowed to relax in darkness for 10 minutes 24 second; then they were excited again for another 40 seconds and then allowed to relax for 12 minutes 24 seconds; finally, they were excited again for 35 seconds.

When the excitation light is kept focused on the cell, the cell's auto-fluorescence drops continuously. But when the excitation light is interrupted and blocked from reaching the excited cell, the fluorophore in the cell from the areas surrounding the excited spot will spread to it, which causes the fluorescence intensity to recover. This is called Fluorescence recovery after photobleaching [1]. It notice that the IFI for G. lamblia has recovered approximately 40% of the first IFI during the first relaxation and 30% of the first IFI during the second relaxation.

6.16 The ONF spectra for G. lamblia during the decay of its IFI

The ONF data during the decay and recovery of IFI are normalized to compare their spectral shape. When figure (6.27) is normalized as in figure (6.28) where the recovered signal gets a little broadening to the right. The initial excitation lasted for 65 seconds; the laser was blocked and the G. lamblia cysts were allowed to relax in darkness for 10 minutes 24 second; then they were excited again for another 40 seconds and then allowed to relax for 12 minutes 24 seconds; finally, they were excited again for 35 seconds. Figure (6.29) shows the first ten ONF of G. lamblia upon the initiation of excitation at 458 nm, where the excitation power out of the excitation fiber is 10 mW and the integration time is 4 seconds. The spectra are all normalized to their maximal as in figure (6.30). The figure shows that during the initial decay of the IFI, the ONF are still reproducible in shape even though photobleaching was decreasing the IFI by a substantial amount.

However, Figure (6.31) shows the ONF spectra of G.lamblia after 80 second and 180 second of excitation with that at the beginning of the excitation. The excitation wavelength is 458 nm, with power out of the excitation fiber is 10 mW and the integration time is 4 seconds. In addition, after longer excitation time, the ONF spectra are broadened compared to the initial one. As in figure (6.32) that compares the ONF data for of G. lamblia after 80 second and 180 second of excitation with that at the beginning of the excitation. This concludes that the ONF spectra are for broadening foe longer continuous excitation time until the broadening is stopped.

6.17 Discussions

Another main limitation is the finite duration of emission as a result of photobleaching (Photodestruction of fluorophores). It always depends on the presence of molecular oxygen, which shortens the fluorophore's dark triplet excited state by quenching; producing the highly reactive singlet oxygen that then attacks the fluorophore and bleaches it. Removing oxygen will prolong the fluorophore lifetime with respect to photobleaching but at the same time will increase the triple-state lifetime [3].

However, due to that thousands of different chemical reactions take place within the microorganism's cells, Such as diverse activities as the synthesis and breakdown of chemical building blocks and macromolecules, the conversion of chemical energy, and the transmission of genetic information [1]. In addition, living organisms have *enzymes* to speed up the rate of chemical reactions and the microorganism's cells manufacture several thousand different enzymes, each enhancing the rate of different chemical

reaction [1]. These can be a factor of different reactions of the continuous excitation on the microorganisms compared to the G. lamblia cysts in the factor of time.

The photobleaching of G. lamblia may due to chemical reactions of the excited molecule, which destroy it or destroy its fluorescence. The speed of the photobleaching is proportional to the fraction of the total time that the molecule of the cell spends in the excited states where the ground state is stable. The fraction of the time that the molecule spends in the excited states depends on the how often the molecule is irradiated in the excited state and how long it is stays there each time [4].

However, when *Giardia lamblia* is excited at 401 nm under the same excitation power used for 458nm excitation, the fluorescence intensity levels off at a much higher value relative to its maximum during its decay.

Furthermore, the G.lamblia cell is excited with continuous and constant illumination intensity, which means that the molecules of the cell are excited and reexcited at same rate. Thus G.lamblia is bleached fast at 458 nm excitation is due to molecules spending of longer of time in the excited state which means there is more chances for molecules of the G.lamblia cell to decomposition. In contrast, G.lamblia is bleached slower at 401 nm excitation.

On other hand, the speed (lifetime) of bleaching G.lamblia has been changed by changing the illumination intensity. Thus, it is important to know that the bleaching lifetime (speed) of the intrinsic fluorescent molecule in the G.lamblia cell to destroy the molecule of the cell controlled by the time and the exposure intensity.

During the fluorescence experiment, the microorganisms (G. lamblia, Paramecium, Rotifer, and G. muris) studied in this work were observed to emit time-dependent

fluorescence intensity under continuous laser excitation. The intensity of G. lamblia tends to decrease rapidly at the beginning of the excitation. The decay gradually slows as the excitation time is increased until the intensity levels off to a relative stable value. Although, as shown in chapter 3, G. lamblia shows similar fluorescence spectrum to Paramecium and Rotifer under 458 nm excitation, there is a clear difference between them in the decay of the fluorescence intensity at this excitation wavelength. Giardia lamblia is observed to show a highly reproducible decay as a function of excitation time under fixed excitation intensity. In contrast, due to their complex internal structure as well as motility and rapid lyses of prepared sample, both Paramecium and Rotifer exhibit highly unstable decay as a function of excitation time. It probably that, for Rotifer and Paramecium uncontrolled or unknown changes in the environment may cause spectral diffusion and changes in quantum efficiency.

On the other hand, the clearly different decay feature in the fluorescent intensity of Giardia, paramecium, and rotifer reveals that the excitation dynamics is different in these organisms. G.lamblia cyst has the smallest cell volume and is entirely covered by the laser excitation, while paramecium and rotifer are in general larger than the excitation spot. Therefore, the whole ensemble of fluorophores in G.lamblia is excited and bleached, whereas only a part of the paramecium and rotifer are. Over the time scale of the experiment, paramecium and rotifer can refresh the fluorophores more effectively than G.lamblia. Therefore, the decay of fluorescence intensity in paramecium and rotifer tends to decay slower than G.lamblia.

To help understand the decay of IFI for microorganisms, continuous excitation at the same wavelengths as those used for G. lamblia was also applied to tryptophan and FAD in aqueous solutions (data not shown here). In contrast to the decay of IFI for microorganisms, tryptophan and FAD show no decay in their IFI during the experiment. This is understandable because tryptophan and FAD do not go through the cellular photobleaching as the microorganisms do. The result also indicates that the decay of IFI for microorganisms are not due to photochemical changes of the fluorophores themselves.

6.18 Conclusion

The fluorescence intensity for G. lamblia cysts undergoes a non-exponential decay under continuous excitation at all the laser wavelengths used (401 nm, 458 nm, and 496 nm). The decay is highly reproducible in shape, in contrast to other microorganisms.

6.19 Reference

1. A.D. Bray, J. Lewis, M. Raff, K. Roberts, and J. D. Watson, Molecular Biology of The Cell, 2nd Ed, (Garland Publishing, Inc. New York & London 1989).
2. W. P. Ambrose, P. M. Goodwin, J. C. Martin, and R. A. Keller, "Single molecule detection and photochemistry on a surface using near-field optical excitation," Physical Review Letters. 72, 160-163 (1994).
3. S. Weiss, " Fluorescence spectroscopy of single biomolecules," Science 283, 1676-1683 (1999).
4. T. Hirschfeld, " Fluorescence background discrimination by prebleaching," The Journal of Histochemistry and Cytochemistry. 27, 96-101 (1979).

6.19 Figures

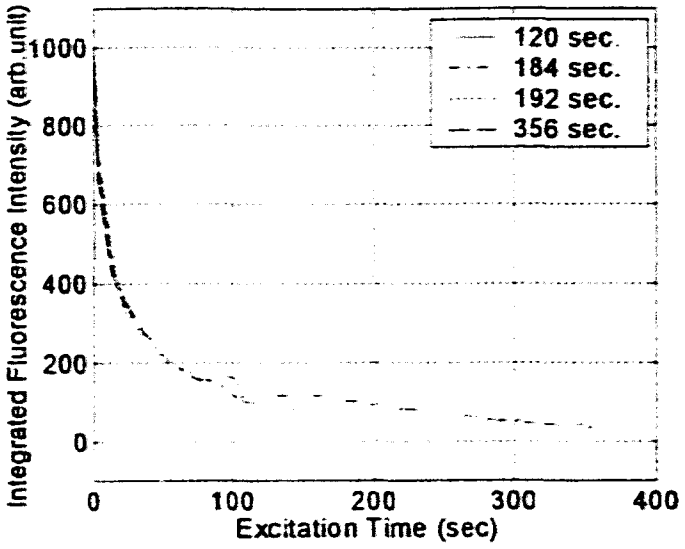

Fig. 6.1. Normalized a batch of integrated fluorescence intensity decay from G. lamblia, that is 4 days old, Pf was 10 mW, and excited at 458 nm. Integration time is 4 seconds.

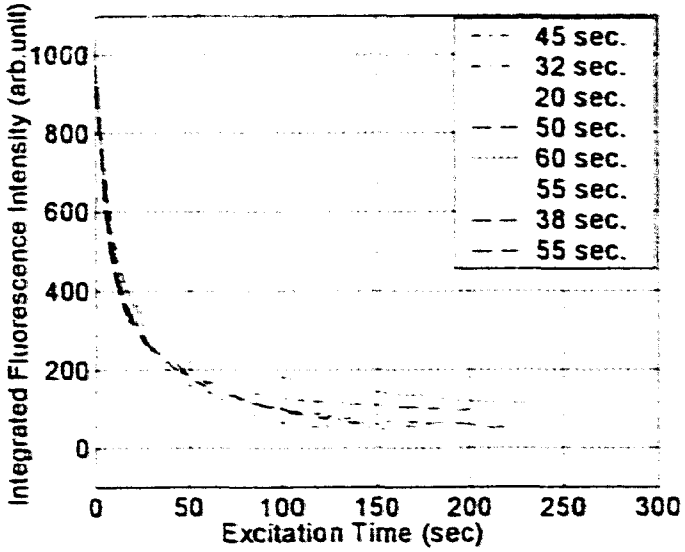

Fig.6. 2. Normalized a batch of integrated fluorescence intensity decay from G. lamblia, that is 60 and 111days old, Pf was 10 mW, and excited at 458 nm. Integration time is 4 seconds.

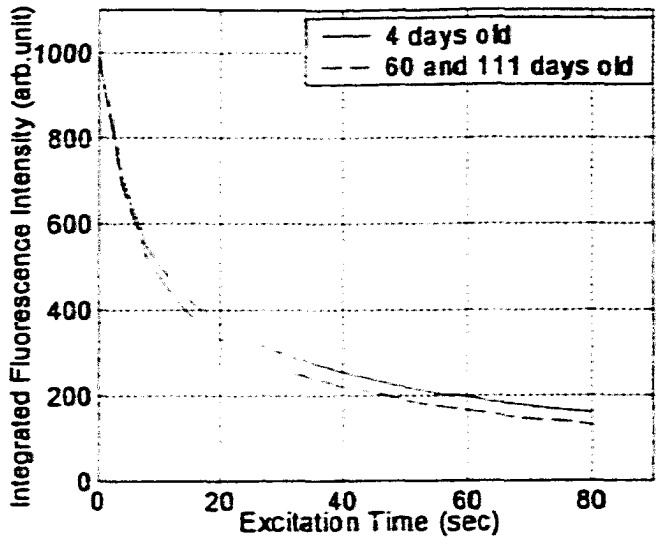

Fig. 6. 3. Comparison of the averaged IFI decays from very old cysts 60 to 111 days old (dashdot) and very young ones 4 days old (solid). Pf was 10 mW, and excited at 458 nm. Integration time is 4 seconds.

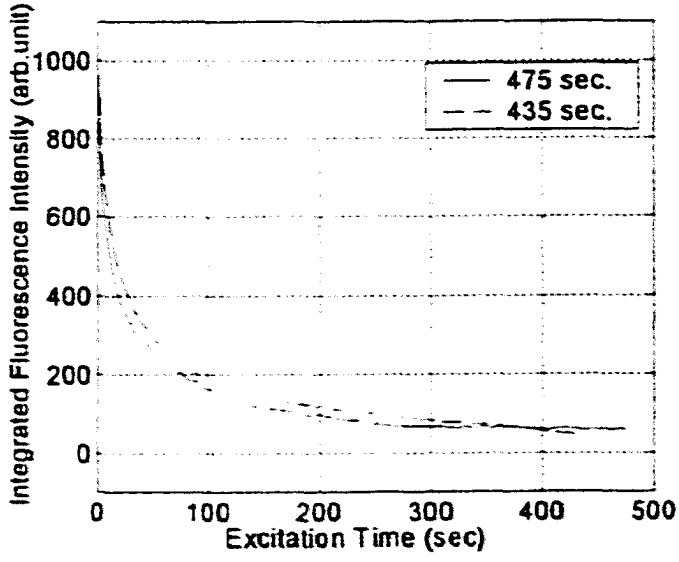

Fig. 6. 4. Normalized a batch of integrated fluorescence intensity decay from G. lamblia, that is 47 and 50 days old. Pf was 10 mW, and excited at 458 nm. Integration time is 5 seconds.

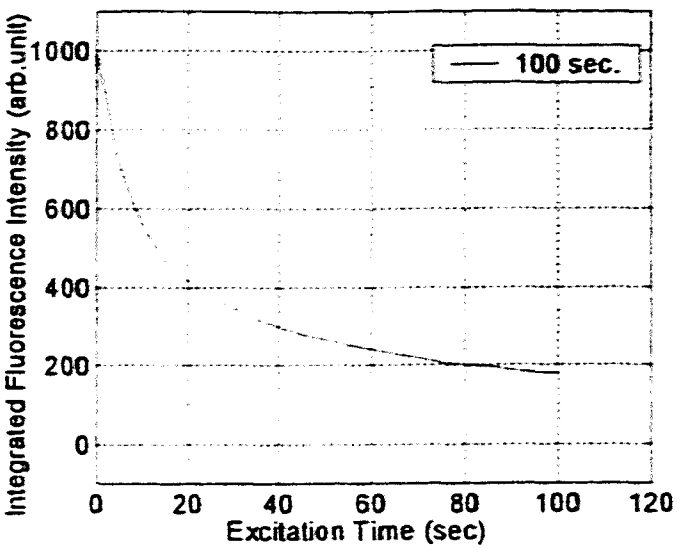

Fig. 6.5. Normalized a batch of integrated fluorescence intensity decay from G. lamblia, that is 5 days old, Pf was 10 mW, and excited at 458 nm. Integration time is 5 seconds.

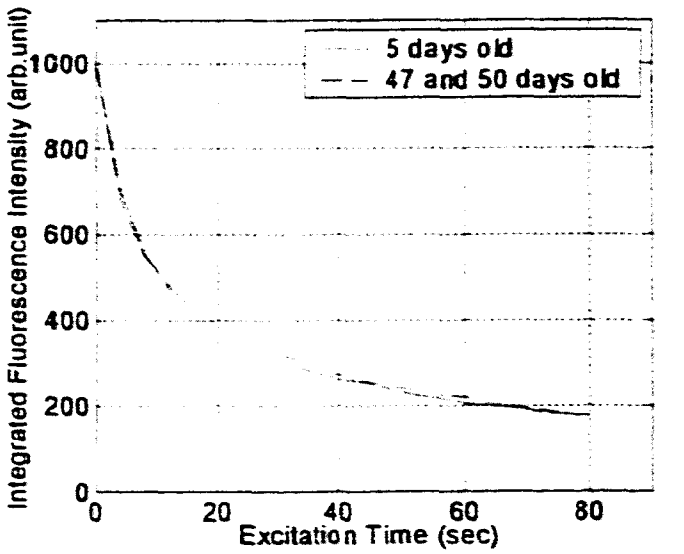

Fig. 6.6. Comparison of the averaged IFI decays from old cysts 47 to 50 days old (dashdot) and very young ones 5 days old (solid). Pf was 10 mW, and excited at 458 nm. Integration time is 5 seconds.

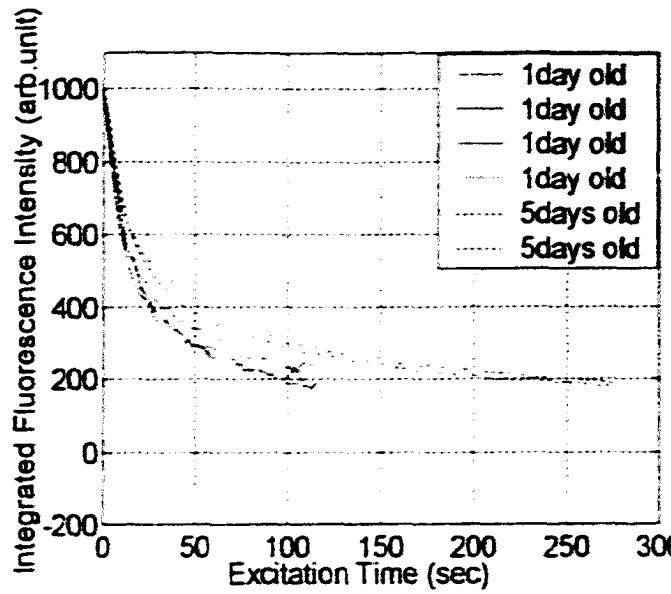

Fig. 6.7. Normalized a batch of integrated fluorescence intensity decay from G. lamblia, that is 1 to 5 days old, Pf was 2.5 mW, and excited at 458 nm. Integration time is 4 seconds.

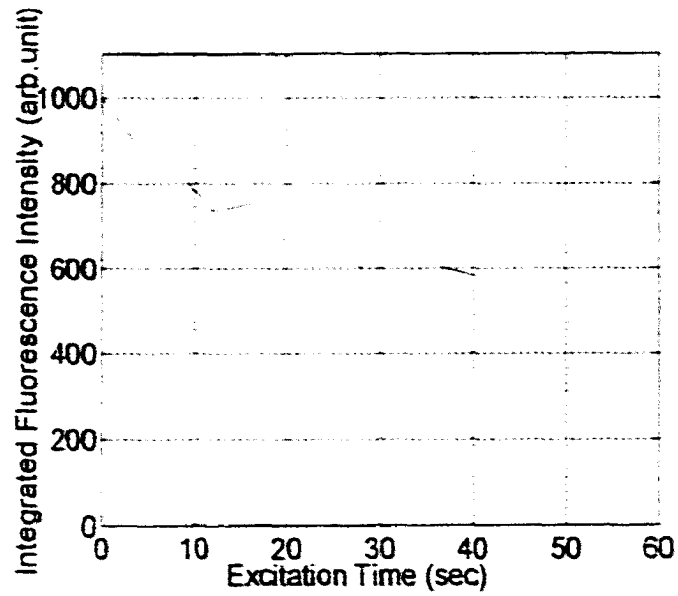

Fig. 6.8. Normalized a batch of integrated fluorescence intensity decay from single G. lamblia, that is 19 days old, Pf was 10 mW, and excited at 458 nm. Integration time is 4 seconds.

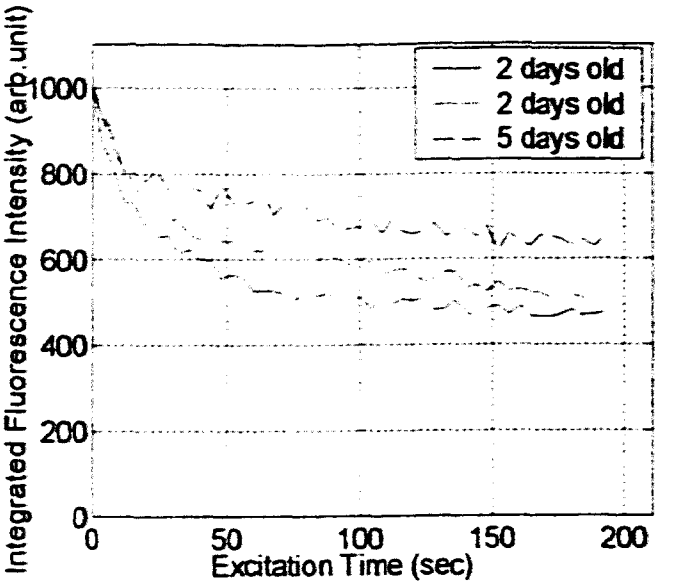

Fig. 6.9. Normalized a batch of integrated fluorescence intensity decay from G. lamblia, that is 2 to 5 days old, Pf was 2.2-2.5 mW, and excited at 401 nm. Integration time is 4 seconds.

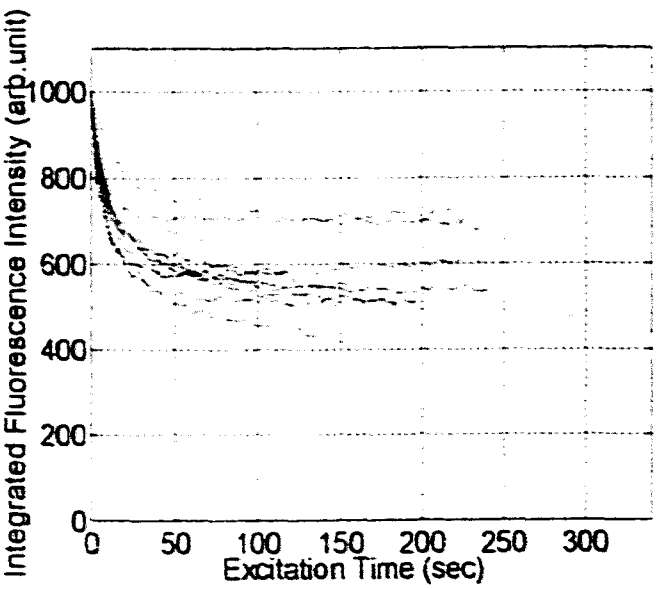

Fig. 6.10. Normalized a batch of integrated fluorescence intensity decay from G. lamblia, that is 32 days old, Pf was 2.2-2.5 mW, and excited at 401 nm. Integration time is 4 seconds.

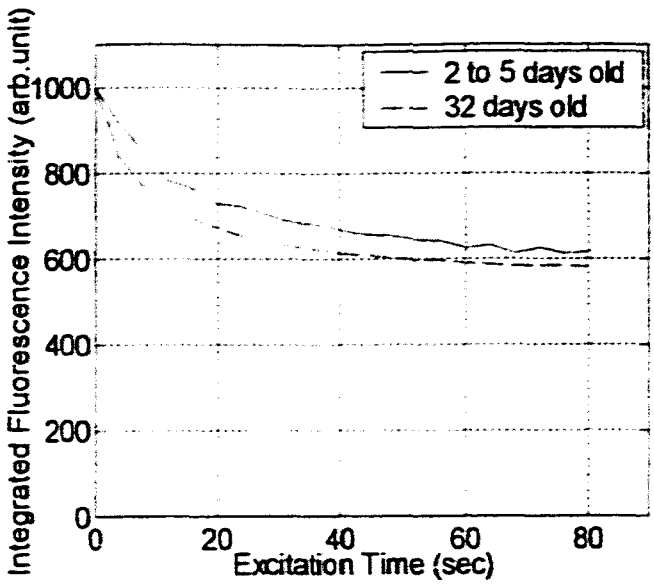

Fig. 6.11. Comparison of the averaged IFI decays from old cysts 32 days old (dashdot) and young ones 2 to 5 days old (solid). Pf was 2.2-2.5 mW, and excited at 401 nm. Integration time is 4 seconds.

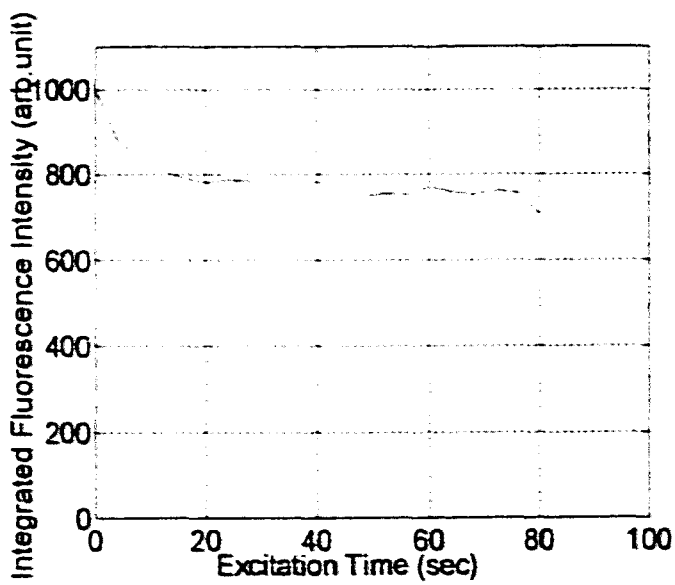

Fig. 6.12. Normalized a batch of integrated fluorescence intensity decay from single G. lamblia, that is 36 days old. Pf was 2.2-2.5 mW, and excited at 401 nm. Integration time is 4 seconds.

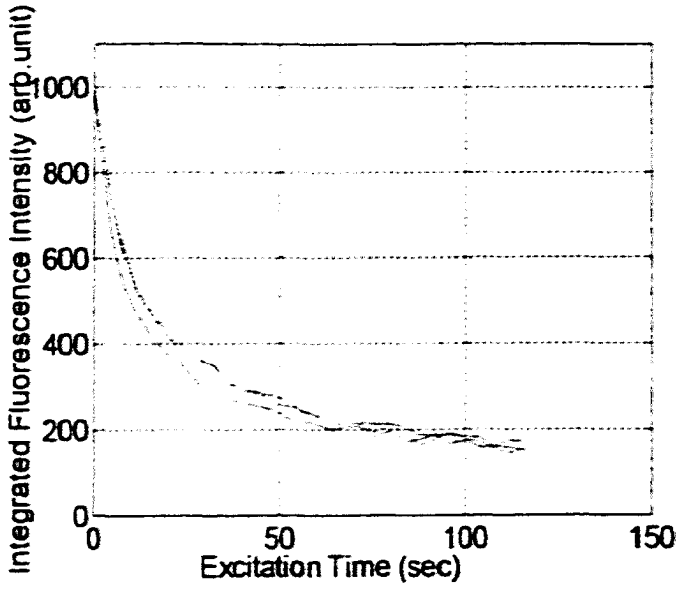

Fig.6. 13. Normalized a batch of integrated fluorescence intensity decay from G. lamblia, that is 2 days old. Pf was 10 mW, and excited at 496 nm. Integration time is 4 seconds.

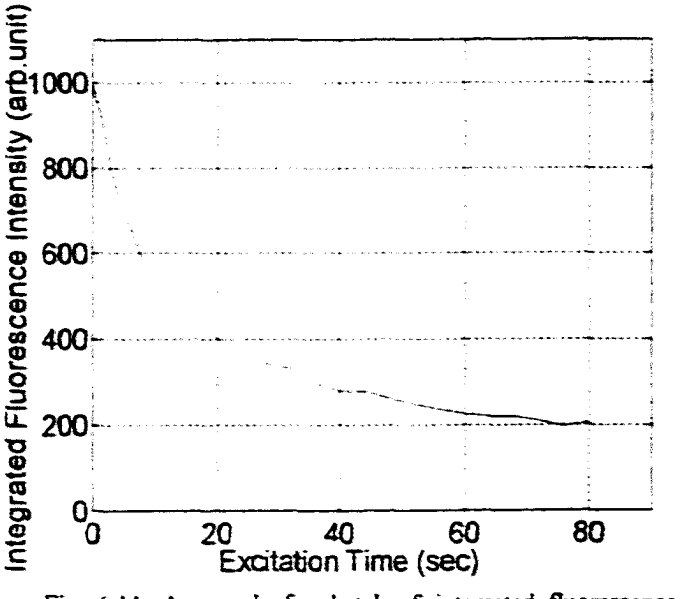

Fig. 6.14. Averaged of a batch of integrated fluorescence intensity decay from G. lamblia, that is 2 days old. Pf was 10 mW, and excited at 496 nm. Integration time is 4 seconds.

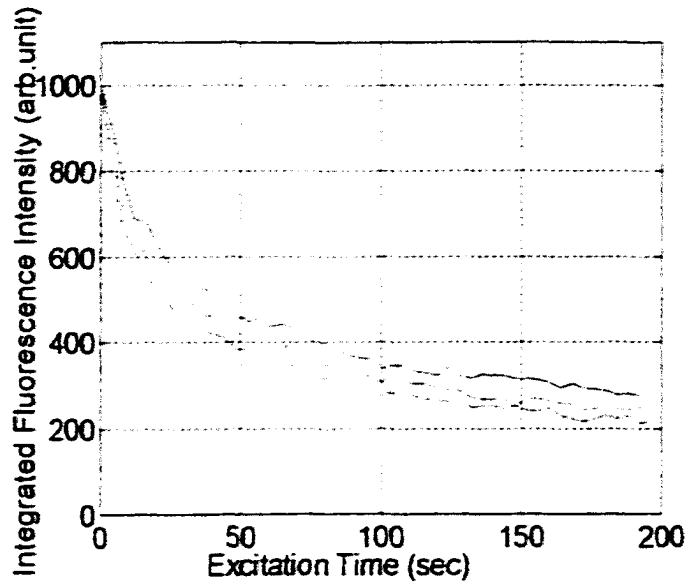

Fig. 6.15. Normalized a batch of integrated fluorescence intensity decay from G. lamblia, that is 5 days old, Pf was 2.5 mW, and excited at 496 nm. Integration time is 4 seconds.

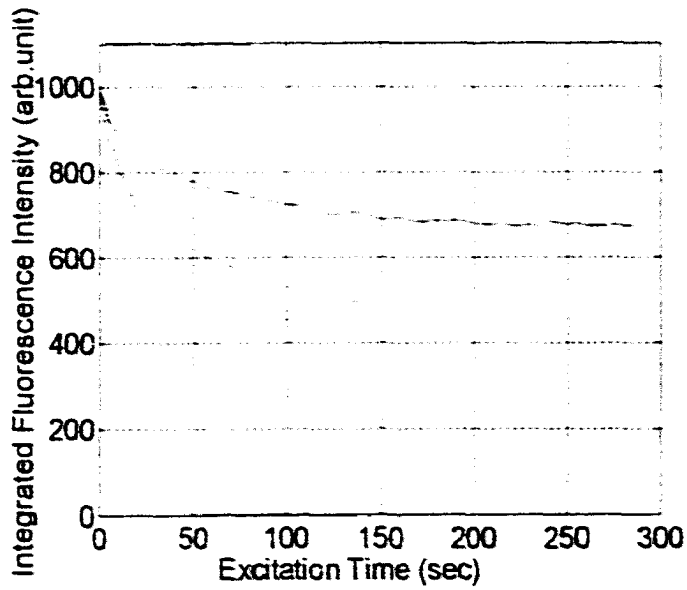

Fig. 6.16. Normalized a batch of integrated fluorescence intensity decay from Paramecium of sample #1, Pf was 10 mW, and excited at 458 nm. Integration time is 5 seconds.

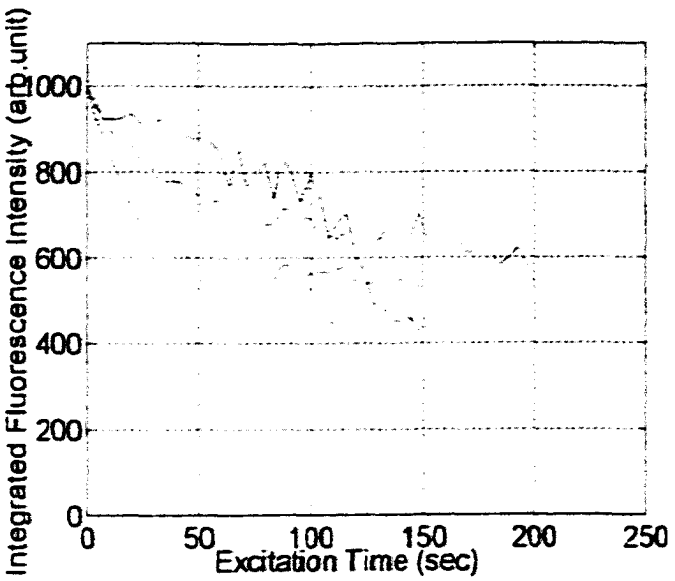

Fig. 6.17. Normalized a batch of integrated fluorescence intensity decay from Paramecium of sample #2. Pf was 2.2-2.5 mW, and excited at 401 nm. Integration time is 4 seconds.

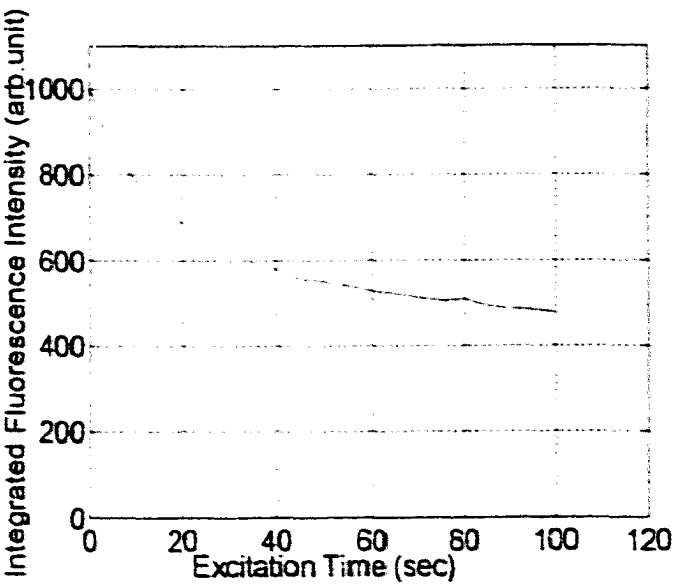

Fig. 6.18. Normalized a batch of integrated fluorescence intensity decay from Rotifer of sample A. Pf was 10 mW, and excited at 458 nm. Integration time is 5 seconds.

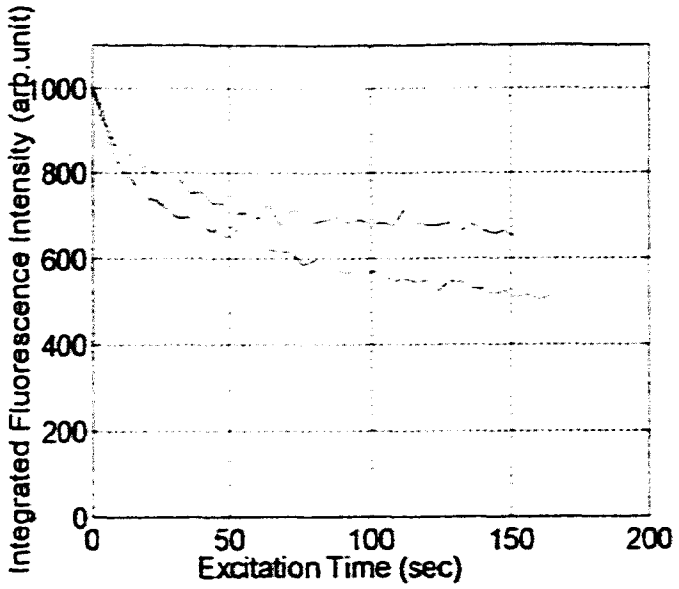

Fig. 6.19. Normalized a batch of integrated fluorescence intensity decay from Rotifer of sample A. Pf was 10 mW, and excited at 458 nm.Using objective lens 10X. Integration time is 4 seconds.

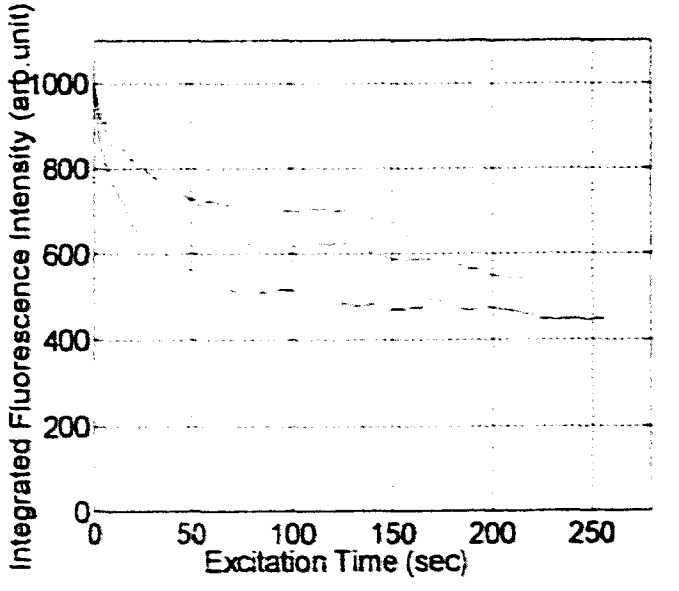

Fig. 6.20. Normalized a batch of integrated fluorescence intensity decay from Rotifer of sample B. Pf was 2.2-2.5 mW, and excited at 401 nm. Integration time is 4 seconds.

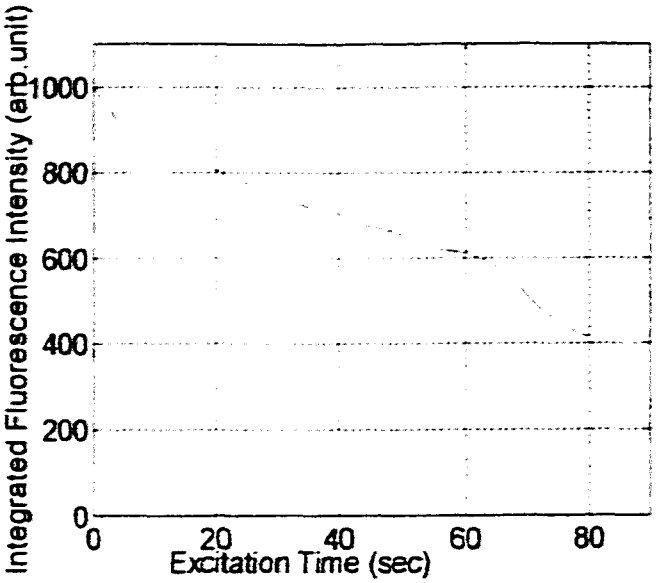

Fig. 6.21. Normalized a batch of integrated fluorescence intensity decay from Rotifer of sample A, Pf was 10 mW, and excited at 496 nm. Using objective lens 10X. Integration time is 4 seconds.

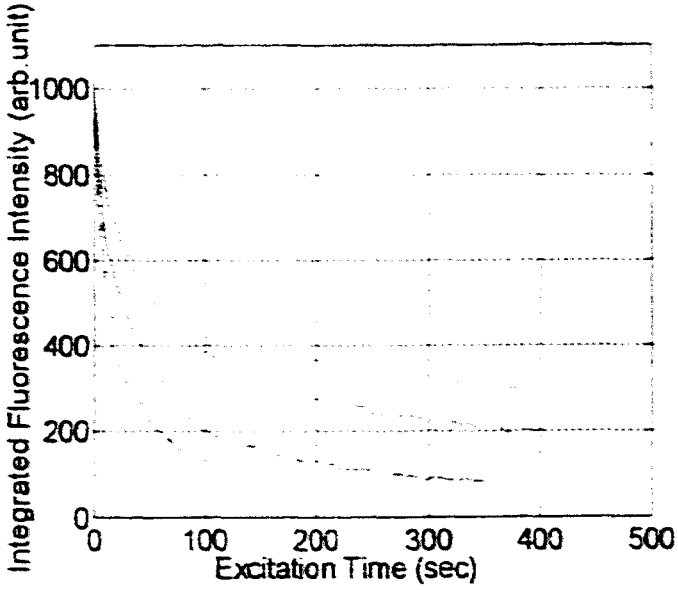

Fig. 6.22. Normalized a batch of integrated fluorescence intensity decay from G. muris, that is 1 day old. Pf was 10 mW, and excited at 458 nm. Integration time is 4 seconds.

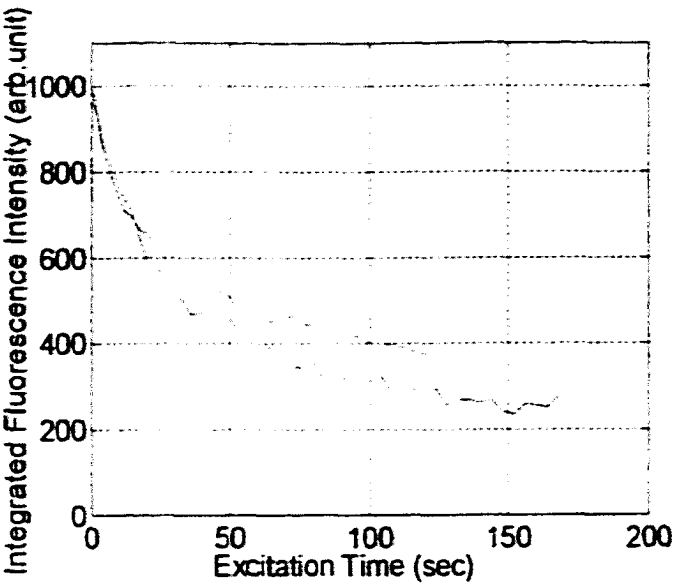

Fig. 6.23. Normalized a batch of integrated fluorescence intensity decay from single G. muris, that is 1 day old, Pf was 10 mW, and excited at 458 nm. Integration time is 4 seconds.

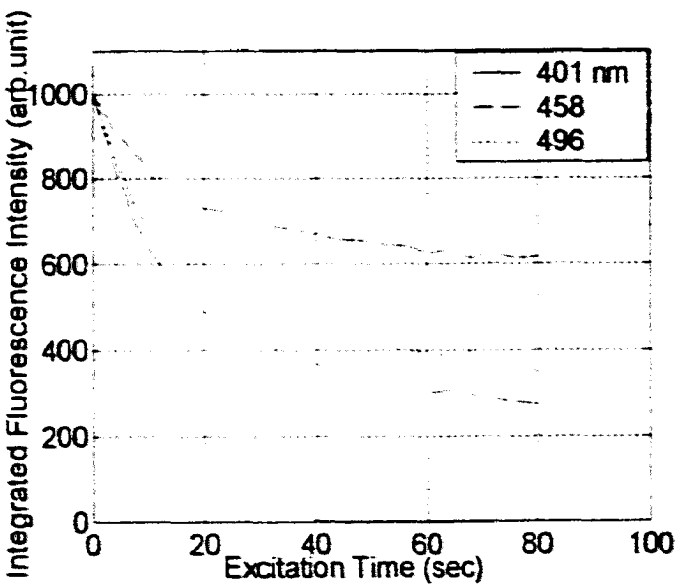

Fig. 6.24. Comparison of the IFI decays for G.lamblia cysts excited at 401 (solid), 458 (dashdot), and 496 nm (dotted) and collected with integration time was 4 seconds, Pf was 2.5 mW.

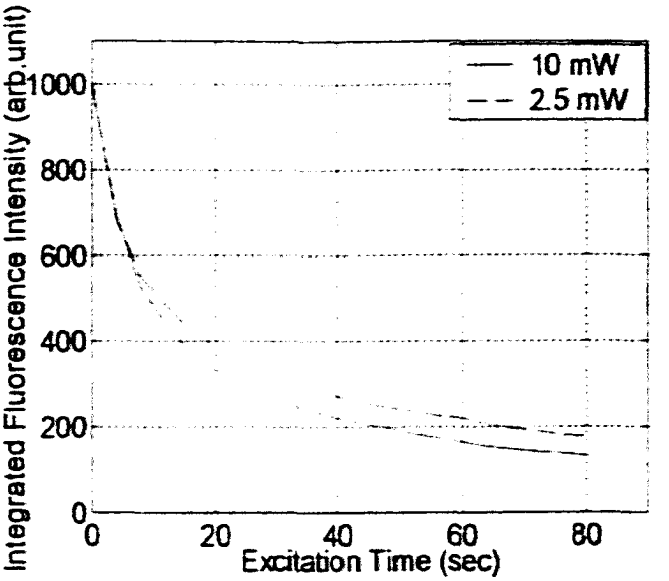

Fig. 6.25. Comparison of the IFI decays for G.lamblia cysts excited at 458 nm with excitation power out of the excitation fiber 10 mW (solid) and 2.5 mW (dashdot), and collected with integration time was 4 seconds.

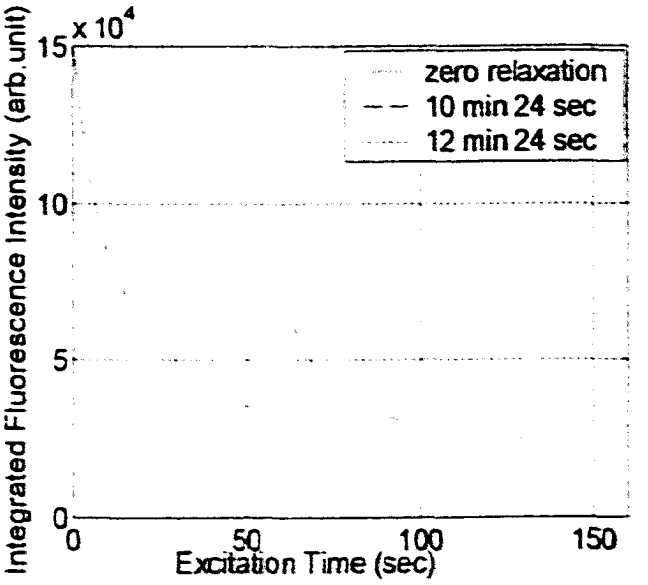

Fig. 6.26. The IFI decays recovery for G.lamblia under 458 nm excitation, the excitation was interrupted during the photobleaching for two time each time for 10 minutes 24 seconds. Pf was 10 mW, and integration time was 5 seconds.

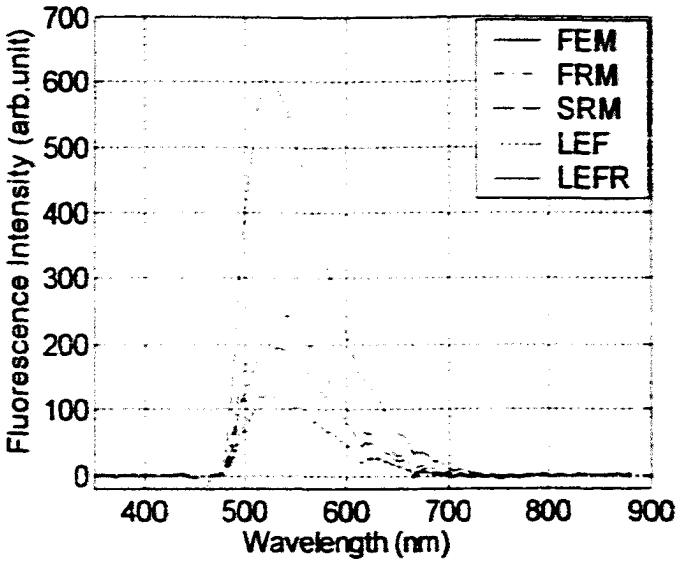

Fig. 6.27. The ONF spectral recovery shape for G.lamblia under 458 nm excitation, the excitation was interrupted during the photobleaching for two time each time for 10 minutes 24 seconds. Pf was 10 mW, and integration time was 5 seconds.

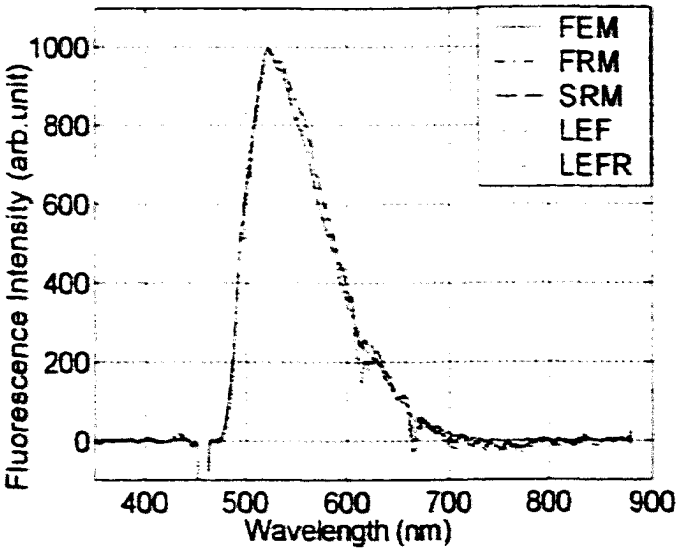

Fig. 6.28. Normalized the ONF spectral recovery shape for G.lamblia under 458 nm excitation, the excitation was interrupted during the photobleaching for two time each time for 10 minutes 24 seconds. Pf was 10 mW, and integration time was 5 seconds.

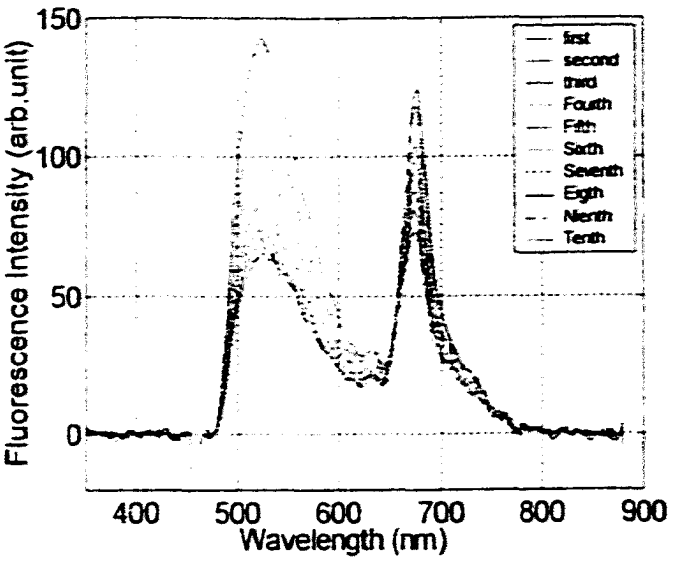

Fig. 6.29. First ten ONF spectra of G.lamblia under 458 nm excitation, the power out of the excitation fiber was 10 mW, the integration time was 4 seconds.

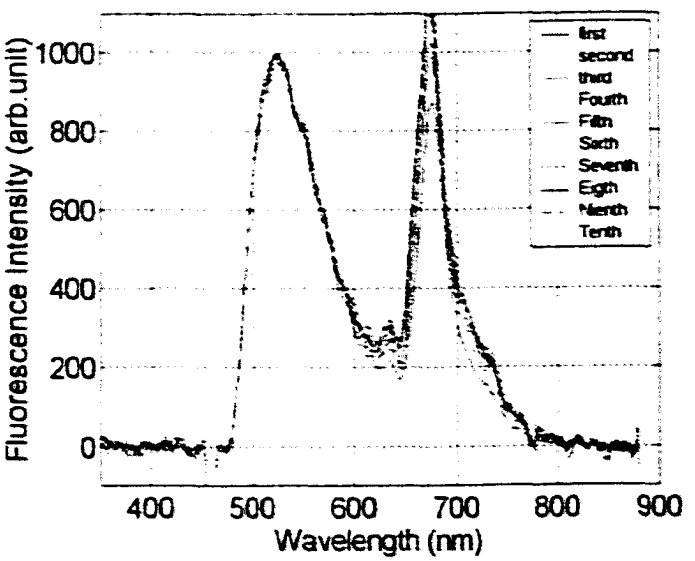

Fig. 6.30. Normalized the first ten ONF spectra of G.lamblia under 458 nm excitation, the power out of the excitation fiber was 10 mW, the integration time was 4 seconds.

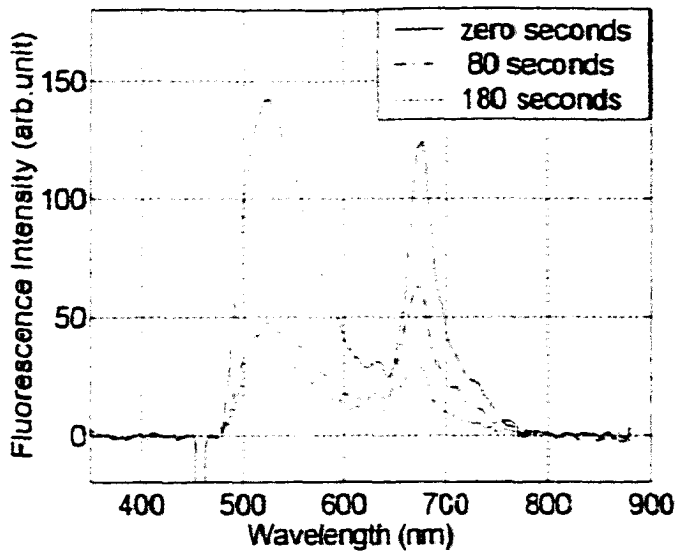

Fig. 6.31. The ONF spectra of G.lamblia after 80 seconds and 180 seconds of excitation with that at the beginning of the excitation. The excitation wavelength 458 nm with Pf was 10 mw, and integration time is 4 seconds.

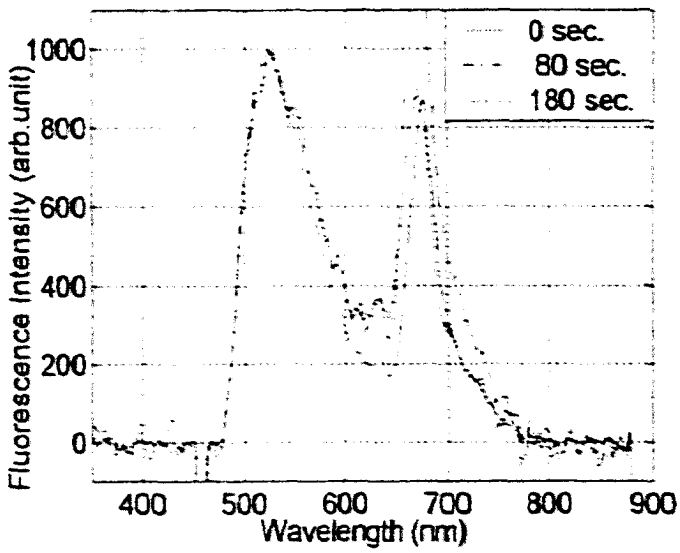

Fig. 6.32. Normalized of the ONF spectra of G.lamblia after 80 seconds and 180 seconds of excitation with that at the beginning of the excitation. The excitation wavelength 458 nm with Pf was 10 mw, and integration time is 4 seconds.

Chapter 7

Future Research Directions

This work breaks ground for the development of fluorescence probes for detecting *Giardia lamblia* cysts. Although the current technique is indispensable a microscope and thin sample medium, future development shoudl aim towards fiber optical dip probe for *in situ* remote sensing. While the laser out of the probe needs to be focused to microscopically sized spots in order to excite fluorescence signal from the cysts, the location of the cysts needs to be first determined by optical back-scattering methods that scan the natural water for particles similar in size to G. lamblia cysts. In such an application, the 401 nm blue laser excitation has the shortest wavelength that is not strongly absorbed by water and the most effective for distinguishing the cysts from other protozoa. At the same time, it may be necessary to combine the ONF spectroscopy with flow cytometry (FC) techniques to facilitate the detection of cysts in the background of other natural fluorophores in real water. Besides distinguishing G. lamblia cysts from other microorganisms, it is important to distinguish live G. lamblia cysts from dead ones through ONF characteristics. Beyond the work on G. lamblia cysts, it will be necessary to study other pathogenic microorganisms such as Cryptosporedium oocysts, which are smaller than G.lamblia cysts but more dangerous to public health.

Chapter 8

Conclusion

The auto-fluorescence of G. lamblia cysts has been successfully detected and identified using 458 and 401 nm excitation with a fiber-optical fluorescence microscopy setup. Excitation at 401 nm results in a distinctive ONF spectral shape of G. lamblia cysts from other microorganisms. The peak of the ONF spectrum of G.lamblia cysts largely agrees with the aromatic amino acid L- tryptophan in aqueous solution at all the excitation wavelengths used. In addition, a reproducible decay of the fluorescence intensity is observed in *Giardia lamblia cysts* under continuous excitation compared to other protozoa.

Bibliography

Chapter 1

1. G.F. Craun, "Waterborne Outbreaks of Giardiasis, Current Statues," In: Giardia and Giardiasis, S. L. Erlandsen, and E. A. Meyer Eds. (Plenum Press, New York, 1984), pp. 243-261.
2. P. Willis and B. Hammond, "Advances in Giardia Research," The University of Calgary Press (1987).
3. G. J. Tortora, B. R. Funke, and C. L. Case, Microbiology: An Introduction, 4th ed. (Benjamin/Cumming, Redwood City, CA, 1992), pp. 313-319.
4. M. W. LeChevallier, W. D. Norton, and T. B. Atherholt, "Protozoa in open reservoirs," J. Am. Water Works Assoc. **89**, 84-96 (1997).
5. S. T. Bagley, M. T. Auer, D. A. Stern, and M. J. Babiera, "Sources and fate of Giardia Cysts and Cryptosporidium Oocysts in surface waters," J. Lake and Reserv. Manage. **14**, 379-392 (1998).
6. S. L. Erlandsen and E. A. Meyer, Giardia And Giardiasis, (Plenum press, New York 1984).
7. Lechevallie, M.W. ET AL., Giardia and Cryptosporidium in water Supplies, AWWARF, Denver, (1991).
8. D. A. Stern, "Monitoring for Cryptosporidium spp. and Giardia spp. and human enteric viruses in the watersheds of the New York City water supply system," http://www.epa.gov/owow/watershed/proceed/stern.html
9. G. Vesey, et al., "Appliction of Flow Cytometry Methods for the Routine Detection of Cryptosporidium and Giardia in Water," Cytometry.**16**, 1-6 (1994).

10. G. Vesey, et al., "Detection of Specific Microorganisms in Environmental Samples Using Flow Cytometry," Methods in Cell Biol. **42**, 489 (1994).

11. IC. Bacon, et al., "Quantitative Classification of Cryptosporidium Oocysts and Giardia Cysts in Water Using UV/VIS Spectroscopy," BIOS: Biomedical Optics Conference (1995).

12. K. Patten, et al., "Rapid Methods for On-line Detection of Cryptosporidium Oocysts and Giardia Cysts," Proc. AWWA WQTC, San Francisco, Calif (1994).

13. D. L. Cruz, A. Armah, and M. Sivaganesan, "Detection of Giardia and Cryptosporidium spp. in Source Water Samples by Commercial Enzyme Immunoassay Kits," Proc. AWWA WQTC, San Francisco, Calif (1994).

14. C. L. Mayer, and C. J. Palmer, "Evaluation of PCR, Nested PCR, and Fluorescent Antibodies for Detection of Giardia and Cryptospridium Species in wastewater," Appl. Envir. Microbiol. **62**, 2081 (1996).

15. C. Water, P. Hibler, "An Overview of the Techniques Used for Detection of Giardia Cysts in Surface Water", Advances In Giardia Research, pp.197-204, 1988.

16. M. W. LeChevallier, ET AL. "Evaluation of the Immunofluorescence Procedure for Detection of Giardia Cysts and Cryptospordium Oocysts in Water." Appl. Envir. Microbiol. **61**,690 (1995).

17. E. C. Nieminski, Frank W. Schaefer III, Jerry E. Ongerth, "Comparison of Two Methods for Detection of Giardia Cysts and Cryptosporiidium Oocysts in Water," Appl. And Envir. Micro. **61**, 1714-1719 (1995).

18. "Development of Performance Evaluation Sample Preparation Protocols for Giardia Cysts and cryptosporidium Oocysts," EPA Contract No. 68-C3-0365. USEPA Water Docket (1996).

19. B. R. Dixon, M. Parenteau, C. Martineau, and J. Fournier, "A comparison of conventional microscopy, immunofluorescence microscopy and flow cytometry in the detection of Giardia lamblia cysts in beaver fecal samples," J. Immuno. Methods. **202**, 27-33 (1997).

20. L. Thiriat, F. Sidaner, and J. Schwartzbrod, "Determination of Giardia cyst viability in environmental and faecal samples by immunofluorescence, fluorogenic dye staining and differential interference contrast microscopy," Lett. Appl. Microbiol. **26**, 237-242 (1998).

21. H. A. Lindquist, A. dufour, L. Wymer, and F. Schaefer III, "Criteria for evaluation of proposed protozoan detection methods," Journal of Microbiology Methods. 37,33-43 (1999).

22. A. Ashendorff, M. Principe, A. Seeley, J. Laduca, L. beckhardt, W. Faber, and J. Mantus, " Watershed protection for new york city's supply," Journal AWWA. **89**,75-88 (1997).

23. G. F. Craun, " surface water supplies and health," Journal AWWA. **80**, 40-52 (1988).

24. R. Hoffman, J. Standridge, A. Prieve, J. Cucunato, and M. Bernhardt, " Using flow cytometry to detect protozoa," Journal AWWA. **89**, 104-111 (1997).

25. S. K. Stephen, J. L. Riggs, P. D. Dileanis, and T. J. Suk. "Isolation and detection of Giardia Cysts from water using direct immunofluorescence," Water resources bulletin, American water resources association. **22**, (1986).

26. J. L. Riggs, K. W. Dupuis, Koichi Nakamura, and David P. Spath, "Detection of Giardia lamblia by Immunofluorescence," Appl. And Envir. Micro. **45**, 698-700 (1983).

27. Walter Jakubowski, *Giardia methods workshop*, Denver, Colorado, 1-12 (1984).

28. W. Jakubowski, S. Boutros, W. Faber, R. Fayer, W. Ghiorse, M. LeChevallier, J. Rose, S. Schaub, A. Singh, and M. Stewart, "Environmental methods for Crypyosporifium," Journal AWWA. 107-121 (1996).

Chapter 2

1. Ocean Optics, Inc. http://www.OceanOptics.com/

2. R. Kingslake, Applied Optics and Optical Engineering, Vol. IV, Optical Instruments Part I, (Academic Press, New York/London, 1967).

3. R. Kingslake, "Applied Optics and Optical Engineering," III, Optical Components, (Academic Press, New York/London, 1965).

4. D. Malacara, Geometrical and Instrumental Optics, 25, methods of Experimental Physics, (Academic Press, Inc. Boston, 1988).

Chapter 4

1. Paramecium caudatum, Ehrenberg, 1838, http://www.microscopy-uk.org.uk/mag/articles/param1.html/.

2. Introduction to the Rotifera - Introduction to the Rotifera Rotifers: http://www.ucmp.berkeley.edu/phyla/rotifera/r

3. Summary-Parasites, DigestiveSystem (i) Giardiamuris. http://ourworld.compuserve.com/homepages/theb

4. Water filters & Giardia Distilled Wisdom, Alan Dove, Bill Tuthill, 1995. http://www.fc.net/~tdeagan/water/one.html

Chapter 5

1. D. Alberts, J. Bray, M. Lewis, K. Raff, and J. D. Watson, Molecular Biology of the Cell, Second Ed.,(Garland Publishing, Inc. New York & London 1989).

2. K. Mathews, K. E. Van Holde, Biochemistry, (The Benjamin/Cummings Publishing Company, Inc. 1983).

3. L. J. Kleinsmith, and V. M. Kish, Principle of Cell and Molecular Biology, Second Ed., (HarperCollins College Publishers, 1995).

4. Branden and J. Tooze, Introduction to Protein Structure, Second Ed., (1999).

5. T. Timperman, K. E. Oldenburg, and J. V. Sweedler, "Native Fluorescence Detection and Spectral Differentiation of Peptides Containing Tryptophan and Tyrosine in Capillary Electrophoresis," Analytic Chemistry. 67. 3421-3426,1995.

6. Yariv, Amnon, Quantum Electronics, (John Wiley & Sons, Inc., New York, 1975).

7. E. A. Permyakov, Luminescence Spectroscopy of Protein (CRC, Boca Raton, FL, 1993).

8. R. Lakowicz, "On Spectral Relaxation in Proteins," Photochem. Photobiol. 72, 421-437 (2000).

9. S. V. Konev, Fluorescence and Phosphorescence of Proteins and Nucleic Acids (Plenum, New York, 1967).

10. R. Lakowicz, "Protein fluorescence," in Principles of Fluorescence Spectroscopy, 2nd ed., J. R. Lakowicz ed. (Kluwer/Plenum, New York, 1999).

11. R. R. Alfano and A. Katz, "Photonic pathology, fluorescence and raman spectroscopy for tissue diagnosis and characterization," in Analytical use of fluorescent probes in Oncology, Kohen and Hirschberg, eds. (Plenum, New York, 1996).

12. P. Demchenko, Ultraviolet Spectroscopy of Proteins (Springer, New York 1981).

13. E. D. Owen, "Principles of photochemical reactions," in Organic Compounds in Aquatic Environments, S. D. Faust and J. V. Hunter, eds. (Marcel Dekker, Inc. New York 1971).

14. L. J. Kleinsmith and V. M. Kish, Principles of cell and molecular biology, 2nd ed. (HarperCollins, New York, 1995).

15. M. Monici, R. Pratesi, P. A. Bernabei, R. Caporale, P. R. Ferrini, A. C. Croce, P. Balzarini, and G. Bottiroli, "Natural fluorescence of white blood cells: spectroscopic and imaging study," J. Photochem. Photobiol. **30**, 29-37 (1995).

16. M. Roederer and R. F. Murphy, "Cell-by-cell autofluorescence correction for low signal-to-noise systems: application to epidermal growth factor endocytosis by 3T3 fibroblasts," Cytometry. 7, 558-565 (1986).

17. C. Benson, R. A. Meyer, M. E. Zaruba, and G. M. McKhann, "Cellular autofluorescence - is it due to flavins," J. Histochem. Cytochem. 27, 44-48 (1979).

18. G. Cinelli, A. Ferrari, V. Pellegrini, M. Tyagi, M. Giacca, and F. Beltram, "The enhanced green fluorescent protein as a tool for the analysis of protein dynamics and localization: local fluorescence study at the single-molecule level," Photochem. Photobiol. 71, 771-776 (2000).

19. Encarta Learning Zone, Amino Acids, http://encarta.msn.com/find/Concise.asp?z

20. Encarta Learning Zone, Protein, http://encarta.msn.com/find/Concise.asp?ti

21. Amino acids, http://chemed.chem.purdue.edu/genchem/topicreview/bp/1biochem/amino2.html

22. T. Ha, Th. Enderle, D. F. Ogletree, D. S. Chemla, P. R. Selvin, and S. Weiss, "Probing the interaction between two single molecules: Fluorescence resonance energy between a single donor and a single acceptor," Proc. Natl. Acd. Sci. **93**, 6264-6268 (1996).

23. Erwin J. G. Peterman, Sophie Brasselet, and W. E. Moerner, " The fluorescence dynamic of single molecules of green fluorescent protein," J. Phys. Chem. A **103**, 10553-10560 (1999).

24. Mita Chattoraj, Brett A. king, Gerold U. Bublitz, and Steven G. Boxer, " Ultra-fast excited state dynamics in green fluorescence protein: Multiple states and proton transfer," Proc. Natl. Acad. Sci. **93**, 8362-8367 (1996).

25. Robert M. Dickson, Andrew B. Cubitt, Roger Y. Tsien, and W. E. Moerner, " On/off blinking and switching behavior of single molecules of green fluorescent protein," Nature **388**, 355-358 (1997).

26. T. M. H. Creemers, A. J. Lock, V. Subtramaniam, T. M. Jovin, and S. Volker, " Three photoconvertible forms of green fluorescent protein identified by spectral hole-burning," Nature Structural Biology **6**, 557-560 (1999).

27. Ling Zang and Michael A. J. Rodgers, " Formation of tryptophan radicals in irradiated aqueous solutions of hexachloroplatinate(IV): a flash photolysis study," Photochemistry and photobiology **70**, 565-567 (1999).

28. Christine Pokalsky, Peter Wick, Etti Harms, Fred E. Lytle, and Robert L. Van Etten, "Fluorescence resolution of the intrinsic tryptophan residues of bovine protein tyrosyl phosphatase," The Journal of Biological Chemistry. 270, 3809-3815 (1995).

29. Alexander A. Voityuka, Maria-Elisabeth Michel-Beyerlea and Notker Rōscha, " Protonation effects on the chromophore of green fluorescent protein. Quantum chemical study of the absorption spectrum, " Chemical Physics Letters 272(3-4), 162-167 (1997).

30. B. Anfinsen, Jr., M. L. anson, Kenneth Bailey, and John T. Edsall, Advances in protein chemistry, Academic Press 17, (1962).

31. Douglas L. Heintzelman, Reuben Lotan, Rebecca R. Richards-Kortum," Characterization of the autofluorescence of polymorphonuclear leukocytes, mononuclear leukocytes and cervical epithelil cancer cells for improved spectroscopic discrimination of inflammation from dysplasia," Photochemistry and Photobiology. 71,327-332 (1999).

32. Brockhinke, R. Plessow, P. Dittrich, K. Kohse-Hoinghaus," Analysis of the local conformation of proteins with two-dimensional fluorescence techniques," Appl. Phys. B71, 755-763 (2000).

33. T. Timperman, K. E. Oldenburg, and J. V. Sweedler, "Native fluorescence detection and spectral differentiation of peptide containing tryptophan and tyrosine in capillary electrophoresis," Anal. Chem. 67, 3421-3426 (1995).

34. J. E. Aubin, " autofluorescecne of visible culture Mammalian cells," The Journal of Histochemistry and Cytochemistry. 27, 36-43 (1979).

35. J. Soltys, Giardia lamblia: cell biology and microscopy of one of the most primitive eukaryotes,http://www.geocities.com/CollegePark/Lab/4551/.

Chapter 6

1. A.D. Bray, J. Lewis, M. Raff, K. Roberts, and J. D. Watson, Molecular Biology of The Cell, 2nd Ed, (Garland Publishing, Inc. New York & London 1989).
2. W. P. Ambrose, P. M. Goodwin, J. C. Martin, and R. A. Keller, "Single molecule detection and photochemistry on a surface using near-field optical excitation," Physical Review Letters. 72, 160-163 (1994).
3. S. Weiss, " Fluorescence spectroscopy of single biomolecules," Science 283, 1676-1683 (1999).
4. T. Hirschfeld, " Fluorescence background discrimination by prebleaching," The Journal of Histochemistry and Cytochemistry. 27, 96-101 (1979).